Doctoral Thesis

Design and modeling of the hydraulic control rod drive mechanism for passive in-core cooling system

In Guk Kim

Department of Nuclear Engineering

Graduate School of UNIST

2019

Design and modeling of the hydraulic control rod drive mechanism for passive in-core cooling system

In Guk Kim

Department of Nuclear Engineering

Graduate School of UNIST

Design and modeling of the hydraulic control rod drive mechanism for passive in-core cooling system

A dissertation
submitted to the Graduate School of UNIST
in partial fulfillment of the
requirements for the degree of
Doctor of Philosophy

In Guk Kim

2019. 01.05

Approved by

Bang, In Cheol

Advisor

Prof. In Cheol Bang

Design and modeling of the hydraulic control rod drive mechanism for passive in-core cooling system

In Guk Kim

This certifies that the dissertation of In Guk Kim is approved.

01.05.2019

signature

Advisor: In Cheol Bang

signature

Ji Hyun Kim

signature

Young-Bin Park

signature

Jae Yung Lee

signature

Ki Yong Choi

Abstract

The safety system in nuclear power plants has become a crucial topic owing to the massive damages inflicted by nuclear disasters. After the Fukushima accident in Japan, the importance of passive safety system has significantly increased, and additional safety systems to mitigate the impact of design extension conditions are constantly being proposed and developed. In Korea, various passive safety systems have been studied, including the hybrid safety injection tank (hybrid-SIT), passive auxiliary feed-water system (PAFS), passive emergency feed-water system, and passive containment cooling system (PCCS). The operation of passive safety systems do not require additional electric or diesel power source for system operation. Especially, a passive in-core cooling system (PINCs) is currently being studied toward a fully passive safety system at the Ulsan National Institute of Science and Technology. A PINCs comprises hybrid control rod assemblies, a hydraulic control rod drive mechanism (CRDM), and a natural circulation loop to remove the decay heat of the nuclear fuels. The hybrid control rod assemblies perform the roles of both a control rod for controlling the reactor power and a heat pipe for removing the decay heat in case of an accident.

To achieve the optimal design of PINCs, there are several requirements: 1) in-vessel CRDM strategy, 2) possible geometry for heat removal, and 3) good passivity. The in-vessel type reactor vessel with a hydraulic control rod drive mechanism (CRDM) is one possible approach to enhance the safety features of nuclear power plants, that can reduce the penetration defect and control rod ejection accident. Previous studies have proposed the hydraulic control system for small modular reactors and research reactors, for advantages such as the in-vessel strategy and enhanced passivity. However, due to the nonlinearities, complex flow area, and requirement of delicate position control, it is difficult to achieve the specific design and model validation. Therefore, to achieve a feasible design of hydraulic CRDM for PINCs, this research is focused on the study of a flow-induced pressure and flow behavior inside the hydraulic system with developing the theoretical model, which is characterized by the geometry of control unit, flow control system, and condition of the hybrid control rod.

Thus, the first chapter includes the design and modeling of hybrid control rod based on the experiment. In similar previous researches, the heat transfer performance of pressurized hybrid heat pipe-control rod was reported for enhancing the heat transfer performance. However, the study focused on single hybrid control rod and did not consider the elevation control of the control rod, pressure boundary of PINCs, and the connection between the control rod and the condenser section. Therefore, this study extends the experimental works with the developed control system and revises the design of hybrid control rod. Specifically, a hybrid control rod with varied length using two parts of the tubes and linear ball bearing system is proposed. This concept can effectively control the operation of the hybrid control rod and it is possible to optimize the heat performance of PINCs. At the upper plenum of the pressurized

vessel, the condenser of the hybrid control rods is sealed by welding. The linear ball bearings are located at the bottom of the condenser which is connected to the evaporator section, including the neutron absorbing material and working fluid. Therefore, in steady state, the length of the shutdown hybrid control rod is minimized as it is located in the upper plenum of the reactor vessel, and the thermal performance is degraded due to the decrease in temperature difference between reactor coolant and working fluid. During rod drop, the length of the hybrid control rod increases, and the operational temperature of the hybrid control rod is decreased. In this chapter, the thermal performance of the hybrid control rod is presented using the experimental results and previous studies.

The following chapter explain the possible geometry of hybrid control rod and hydraulic CRDM inside the nuclear power plant. PINCs must be capable of passively removing the decay heat from the nuclear fuel and transfer it to the water pool located at the top of the reactor vessel without alternative power. During operation, the CRDMs are key devices for controlling the reactor power and shutting down the reactor in the event of an accident. For commercial pressurized water reactors, the magnetic jack type CRDM has been developed and widely used due to its simple mechanism based on electric signals. It requires a large space on the top of reactor vessel. In Chapter 3, to achieve the geometry for heat removal, the conceptual hydraulic CRDM is designed with hybrid control rods inside the reactor vessel. In hydraulic CRDMs, the forces such as gravitational force, buoyancy force, frictional force, and the pressure difference between the cylinder and outside pool are dominant parameters and these forces are at equilibrium during the steady state condition. Based on the force balance equation, it is found that the relationship between the forces depends on the inlet mass flow rate and pressure difference. The two different geometries, such as conventional hydraulic CRDM and a new type hydraulic CRDM for PINCs are designed, evaluated, and validated to develop the theoretical model. The developed models demonstrated a reasonable accuracy in comparison with the experimental results and previous studies. Based on the elevation control test and control rod-drop test, the transient control model was also validated. In previous chapters, experiments were conducted, and theoretical models were validated. However, the conditions for application of hydraulic systems are high temperature and pressure in comparison with experimental conditions. In Chapter 4, the parameters crucial for CRDM performance are determined based on the driving mechanism and force balance equation. Then, the specific design of hydraulic CRDM is described and mass flow rate during the steady flow rate and rod drop are theoretically analyzed. Finally, the thermal performance and design of PINCs in commercial PWR are determined, and the discussions for enhancing the accuracy and safety of PINCs are presented.

Contents

List of Figures

List of Table

Nomenclature

A	Area	[m^2]
C	Constant	[-]
D	Diameter	[m]
F	Force	[N]
f	Frictional force	[N]
g	Gravitational acceleration	[m/s^2]
G_m	Mass flux	[kg/m^2s]
l	Length	[m]
$\dot{m}$	Mass flow rate	[kg/min]
n	number of moles of gas	[mol]
P	Pressure	[Pa]
ΔP	Pressure difference	[Pa]
r	Radius	[m]
R	ideal gas constant	[J/mol·K]
R	Thermal Resistance	[°C/W]
Re	Reynolds number	[-]
S	Head loss	[m]
Vol	Volume	[m^3]
V	Velocity	[m/s]
Y	Position	[m]

Greek symbols

ρ	Density	[kg/m^3]
ν	Viscosity	[kg/ms]
ω	Friction coefficient (bearing)	[-]
λ	Darcy friction factor	[-]

Subscripts

atm	*atmosphere*
b	*buoyancy*
bearing	*ball bearing*
B_4C	*boron carbide*
c	*cylinder*
clad	*cladding*
con	*condenser*
c,cs	*cross section of the cylinder*
CRDM	*control rod drive mechanism*
e	*evaporator*
fluid	*fluid*
fr	*friction*
g	*gravitation*
gt,cs	*cross section of the guide tube*
hcr	*hybrid control rod*
i	*initial*
in	*inner*
inp	*input*
max	*maximum*
min	*minimum*
num	*number*
out	*outer*
p	*pressure*
s	*seal material*
spring	*spring*

Chapter 1. Introduction

1.1 Research background and motivation

The safety systems in nuclear power plants are an important topic owing to their enormous effect on the environment and society. Especially, the need for developing a safety system to prevent or mitigate unexpected accidents has dramatically increased after the Fukushima accident in 2011. During station blackout (SBO) such as that occurred in the Fukushima accident, the active safety systems cannot be operated. Therefore, various passive safety systems have been suggested and designed for nuclear power plants including the hybrid safety injection tank (H-SIT), integrated passive safety system (IPSS), passive auxiliary feed-water system (PAFS), and passive containment cooling system (PCCS) [1.1-1.6]. The hybrid-SIT system is based on a new concept of passive safety system by using the safety injection system in conventional PWR. The mechanism of H-SIT depends on a natural circulation between SIT and reactor vessel by gravitational force, in the event of SBO and non-depressurized accident[1.1]. The IPSS is proposed as a type of passive supplement for previous safety systems, therefore, it reinforces safety enhancements. Independent passive safety systems are installed in the nuclear power plants. These systems are operated by natural forces, including the natural convection, gravitational force, and pressure differential force [1.2]. The PAFS is a well-known passive safety system comprising a steam supply pipe, heat exchanger to condense the steam inside cooling tank, a return pipe, and a condensation cooling tank outside containment building. This system modifies the auxiliary feed-water system by connecting a condensation heat exchanger and a passive condensation cooling tank. The PAFS removes the core heat from the primary system and transfers it to the secondary system of steam generator [1.3,1.4]. The PCCS is one of the main passive safety systems to enhance the containment integrity and safety, for advanced nuclear power plants. The PCCS is deployed in the upper of the containment building and consists of a passive containment cooling tank and a heat exchanger that removes heat using natural circulation, passively [1.5, 1.6].

A passive in-core cooling system (PINCs) was proposed and designed to enhance the passive safety for pressurized water reactors (PWRs), small modular reactors (SMRs), and Gen. IV reactors. The PINCs consists of hybrid control rod assembly, a hydraulic control rod drive mechanism (CRDM), and a natural circulation loop to remove the decay heat from the nuclear fuel in case of an accident, especially SBO accident [1.7-1.10]. The components of PINCs are completely passive, to remove the decay heat from the reactor core and transfer it to a natural circulation loop at the tip of the reactor vessel. Fig. 1.1 shows a conceptual design of the PINCs with main components such as; 1) hybrid control rod and 2) hydraulic control rod drive mechanism. Most rod control systems used in large-scale PWRs are located in the top of the reactor vessel and the shafts of control rod assemblies covered by pressure

housings [1.11]. Therefore, a penetrating volume of space is required for the installation of CRDM components in the pressurized vessel. However, an in-vessel hydraulic CRDM has a reduced or negligible penetrated area, a compact geometry of CRDM, and a short control rod assembly in comparison with the general CRDMs in nuclear power plants.

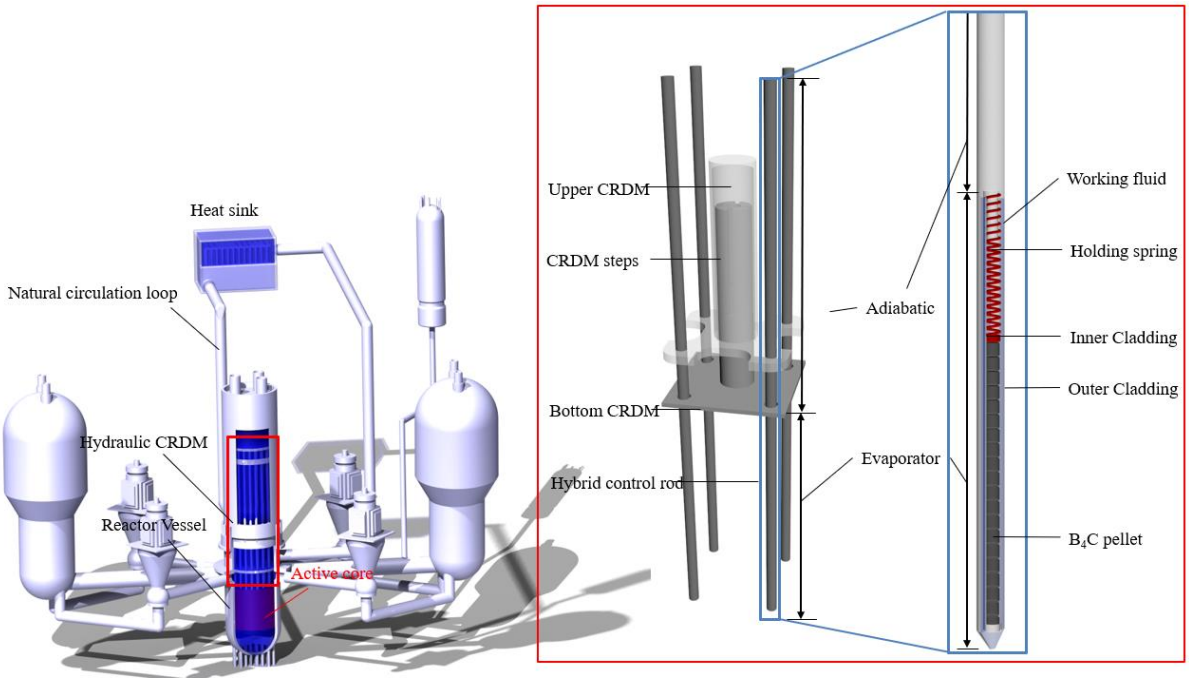

Fig. 1.1 The conceptual design of PINCs with main components; hybrid control rod and hydraulic CRDM [1.21]

1.2 Review on hydraulic control rod drive systems

The control system for the control rod assemblies is a crucial device for controlling the nuclear reaction and perform safety shutdown in case of an accident. The hydraulically driven rod control systems are currently being studied and designed, owing to their advantages such as short control rod assembly, in-vessel application in pressurized water reactors, and good passivity during the reactor shutdown. Various reactor types use the hydraulically driven rod control strategy for advanced reactor control systems. In SMRs, hydraulic CRDMs with a well-designed system have been studied. The IRIS reactor uses a spider type PWR control rod assemblies with hydraulically driven control rod and its design provides various benefits: 1) elimination of mechanical penetrations, penetration cost, and corrosion problem, 2) elimination of rod ejection accident by using the in-vessel strategy, 3) safety shutdown without any additional power [1.12].

In Tsinghua university, the pressure discharged hydraulic control rod drive system (HCRDS) was designed and tested for 5MW and 200 MW research reactors (NHR-5, NHR-200) [1.13, 1.14]. Initially, the design of NHR-5 used the bottom mounted control rod system with hole-patterned elevation control system. The NHR-5 is a water-cooled integrated passive reactor without the primary pump and is operated based on the natural circulation inside the reactor vessel. The HCRDS consists of a circulation loop outside the reactor vessel, a hole-patterned cylinder at the bottom of the reactor core, and two different control units. The control rod assemblies can be both controlled and safely dropped in the reactor core by utilizing the mass flow rate of the working fluid (water) and gravitational force. The design of NHR-200 was based on the previously designed NHR-5, therefore, the HCRDS also was modified using design of NHR-5. The modification was performed considering the enhancement for easy fabrication, to obtain a wide range of operational temperature, and to have a compact core geometry including the hydraulic system, in comparison with those of the NHR-5. In CAREM 25, a key issue of the hydraulic system was the rod drop behavior and the time taken for the rod to reach the bottom of the core. To satisfy the safety requirement of rod drop time, the hydraulic control rod drives (CRDM) offer a change, by connecting the bypass line to the top of the control cylinder for a faster shutdown [1.15]. The final design of the hydraulically driven control rod drive system using water as a working fluid was SBWR-200 suggested by Batheja [1.16]. The integration of hydraulic CRDN was designed for the small nuclear reactor (SBWR-200). In their research, the prototype tests and comparison study were conducted between the theoretical model and experimental results. In Russia, hydraulically driven control rod drives were proposed for applying the sodium-cooled fast reactors (SFRs), especially BN-800 and BN-1200. To achieve the diversity of mechanism of rod control system, the hydraulic CRDMs were used in shutdown control rod assemblies. Fig. 1.2 shows the schematic of hydraulic CRDMs in the previous studies [1.7].

1.3 Introduction to passive in-core cooling system (PINCs)

The concept of PINCs has been designed and developed to utilize the passive emergency system in nuclear power plants, especially in PWRs and SMRs [1.17-20]. The key idea of this system is heat removal using hybrid control rod having the functions of both a control rod and a heat pipe. Therefore, it is possible to remove the heat during non-decompressed accidents such as the SBO accidents. In SBO scenarios, without an alternative power source, PINCs requires the functional capability of removing the heat from the nuclear fuel and transfer it to the outside water tank. Due to the requirement of a hybrid control rod, there are two functions: 1) reactor power control and shutdown and 2) heat removal during reactor accidents [1.21]. Fig. 1.3 shows the schematic of the pressure vessel with PINCs to satisfy these two features. An integrated heat exchanger on the upper plenum of the reactor pressure vessel is considered for the hydraulic CRDM of PINCs. There are fixed condenser sections of the hybrid control rod and movable parts of the hybrid control rod, connected with a hydraulic unit to avoid the issue of the penetration region such as cracks and rod ejection. In case of rod seal failure, the thermal performance of the hybrid control rod is degraded due to increased operational pressure (Two-phase heat transfer → Single phase natural circulation), however, the loss of coolant accident cannot occur (different pressure boundary). The control rod assemblies are considered to possess both full and part strengths. Full-strength assemblies are not inserted in the core and are positioned at the top of the reactor core. However, the part strength assemblies are moved to control the reactivity of the reactor power plant during the steady state. Due to the stroke length of the reference plant (APR1400), the required height of the hydraulic CRDM inside the vessel is 8 m (double of the core height). The full-strength control rod assemblies maintain a minimum rod length under the operation condition. During a reactor accident, the full-strength hybrid control rod assemblies are dropped, and it transfers the decay heat from the nuclear fuel to the condenser of the hybrid control rod. One of the key components of the PINCs is the hybrid control rod, which consists of two layers of metal cladding, neutron absorber, holding spring, and a working fluid. The decay heat of the nuclear fuel is transported by phase change heat transfer of the water inside the cladding structure (Annular flow path). To control the reactor power, the B4C pellets with enriched B10 (neutron absorbing material) for reducing the pellet diameter are inserted inside the metal cladding [1.7].

The hydraulic CRDM inside PINCs has a unique feature, including the stepped shape with different holding flow rates and position-indicated system using the mass flow rate. In previous studies, the hydraulic CRDMs had a fixed holding flow rate, therefore, an indicator is needed to detect the elevation of control rods. The conventional CRDMs needed penetration holes for inserting position indicator, and the peak of the pressure and mass flow rates during the step control. To enhance the hydraulic CRDM, a novel design with stable operating behavior and flow-indicated structure using the stepped cylinders

is developed, as shown in Fig. 1.4.

1.4 Research Objectives and Scope

The present study focuses on the hydraulic CRDM for application of the PINCs with hybrid control rod and its design and model of flow/heat transfer behaviors. This paper includes the major parts such as 1) theoretical model based on the flow-driven force balance equation and its validation using the experimental studies for noble hydraulic CRDM, 2) new-design of the movable hybrid control rod system and experimental studies using single hybrid control rod test facility, 3) validation of the combined system with integrated test facility.

Chapter 1 reviews various hydraulic CRDMs for application in nuclear power plants and introduces the PINCs with major components.

Chapter 2 describes the modified hybrid control rod for solving the critical issues, including the heat loss during steady state and penetration hole on the upper plenum. The present study extends the experimental works with the developed control system and revises the design of the hybrid control rod. Specifically, a hybrid control rod with a varied length which uses two parts of the tubes and linear ball bearing system, is proposed. This concept can control the operation of the hybrid control rod and it is possible to optimize the heat performance of the PINCs. Based on similar previous researches, the enhanced design of the hybrid control rod was proposed.

Chapter 3 presents the design and modeling of the hydraulic CRDM along with its validation. Two different geometries are available to easily explain the difference from previous CRDMs. Based on the force balance equation, it is found that the relationship between the forces depends on the inlet mass flow rate and pressure difference. The two different geometries, such as conventional hydraulic CRDM and a new hydraulic CRDM for PINCs are designed and tested to develop the theoretical model and is validated.

Chapter 4 reports the possible geometry and its specific design during reactor operation. Therefore, in this chapter, the crucial parameters to determine the CRDM performance are proposed based on the driving mechanism and force balance equation. Then, the specific design of the hydraulic CRDM is described and the analysis of mass flow rate and pressure during the steady flow rate and rod drop are theoretically conducted.

Chapter 5 concludes this paper with recommendations for future studies.

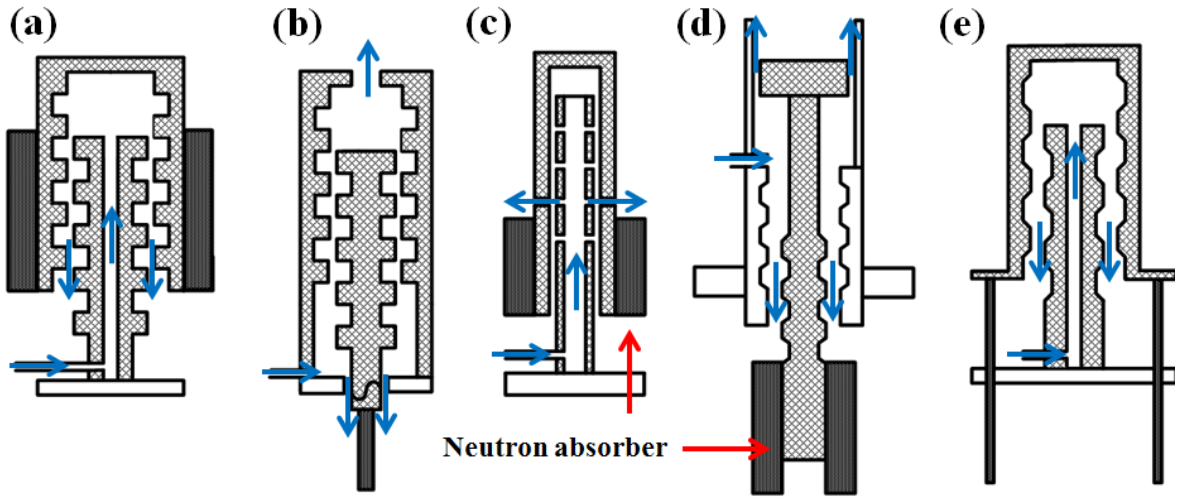

Fig. 1.2. Schematic of hydraulic control rod drive mechanism: (a) SBWR-200, (b) CAREM, (c) NHR-5, (d) NHR-200, and (e) IRIS [1.7]

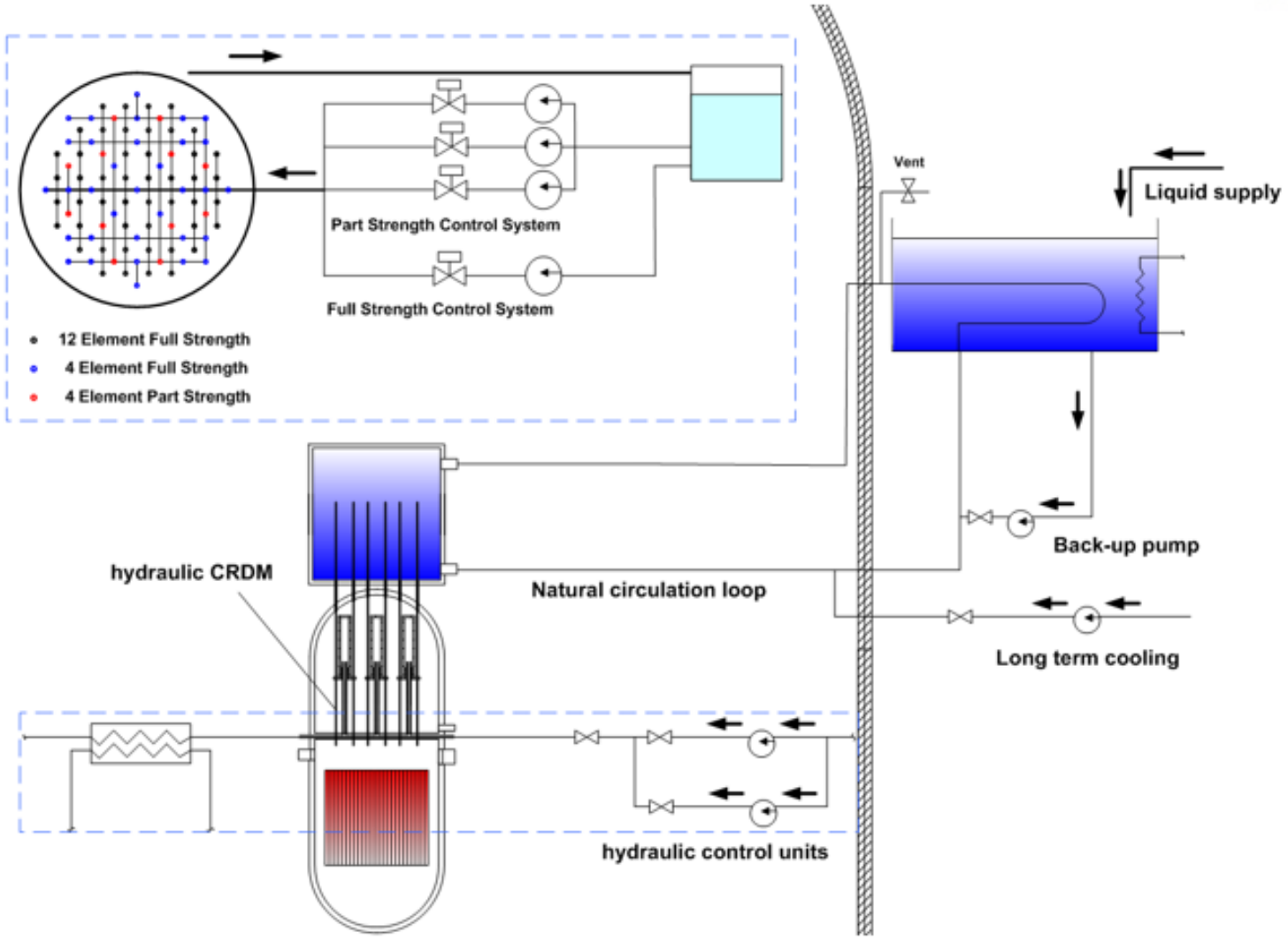

Fig. 1.3 Schematic of the passive in-core cooling system (PINCs)

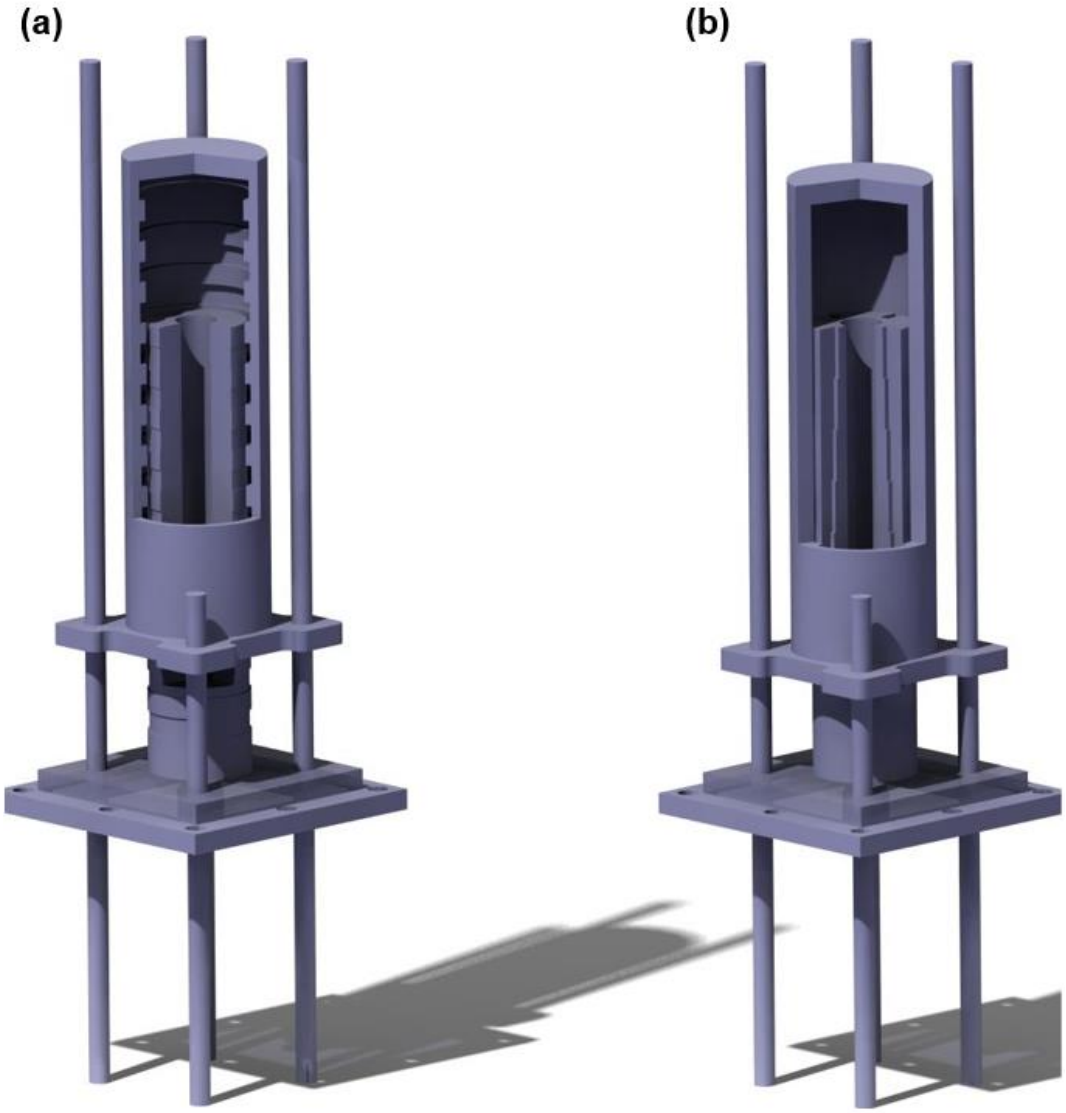

Fig. 1.4 The design of the hydraulic CRDM for previous study and PINCs; (a) Conventional CRDM based on IRIS, (b) Hydraulic CRDM for PINCs

Table. 1.1 The summary of the hydraulically driven rod control system for the nuclear power plants [1.12, 1.13, 1.16, 1.22-1.29]

Researcher	Operation Pressure[Bar] and Temperature [°C]	Geometry and flow rate	Insertion type	Application	Development level	Remarks
Batheja (1987)	Operation pressure : 25 Operation temperature : 223	Number of control rods: 45 Stroke length : 2,300 mm Step length : 100 mm Scram time : 10 sec Flow rate : 1 – 2 kg/s	Bottom up CRDM	BWR, Germany	Prototype Test	Test of the elevation control and free rod drop behaviors
Wang (1993)	Operation pressure : 1.37 Operation temperature : 186	Number of control rods: 32 Flow range : 0.388–0.90kg/s Scram time : 5 sec	Bottom up CRDM	Research Reactor, China(NHR-5)	Preliminary test → Enhancement for NHR-200	Characteristics of the flow channel and flow hole for elevation change Define the effect of the delay time for controlling the elevation
Wang (1993)	Operation pressure : 25 Operation temperature : 140-224		Bottom up CRDM	NHR-200	Conceptual design	
Wang (2002)	Operation pressure : 1.74-2.75 Operation temperature : 66-210		Bottom up CRDM	Research Reactor, China(NHR-5)	Preliminary test	
Bo (2002)	Operation pressure : N/A Operation temperature : 60		Bottom up CRDM	Research Reactor, China(NHR-5)	Preliminary test	
Li (2006)	Operation pressure : 2.5 Operation temperature : ~240	CR :32 Stroke length : 1,500mm Step length :30 mm Scram time : 2.3 sec	Top down CRDM	Desalination and urban heat supply (NHR-200)	Prototype rod control and drop test	Design modification for optimizing the core design
Ricotti (2003)	Operation pressure : 2.0 Operation temperature : ~100	Flow range : 0.25 kg/s Stroke length : 3700mm CR:92	Top down CRDM	IRIS reactor (IMR, Italy)	Preliminary Test	Preliminary tests for hydraulic CRDM with flow control system
Magan (2011)	Operation pressure : 12.25 Operation temperature : 326	Stroke length : 1,400mm CR : 19	Top down CRDM	SMR,Argentina (CAREM project)	Reported PSAR	Conceptual design of full strength (shutdown CRDM) for passive scram
Hibi (2004)	Operation pressure : 15.5 Operation temperature : ~345	N/A	Top down CRDM	SMR, Japan (IMR, 1000MWth)	Conceptual design	Conceptual design of the hydraulic CRDM
Vasilyev (2017)	Operation pressure : 14~17.5 Operation temperature : ~550	Only shutdown	Top down CRDM	BN-800, BN-1200	Design and experiment	Passive shutdown hydraulic CRDM
Liu (2017)	Operation pressure : 1.2 Operation temperature : N/A	Stroke length : N/A Flow rate : ~2.0 kg/s	Top down CRDM	Research Reactor, China(NHR-5)	Experimental test	Weight effect of the hydraulic CRDM
Sun (2017)	Operation pressure : 3.5 Operation temperature : N/A	Stroke length : 2,500mm Flow rate : ~1.6 kg/s	Top down CRDM	PWR application (China)	Test and validation	Analysis of the flow and pressure behaviors during the step-up and down
Qin (2018)	Operation pressure : 3.5 Operation temperature : N/A	Stroke length : 900mm Flow rate : ~4.2 kg/s	Top down CRDM	PWR application (China)	Modeling and its validation	Application of spring damper for reducing the drop impact

Chapter 2. DESIGN AND MODELING OF THE HYBRID CONTROL ROD

2.1 Introduction

The heat pipe applications increased in various fields due to their high thermal performance using phase change heat transfer [2.1-2.16]. Recent reports of heat pipe application in nuclear power plants have focused on the emergency cooling system without any additional power [2.17, 2.18]. In this research, a hybrid control rod is proposed to design of the PINCs for enhancing the nuclear safety. Therefore, detailed information, including the geometry, control method, and mechanism are needed. In previous studies, the hybrid control rod was explained as a passive heat removal device having a neutron absorbing material (named Boron carbide, B_4C). Therefore, it has a unique geometry inside the evaporator, as shown in Fig. 2.1 [2.19].

Generally, heat pipes have a wick structure in container, evaporator, adiabatic region, and condenser. Vapor flow from the evaporator to the condenser is caused by a difference in the vapor pressure. Simultaneously, the liquid flows from condenser to the evaporator driven by the capillary and gravitational forces [2.14]. However, the thermal resistance of the capillary heat pipes increases at the capillary limit because of an insufficient supply of the working fluid. To increase the heat removal capacity of the heat pipes, the thermosyphon heat pipes are used for the hybrid control rod. The thermosyphon heat pipe uses a container with a wickless surface, evaporator, adiabatic region, and condenser. Therefore, it only performs vertically oriented heat transport at high-heat load conditions. Without the capillary structure, the hybrid control rod does not have a capillary limit.

The hybrid control rod has an annular-shaped evaporator due to the neutron absorbing material. In the same research group, studies on the effect of neutron absorbing material, heat transfer performance, operational limit (entrainment limit), and flow visualization were conducted and analyzed [2.19].

While the heat transfer phenomenon in simple geometry was conducted in previous studies, they did not consider the operational problems, including the pressure boundary and heat loss during normal operating condition. Some critical problems of PINCs were 1) movable heat pipe system, 2) isolated pressure boundary, and 3) heat loss under the normal operating condition (steady state). Fig. 2.2 shows the design concept of the hybrid control rod to solve the critical issues.

There are two types of control rod assemblies to control the reactivity and shut down the nuclear reactor: prat-strength assemblies and full-strength assemblies [2.20]. The part-strength assemblies of the control rod control the reactor power, therefore, these assemblies are located inside the reactor core. The commercial CRDMs have a large number of steps (200 steps for APR1400, 1 step = 3/4 inch) [2.21]. In part-strength assemblies, the phase change heat transfer in the hybrid control rod was not considered. The full-strength assemblies are designed for a shutdown system. These assemblies are generally

located at the top of the reactor core under normal operation. The hybrid control rods to remove the decay heat are proposed for the full-strength assemblies. Both the control rod assemblies contain a condenser section welded to the reactor vessel. The condenser section is not movable and the pressure boundary between pressure vessel and the heat sink can be separated. The linear ball bearing is designed and located at the bottom of the condenser section to connect to the adiabatic region of the hybrid control rod. In this geometry, the length of the hybrid control rod is varied according to the operation condition (steady state/accidents).

In this chapter, the design and modeling of the hybrid control rod were conducted to analyze the hydraulic CRDM of PINCs. Therefore, the modeling of hybrid control rod focused on the mechanical operation and operation forces for changing the length of the control rod. To validate the design concept of the hybrid control rod, the single rod control test was conducted. In the experiment, pressure, temperature, and the change of length were measured. Moreover, a simple heat transfer test was conducted to validate the minimized heat transfer during the short length condition (steady state). Finally, the driving forces for controlling the elevation were analyzed based on inside pressure of the hybrid control rod.

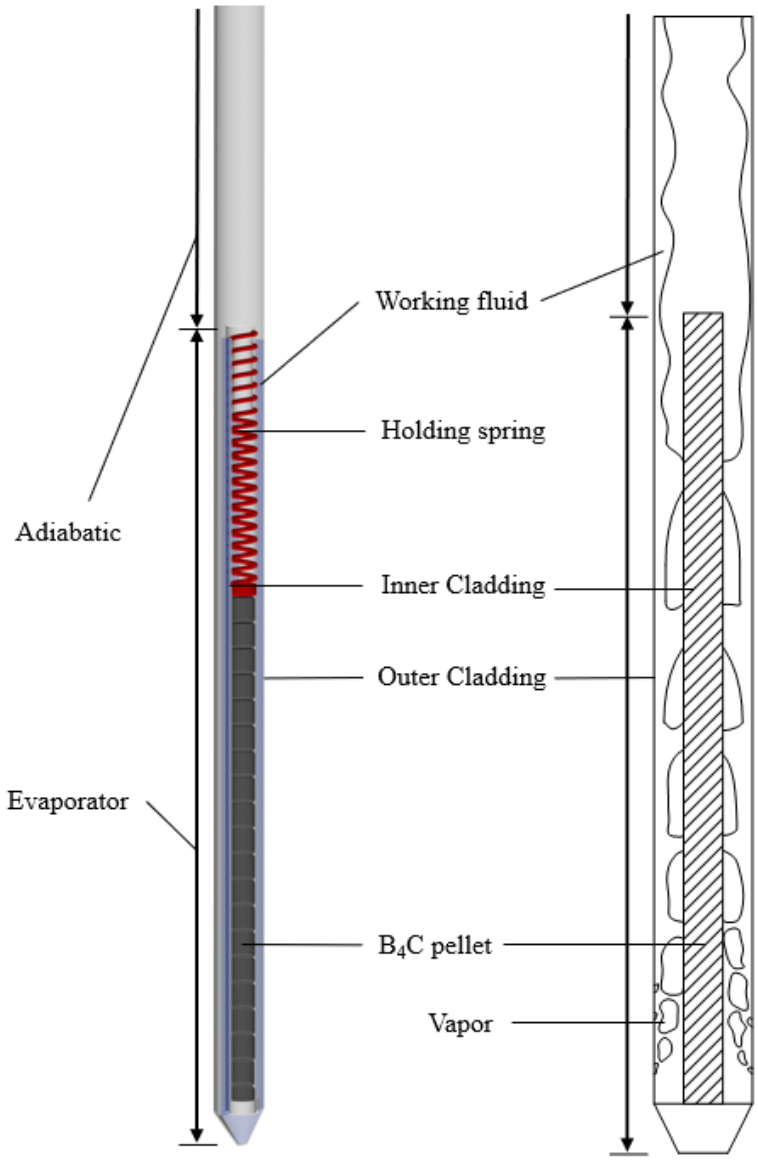

Fig. 2.1 The geometry of the hybrid control rod (Evaporator section) [2.19]

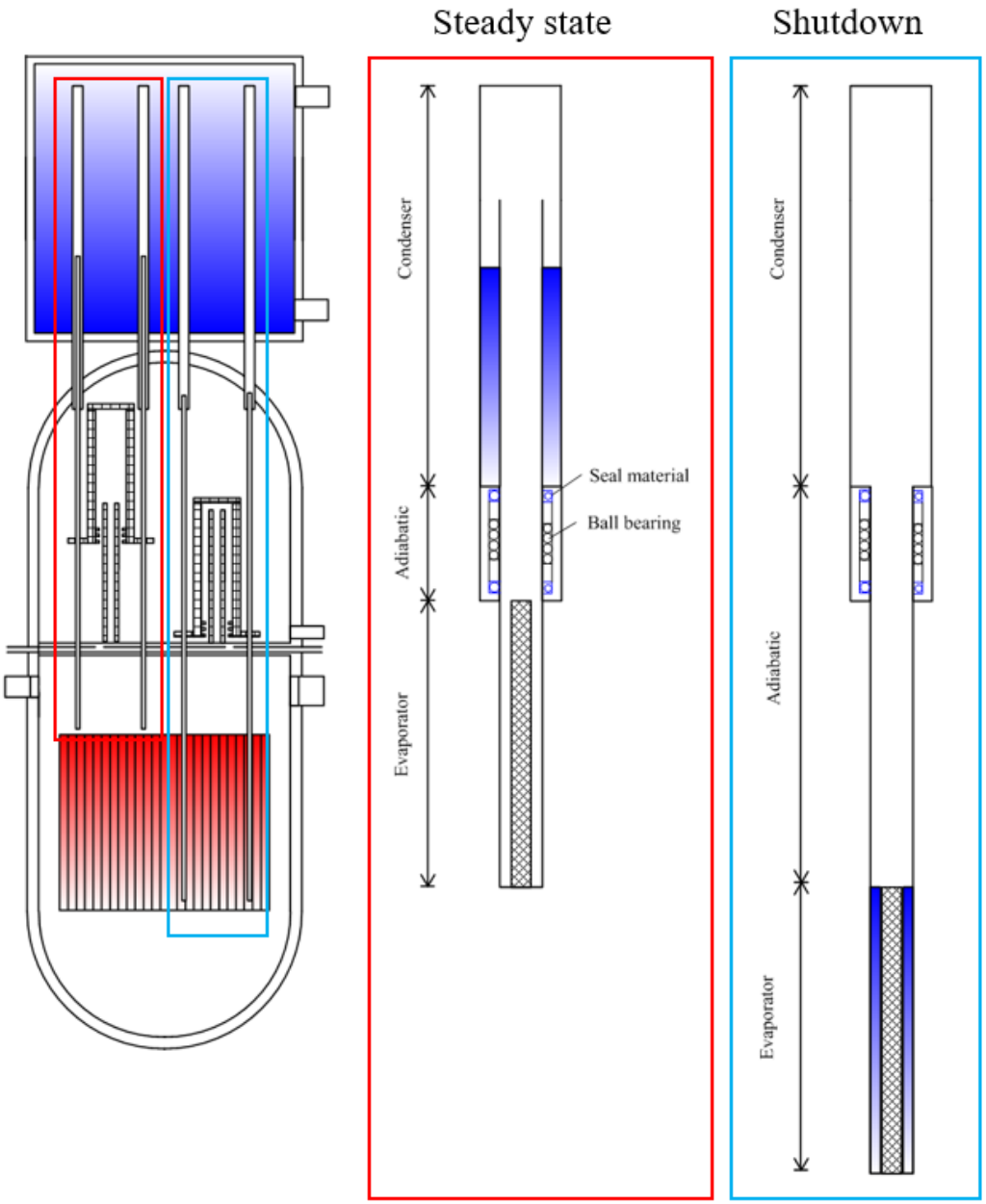

Fig. 2.2 Design concept of hybrid control rod in nuclear power plant under the steady state and shutdown condition

2.2 Driving mechanism and its theoretical models

In this part, the driving mechanism of the hybrid control rod is theoretically explained. The schematics of the hybrid control rod with driving forces are shown in Fig. 2.3(a). In this figure, the force balance equation is given by

$$F_{control} = F_g + F_p + F_{fr} \tag{2.1}$$

The ball bearing device to linearly control the length of the hybrid control rod is considered, therefore, the frictional force at the interface area is one of the main driving forces. Fig. 2.3(b) shows the detailed geometry of the ball bearing device in the test facility. The friction force on the interface area is defined by

$$F_{fr} = \omega F_{bearing} + num \cdot f_{seal} \tag{2.2}$$

In this equation, the values of friction coefficient and seal resistance are used considering the specification documents. The gravitational force for a single hybrid control rod was calculated as a function of length, considering the weight of the working fluid. Due to the annular gap between the condenser and adiabatic walls, the weight of the working fluid is changed according to the length of the hybrid control rod.

$$F_g = (m_{clad} + m_{B4C} + m_{fluid})g \tag{2.3}$$

$$F_g = (m_{clad} + m_{B4C} + m_{fluid,\max} C_1 \frac{L}{L_{\max}})g \tag{2.4}$$

where, the coefficient, C_1, is the geometry parameter to determine the space of the annular gap region. The condition inside hybrid control rod is assumed as an ideal and non-condensable gas. Therefore, the force of pressure difference between the hybrid control rod is calculated using

$$F_p = (P_i - P_{atm})A_c \tag{2.5}$$

$$\frac{P_i Vol_i}{nRT_i} = \frac{P_j Vol_j}{nRT_j} = C \tag{2.6}$$

$$P_i = \frac{P_j Vol_j}{Vol_i} = (C_{v1} + C_{v2} A_c L_j) P_j$$
$$C_2 = \frac{Vol_{fixed}}{Vol_{total}},\ C_3 = \frac{1}{Vol_{total}} \tag{2.7}$$

where C_l is the factor of the fixed volume of the hybrid control rod. The volume expansion/reduction is linearly changed according to the function of length. Finally, to move the hybrid control rod, the linear actuator with tension gauge is used. Therefore, the force required to control the hybrid control rod should be larger than the sum of other forces. By using Eq. 2.1-2.7, the force balance equation is rearranged as:

$$F_{control} = (m_{clad} + m_{B4C} + m_{f,\max} C_1 \frac{L}{L_{\max}}) g$$
$$+((C_2 + C_3 \frac{L}{L_i}) P - P_{atm}) A_c + \omega F_{bearing} + n \cdot f_{seal} \tag{2.8}$$

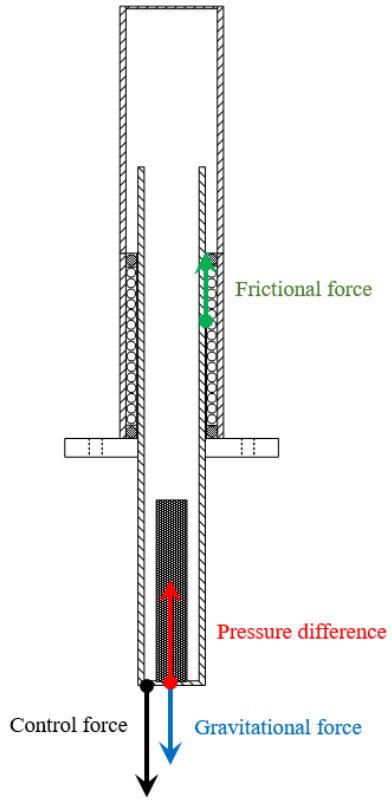

(a) Force balance of the hybrid control rod

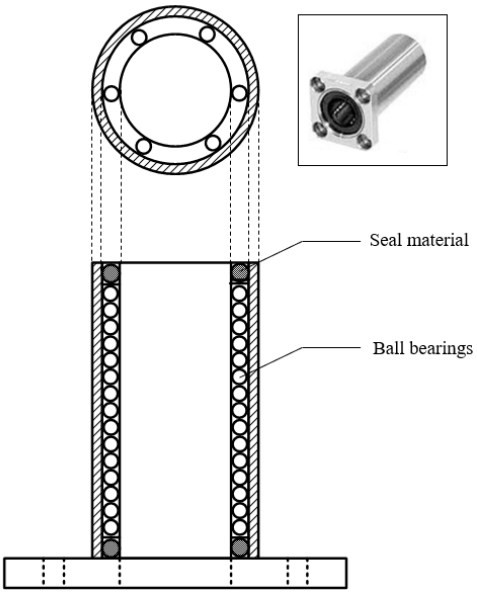

(b) Ball bearing device

Fig. 2.3 The force balance of the hybrid control rod and the schematics of the ball bearing device

2.3 Experimental setup and procedures

To validate the theoretical model of the hybrid control rod system, the single test was conducted according to different pressure conditions. In the hybrid control rod, the enriched boron (B^{10}) was considered due to control the reactor power, therefore, the inner space of the evaporator was decreased. In the tests, a 3-D printed structure (ABS material) was used instead of the neutron absorbing material. The size of the 3-D printed structure was determined by the ratio between the container of the control rod and boron carbide. The tested hybrid control rod used distilled water as the working fluid. The heat transfer performance was tested in a vertical orientation with different length positions. Before the heat transfer tests, the pressure change of each position was measured. Stainless steel was used as the containment of the hybrid control rod, which had outer diameters of 12.7 mm (evaporator and adiabatic) and 19.05 mm (condenser). The total length of the test section was 650 mm. The length of the adiabatic section was changed from 50 mm to 200 mm. Table 2.1 describes the information of the test facility with test conditions. The schematics of the test facility is shown in Fig. 2.4.

2.3.1 Heat transfer test

The experiment on the heat transfer performance is conducted to verify the design of the hybrid control rod. The aim of this test is to show the change in heat transfer performance of the hybrid control rod according to the change in control length. Therefore, control length (ΔL) was considered as a control parameter, which ranged from 0 to 150 mm. The test matrix of the experimental test is given in Table. 2.2.

2.3.2 Length control of the hybrid control rod

The length control of the hybrid control rod was conducted for the measurement of pressure change and control force. The main test parameters are the pressure difference between inside hybrid control rod and outside air, frictional force, gravitational force, and control force for controlling the length of the hybrid control rod. In the length control test, the pressure difference was measured at top of the hybrid control rod. The control force was also measured at bottom of the hybrid control rod with an actuator. During the test, the initial pressure was maintained at a set value, and the actuator was controlled to change the length of the hybrid control rod with a fixed amount of working fluid. Table. 2.3 summarizes the test matrix of the pressure control test.

Table 2.1 Information of the test sections

Parameters		Value	Unit
Total length		650	mm
Evaporator : Adiabatic : Condenser		200:200:250 200:50:250	mm
Containment	Diameter, e	12.7	mm
	Thickness, e	0.889	mm
	Diameter, c	19.05	mm
	Thickness, c	1.24	mm
	material	Stainless steel 316	-
	Thermal conductivity	16.3	W/mK
Inner structure	material	ABS	-
	Diameter	6	mm
	Thermal conductivity	0.6	W/mK

Table 2.2 Test matrix of the experimental test

Parameters	Values	Unit
V_f	100 % (fill ratio of evaporator volume)	%
D_{heated}	10.922	mm
$T_{coolant}$	5.0	℃
Working fluid	Water	-
Initial pressure	10.0 (for heat transfer test) 101.3 – 20 (for pressure measurement)	kPa
ΔL	0, 50, 100, 150	mm

Table. 2.3 Summary of the test matrix of the pressure control test

	Total volume (mm^3)	Control volume (mm^3)	Initial pressure (kPa)	Control length (mm)	Theoretical pressure (after) (kPa)
PC-1	53850.8	19001.0	101.3	50, 100, 150	80.28
PC-2	53850.8	19001.0	80.0	50, 100, 150	63.40
PC-3	53850.8	19001.0	60.0	50, 100, 150	47.55
PC-4	53850.8	19001.0	40.0	50, 100, 150	31.70
PC-5	53850.8	19001.0	20.0	50, 100, 150	15.85

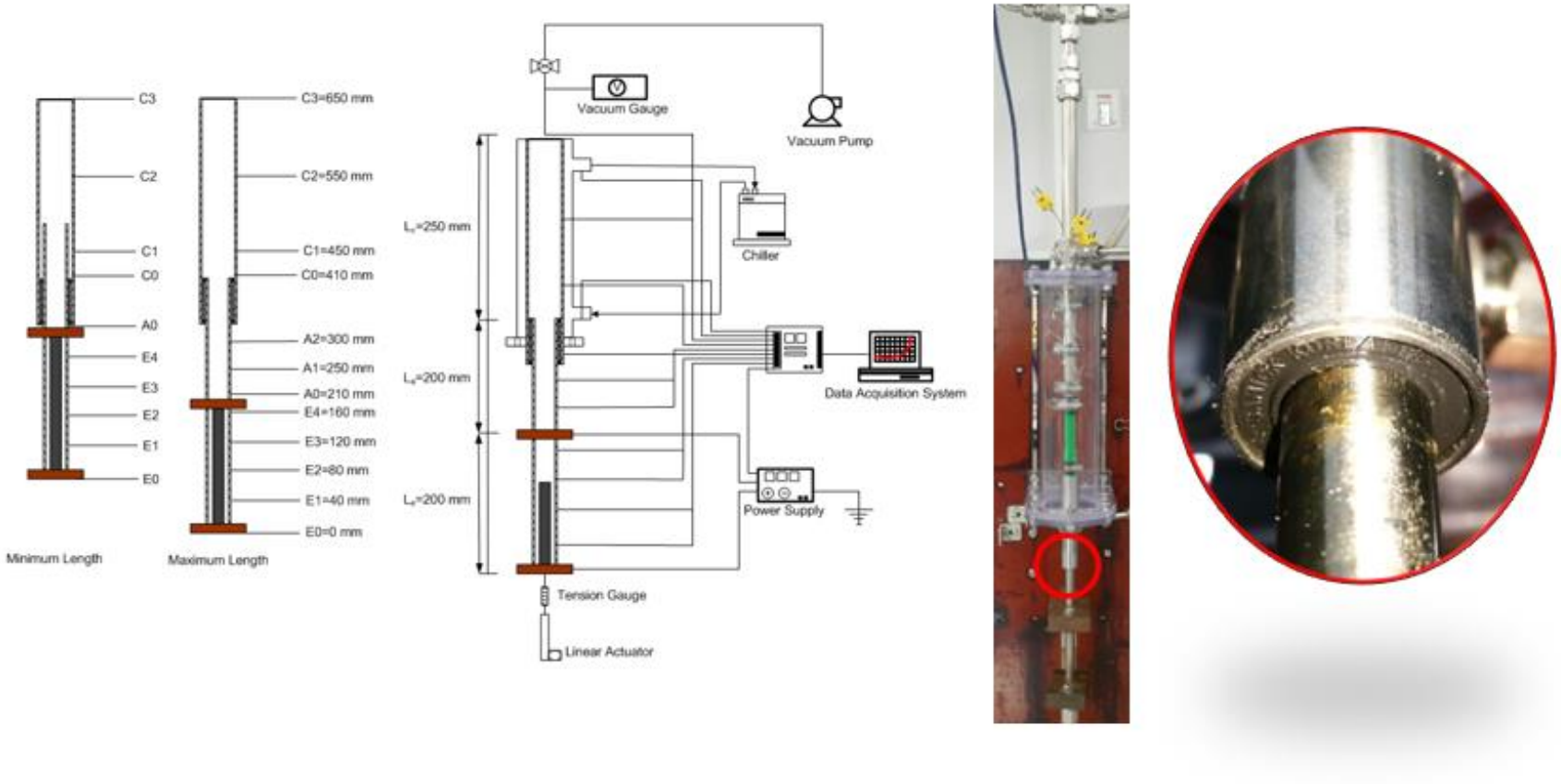

Fig. 2.4 The schematics of the test facility

2.4 Experimental results

In this section, two experiments were performed: 1) heat transfer test with a different length of the hybrid control rod and 2) pressure change according to the initial pressure condition. Both the tests are conducted using a single test facility.

2.4.1 Heat transfer performance of the single hybrid control rod

It is important to demonstrate the heat transfer performance of the hybrid control rod according to the change of length. When using the length control strategy, the hybrid control rod must lower the heat transfer performance at the minimum total length condition. Therefore, in this section, the heat transfer tests of the hybrid control rod were conducted. The mechanically controlled hybrid control rod has a different operational condition according to the position of the hybrid control rod. To determine the performance of the hybrid control rod, there are four different conditions: ΔL=0.0 mm, 50 mm, 100 mm, and 150 mm, as shown in Fig. 2.5. During the experiment, the fill ratio of the working fluid was 100% of the evaporator section. In the minimum length condition (initial condition), the hybrid control rod has a minimum volume of the hybrid control rod, and the annular gap between condenser tube and movable tube was created. Initially, the working fluid was located inside the annular gap and there was no two-phase heat transfer phenomenon.

During the initial condition, the heat pipes have an initial response time to satisfy the two-phase circulation condition. To decrease the start-up time of the hybrid control rod, cooled water is supplied from the condenser at 70 ℃ of the surface temperature of evaporator [2.22]. Fig. 2.6 shows the start-up temperature of the hybrid control rod according to the control length at a heat load of 30 W. The hybrid control rod exhibited nucleate boiling on the evaporator section with a rapid drop in temperature. Due to the periodic nucleate boiling phenomenon, temperature fluctuations in the hybrid control rod were observed (geyser boiling) [2.23, 2.24]. In the case of minimum length condition, the temperatures of the evaporator surface continuously increased at a heat load of 30 W. This indicates that the working fluid was not utilized at the minimum length condition. Therefore, heat transfer occurred by conduction of the containment material and convection of the gas inside hybrid control rod (Fig. 2.7(a)). In the case of maximum length condition, the temperatures of the evaporator surface were stable at the fixed heat load of 30 W, shown in Fig. 2.6(b).

The temperature distributions of the hybrid control rod at various heat loads are shown in Fig. 2.7. The heat load was increased from 30 W to the entrainment limit (operation limit) of 10 W. Each case was iterated three times and the least square method was used to determine the deviation of the experimental results. During the test, the temperature of condensing water was fixed and the temperatures in the

adiabatic section increased slightly due to boiling in the evaporator. In the short length cases, the evaporator temperatures had higher values than long length cases.

From the temperature distribution, the heat transfer performance was determined using the heat transfer coefficient and operation limit of the hybrid control rod. The heat transfer coefficient of the thermosyphon heat pipes can be determined by

$$R_e\left(^\circ C/W\right)=\frac{\overline{T}_e-T_{sat}}{Q_e} \tag{2.9}$$

$$R_{con}\left(^\circ C/W\right)=\frac{T_{sat}-\overline{T}_{con}}{Q_{con}} \tag{2.10}$$

If the amount of heat load in the evaporator equals the amount of heat in the condenser at the steady state condition, the overall thermal resistance is defined by

$$R_o\left(^\circ C/W\right)=\frac{\overline{T}_e-\overline{T}_{con}}{Q_e} \tag{2.11}$$

From the overall thermal resistance of heat pipes, the heat transfer coefficient can be calculated by

$$h_o(W/m^2{}^\circ C)=\frac{q_e''}{\overline{T}_e-\overline{T}_{con}} \tag{2.12}$$

During the test, the maximum error of the input power measurement was approximately 0.5 % and the uncertainties are calculated by

$$\frac{\Delta R_o}{R_o}=\sqrt{\left(\frac{\Delta Q_{inp}}{Q_{inp}}\right)^2+\left(\frac{\Delta(\Delta T)}{\Delta T}\right)^2} \tag{2.13}$$

$$\frac{\Delta h_o}{h_o}=\sqrt{\left(\frac{\Delta q_{inp}''}{q_{inp}''}\right)^2+\left(\frac{\Delta(\Delta T)}{\Delta T}\right)^2} \tag{2.14}$$

The estimated maximum uncertainties in the heat transfer coefficient of the measurement tools and power supply are 5.1%.

From Eq. 2.12, the heat transfer coefficients of the hybrid control rod are shown in Fig. 2.8. The general trendline of the heat transfer coefficients is the same as that of general heat pipes. However, in short length condition of the hybrid heat pipe the value was reduced in comparison with those of the long length conditions. In previous studies, the trendline of the hybrid control rod is similar to the effect of the fill ratio [2.25-2.27]. Therefore, in the minimum length condition (similar to the fill ratio of 0 %), the heat transfer coefficient was significantly reduced.

2.4.2 Change of the pressure and operation condition

To analyze the pressure change of the hybrid control rod, pressure control test were conducted. In the tests, the control parameters were the length of the hybrid control rod and the initial pressure. Table. 2.4 illustrates the detail space of the test facility, including the instrument line. The total volume of the system is approximately 72589.2 mm^3 and the controllable volume is 19001.0 mm^3 during the tests. In the test, the length of the hybrid control rod is controlled from the minimum length to maximum length without additional gases. Therefore, the pressure inside volume is assumed as an ideal gas equation. From the initial pressure condition, the final pressure (maximum length of the hybrid control rod) can be theoretically predicted (Table.2.4). Fig. 2.9 shows the experimental results of the pressure control according to the length of the hybrid control rod. From the experimental results, the pressure of the hybrid control rod is predicted well by the theoretical model. Similarly, the hybrid control rod with a water as a working fluid was also tested and the results were in good agreement with those predicted by the theoretical model. To confirm the force balance of the system, forces at the equilibrium state were measured and comparison study was conducted.

2.5 Validation of the theoretical model

This section presents the comparison between the theoretical model and the experimental results of the driving forces. The test condition is the same as the previous section, therefore, the change of the position is 0, 50 mm, 100 mm, and 150 mm, without other control parameters. During the test, the control force from the actuator was used and this force was measured using the tension gauge. From the force balance equation, the position of the bearing frictional force is fixed. The gravitational force was defined as a function of the change of length. With the increase in length, the amount of working fluid inside of evaporator increased. Therefore, the gravitational force was gradually increased. The pressure differential force of the hybrid control rod was also increased according to the change in control length. In Fig. 2.10(a) and 2.11(b), the fill ratio effect of pressure difference was observed. The working fluid was occupied the space inside the hybrid control rod, therefore, the total volume decreased. In the

case of fill ratio of 100%, the pressure change of the hybrid control rod was slightly increased. In comparison with tension forces in the test facility, the control forces were a good agreement, shown in Fig. 2.11.

Table. 2.4 The detail space of the test facility

		Values	unit
Evaporator and adiabatic	Diameter	10.9	mm
	Length	400.0	mm
	Volume	37325.3	mm^3
Condenser	Diameter	16.6	mm
	Length	250.0	mm
	Volume	53850.8	mm^3
Instruments	Volume of connecting line	1124.0	mm^3
	Volume of pressure gauge line	2248.0	mm^3
	Volume of charge line	2697.6	mm^3
	Volume of inner structure	5655.0	mm^3

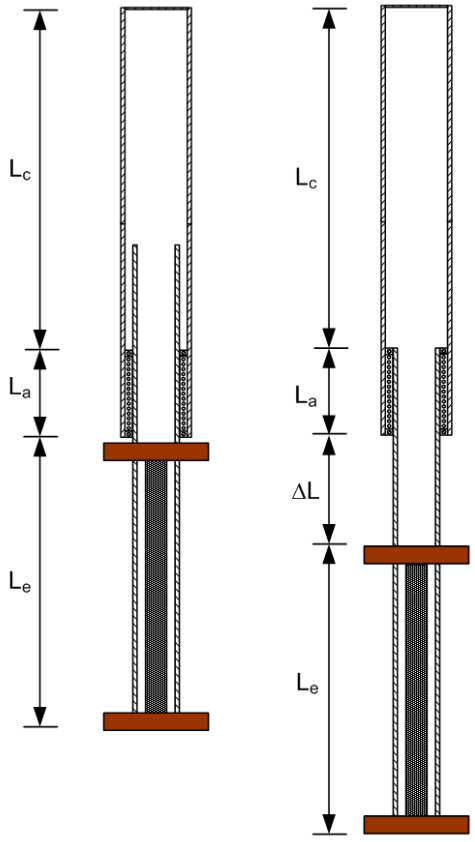

(a) Design of the hybrid control rod

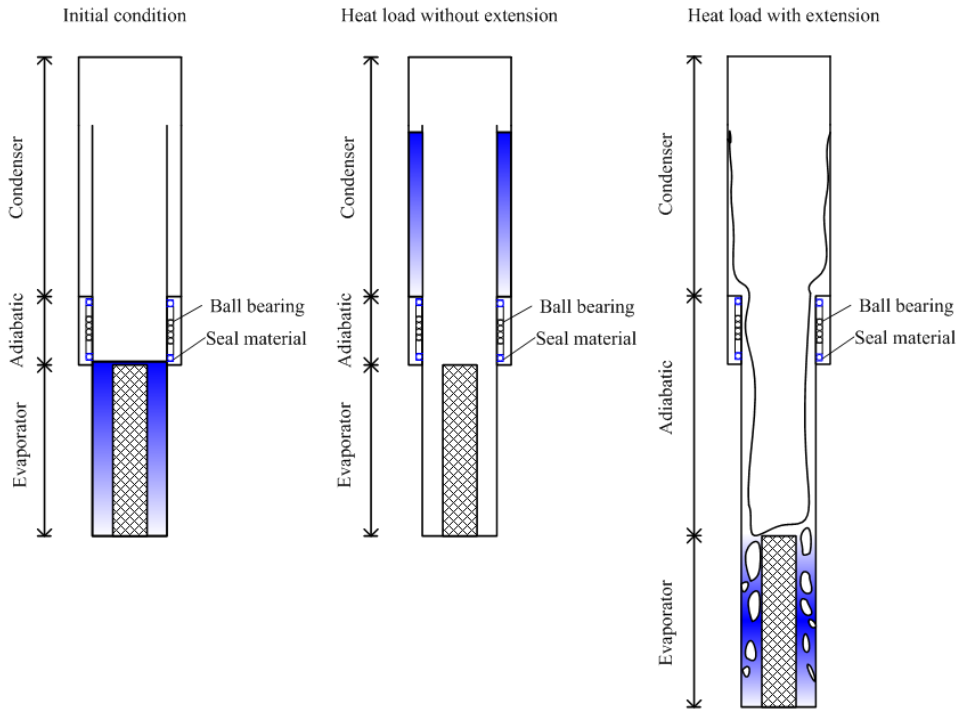

(b) Behavior of the working fluid according to the control length

Fig. 2.5 Design of hybrid control rod for experiment

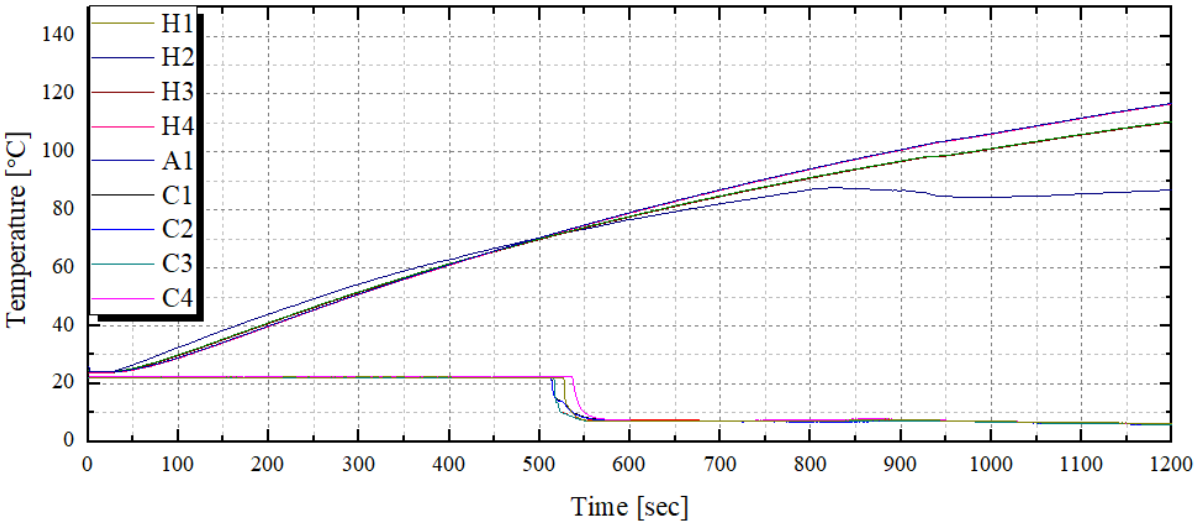

(a) Minimum length

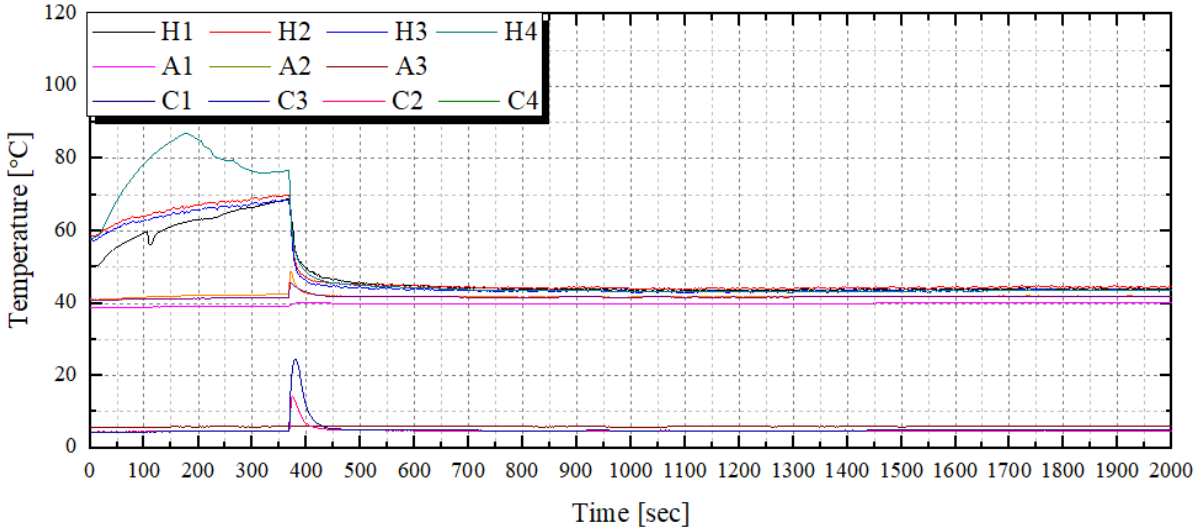

(b) Maximum length

Fig. 2.6 start-up phenomenon of the hybrid control rod at 30 W

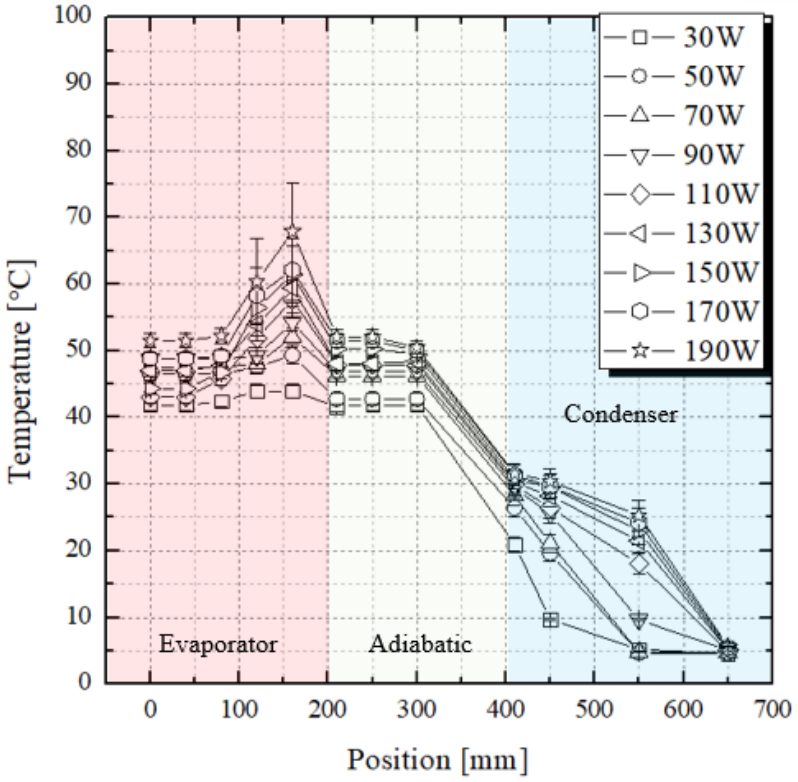

(a) $\Delta L = 150mm$

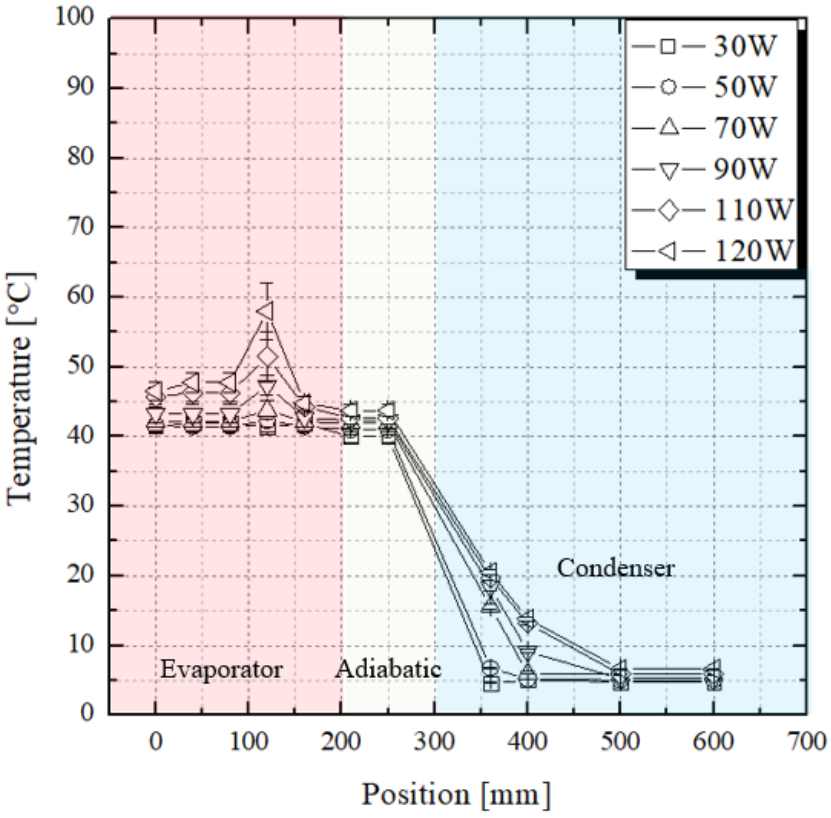

(b) $\Delta L = 100mm$

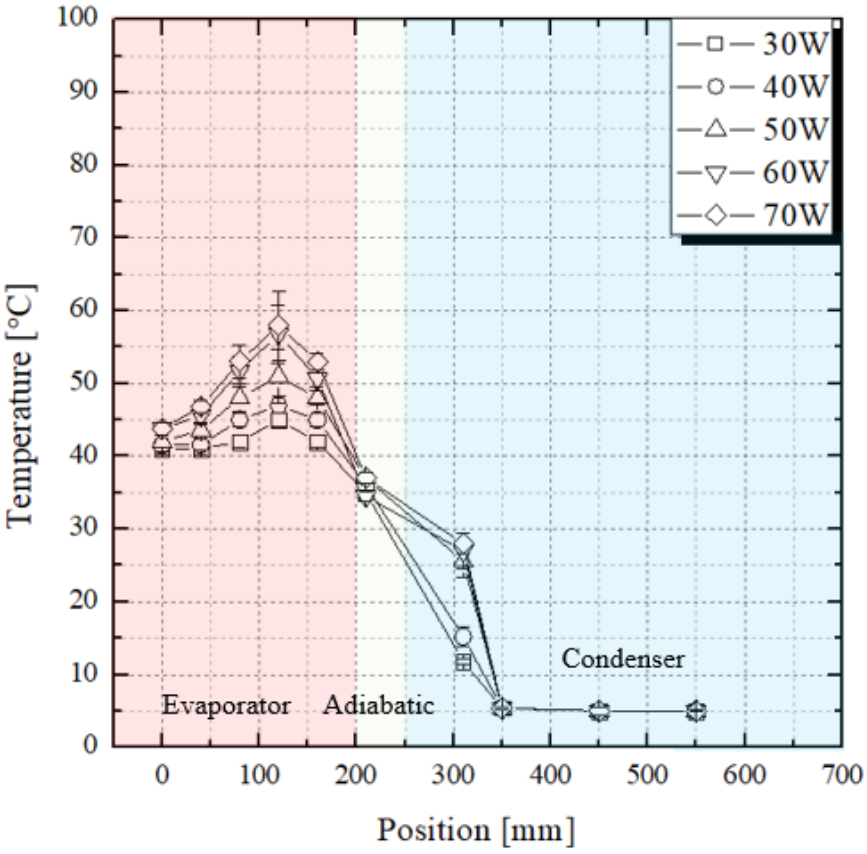

(c) $\Delta L = 50mm$

Fig. 2.7 Temperature distribution of the hybrid control rod

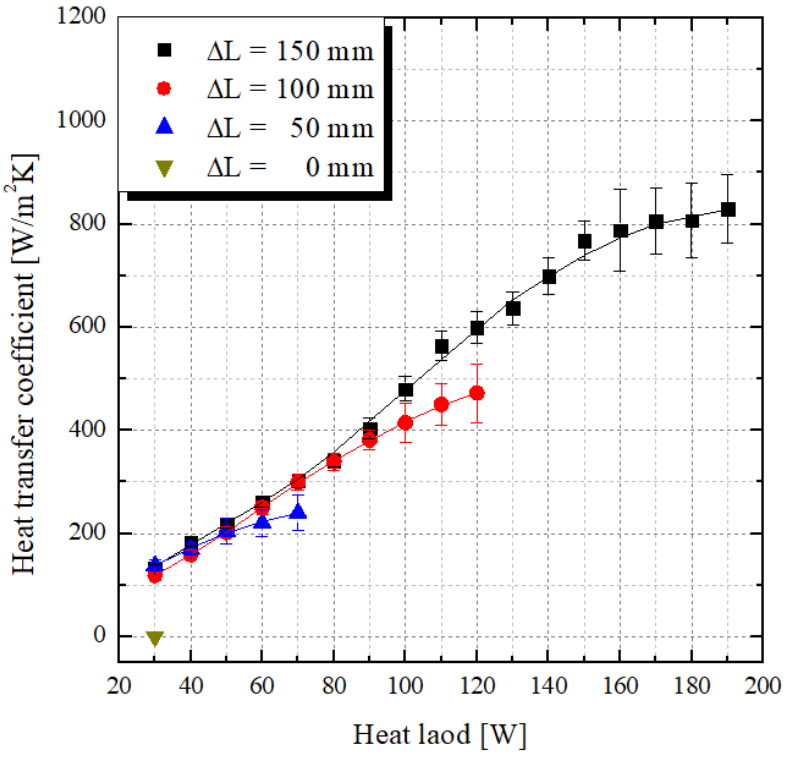

(a) Heat transfer coefficient of hybrid control rod

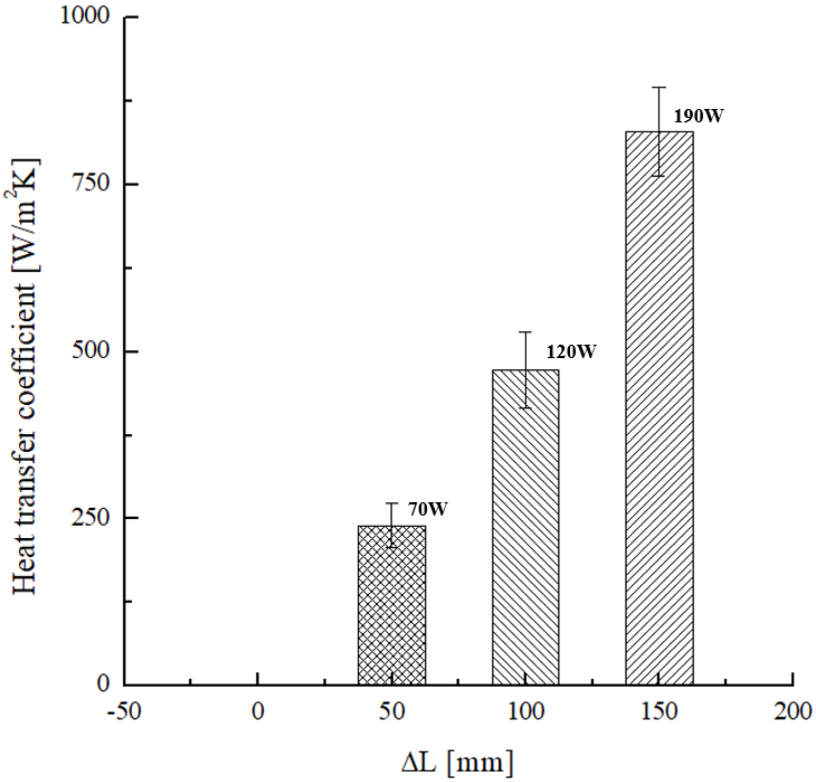

(b) Maximum heat transfer coefficient according to the change of the length

Fig. 2.8 Heat transfer coefficient of hybrid control rod

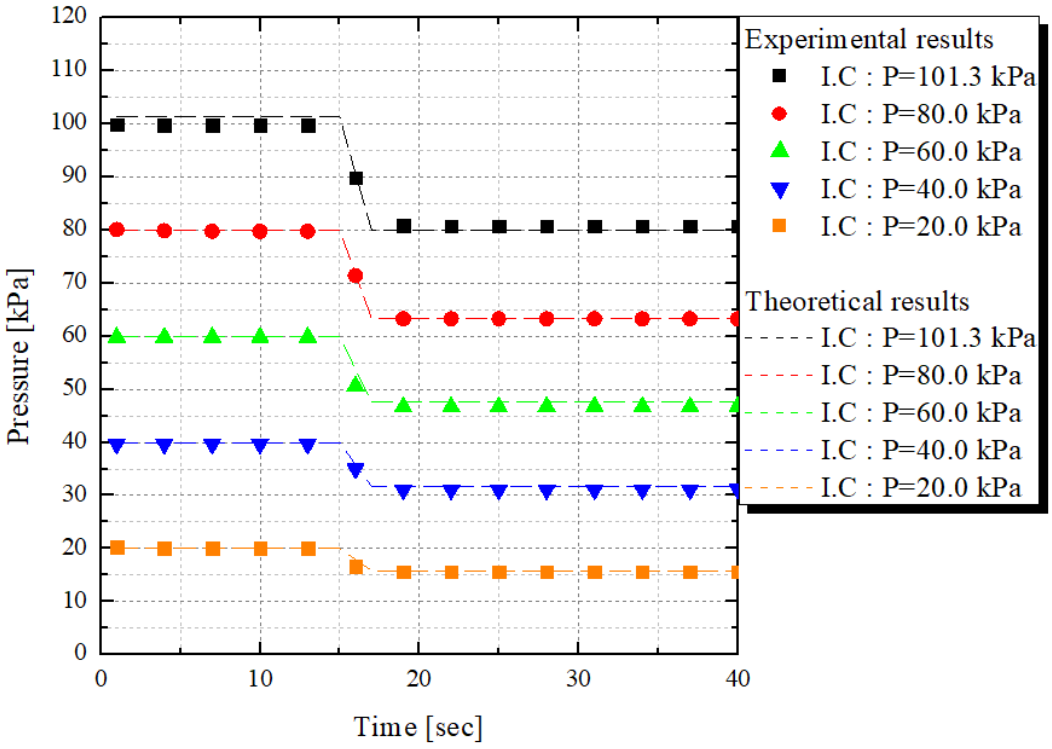

Fig.2.9 Results of the pressure change of the hybrid control rod according to the control length

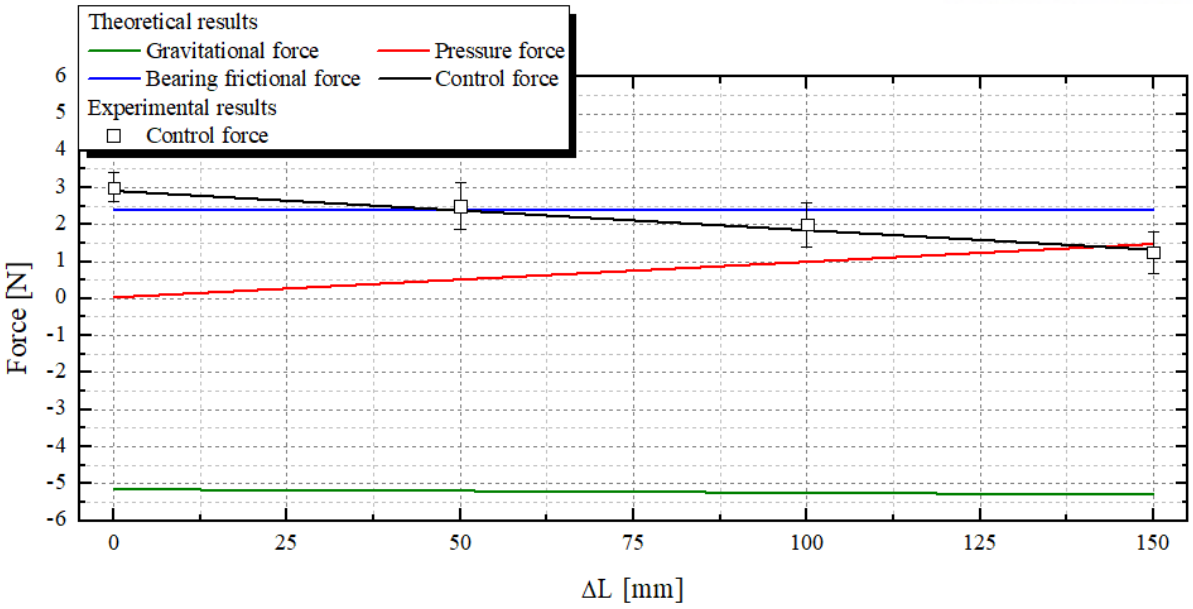

(a) Fill ratio = 0%, P=101.3 kPa

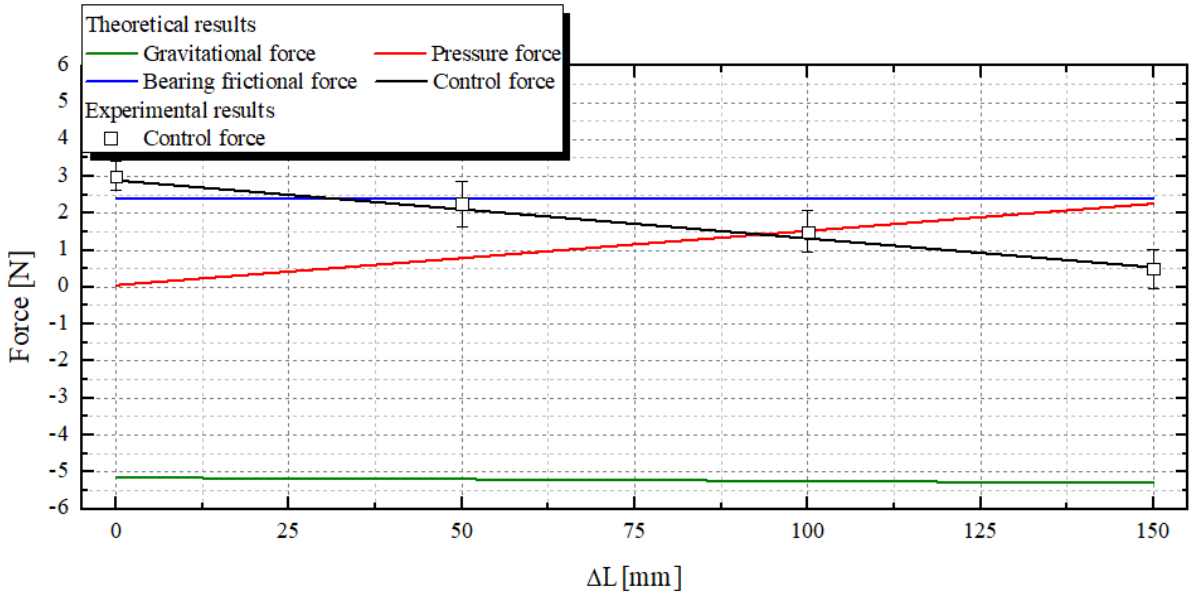

(b) Fill ratio = 100%, P=101.3 kPa

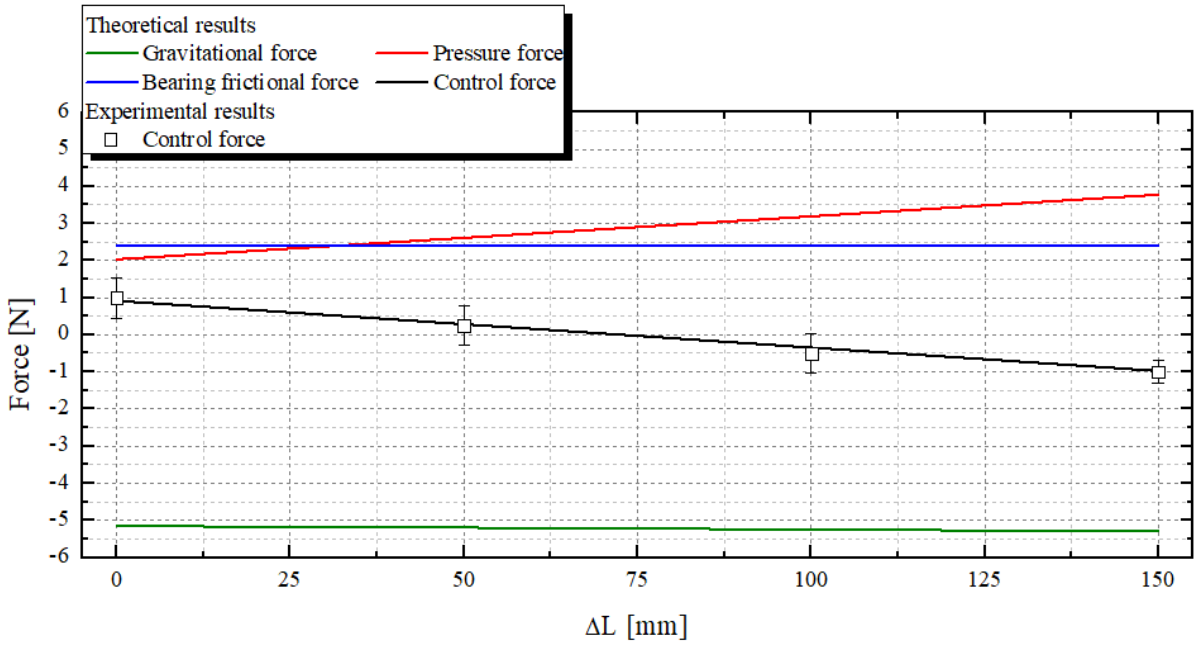

(c) Fill ratio = 100%, P=80.0 kPa

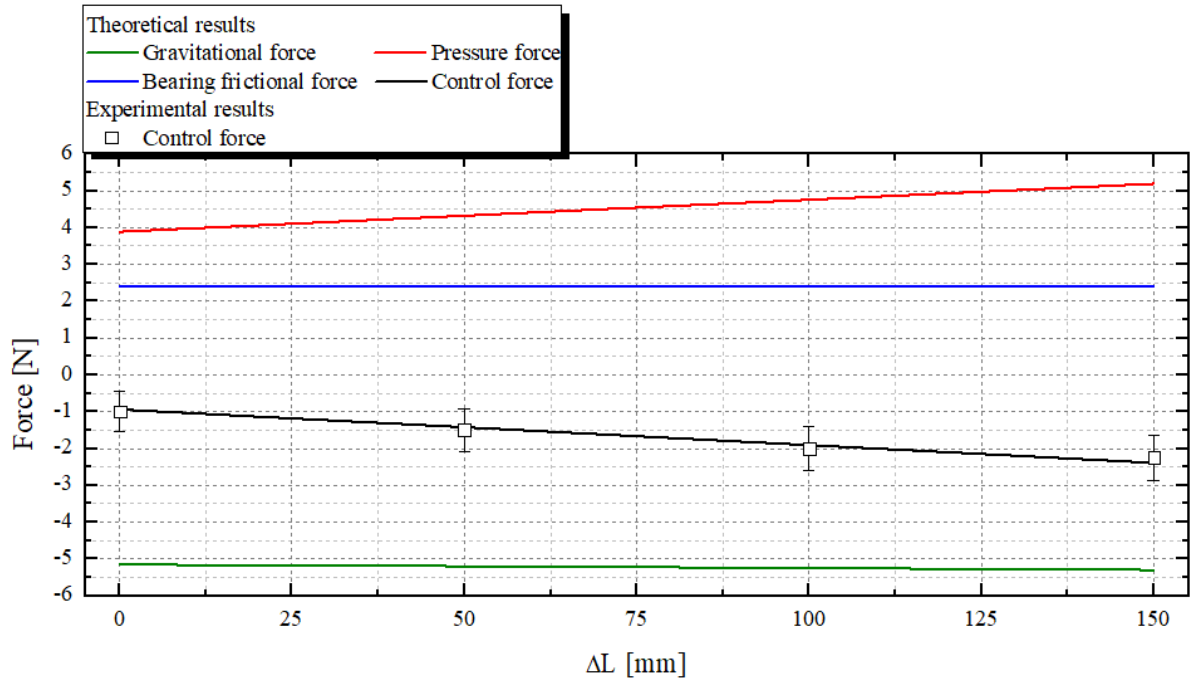

(d) Fill ratio = 100%, P=60 kPa

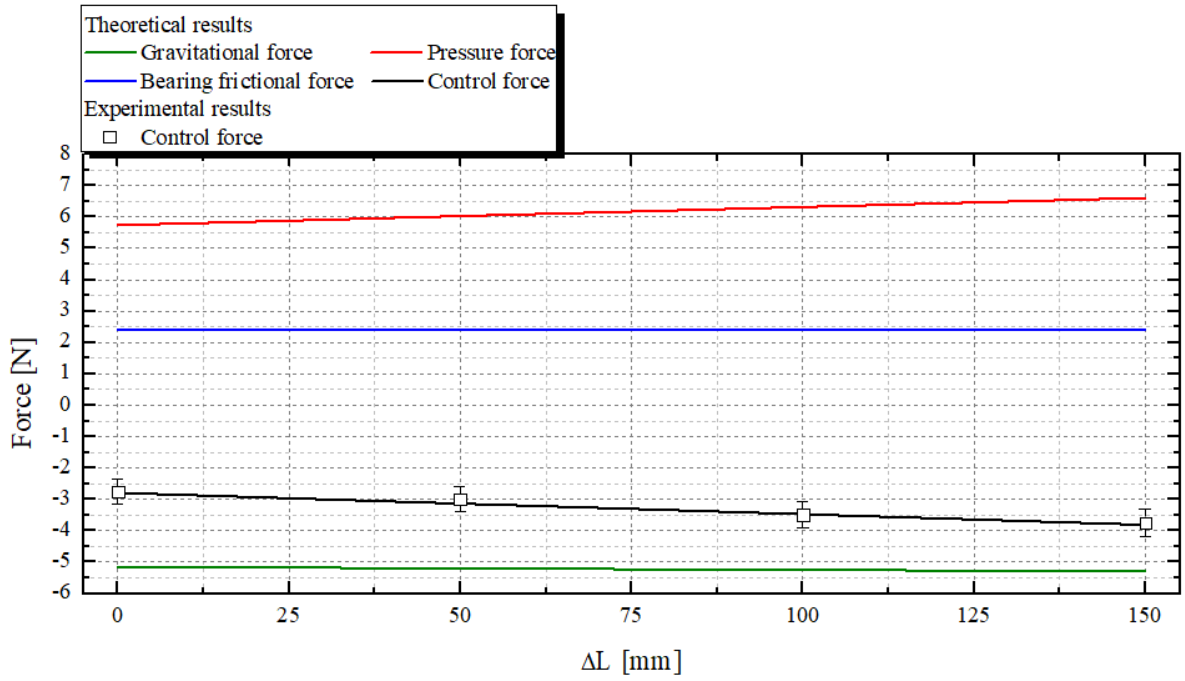

(e) Fill ratio = 100%, P=40.0 kPa

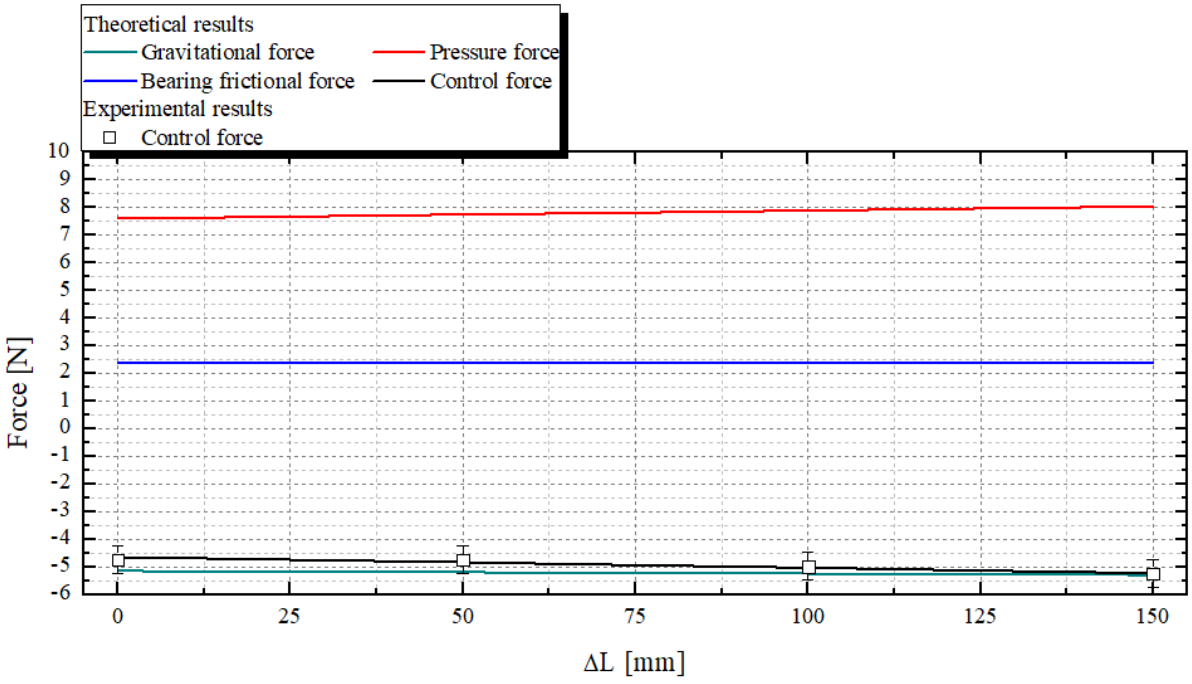

(f) Fill ratio = 100%, P=20 kPa

Fig. 2.10 Theoretical results of the driving forces and the force of the tension gauge according to the change of the length

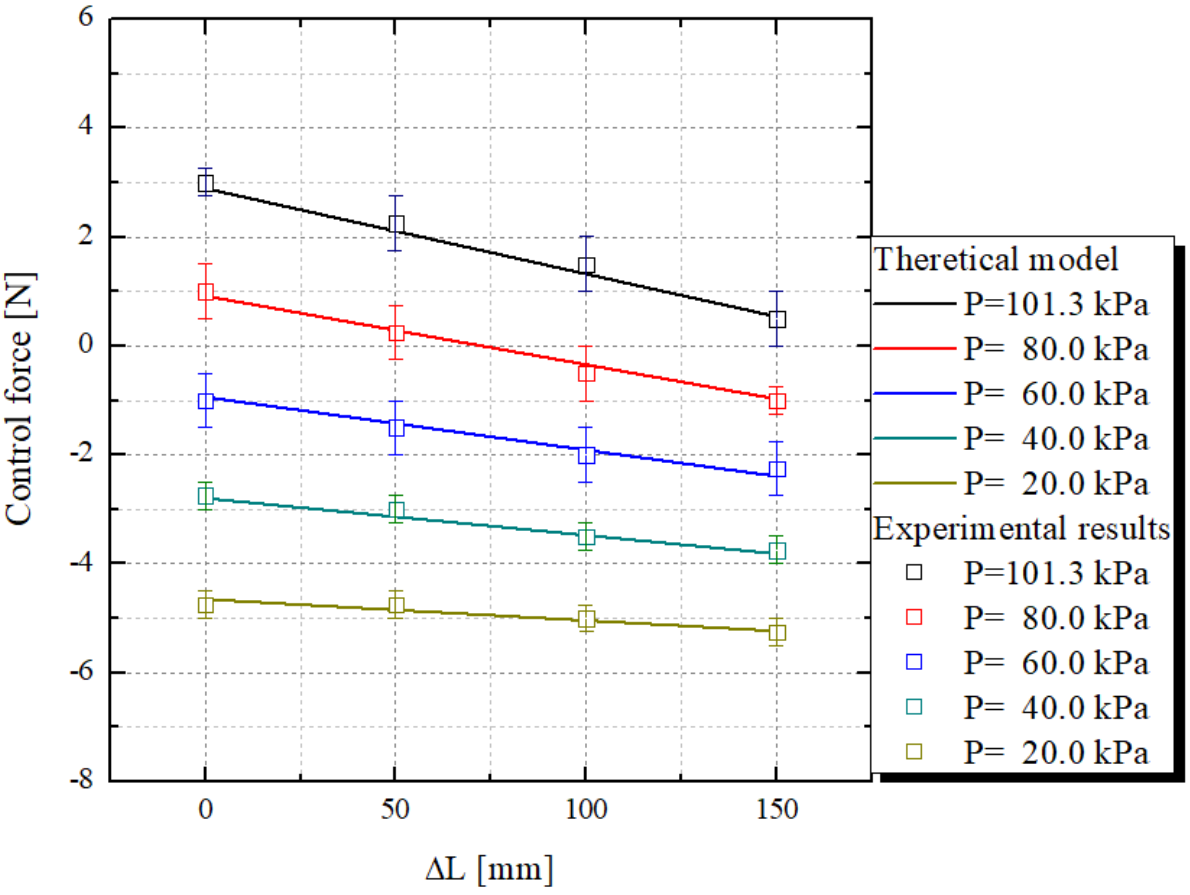

Fig. 2.11 The validation of the theoretical model with the experimental results

Chapter 3. Design and modeling of the hydraulic control rod drive mechanism (CRDM)

3.1 Introduction

The hydraulic control system is currently being studied for controlling the position and force in various fields, including the automobile, mechanical machine, and nuclear power plants. However, it is difficult to predict a high-precise model due to the non-linear and fluctuated motion. In nuclear application, the hydraulic system is used for enhancing the passivity of CRDMs, which has an advantages such as 1) elimination of the penetration hole on the upper plenum of the pressurized vessel, 2) short length of the control rod assemblies, 3) compact and integrated vessel design, and 4) elimination of the rod ejection accident. There are previous researches for developing the hydraulic CRDM with water as a working fluid. Initially, the application of hydraulic CRDM with water was proposed to the nuclear heating plant in Germany [3.1]. This system was designed as bottom mounted CRDM for controlling the boiling water reactor. As an initial design of hydraulic CRDM, the design specification and requirement of CRDM were proposed. In addition, the experiment was conducted to validate the theoretical model under the low temperature condition. In Tsinghua University (1993), the conceptual design of 5 MW nuclear heating reactor (NHR-5) with hydraulic CRDM was described, including the theoretical analysis based on the driving forces from the pressure, buoyance, and gravity [3.2]. This CRDM also had a bottom mounted geometry, which had a complex flow control system. These two concepts had a blade type control element and hydraulic units inside the reactor vessel for controlling the reactivity, therefore, the problems of the fuel compactness and complexity of core design are included. To decrease the control space of hydraulic CRDM, following designs were modified using the top mounted geometry, therefore, modified designs had a high core density and flexibility of the control space. CAREM reactor had a twenty-five control rod drives, operated by the hydraulic driving force [3.3-3.5]. During normal operation condition, hydraulic units are kept in the upper plenum. This device performed the reactor shutdown process in the case of accidents. With shutdown signals, the rod dropped by downward forces when the mass flow rate decreased. In case of SBO accident, the failures of the valve and pump are predicted, and the mass flow rate of the hydraulic circuit is interrupted. Therefore, in this case, the fast shutdown system is operated, passively. Similarly, in the IRIS reactor, the hydraulically driven control rod drive concept has been studying and developing, to apply in innovative BWRs and PWRs [3.6]. To analyze the hydraulic system, the flow control mechanism and geometrical effect of hydraulic drive units were separately explained and modeled. Recently, the design of the NHR-200 is currently being developed based on the design of the NHR-5 [3.7-3.9]. In the modified geometry of hydraulic CRDM (NHR-200), the enhancement to easy fabrication, to get the wide operational range, and to have a compact geometry was achieved. Fig. 3.1 shows the flow of CRDM development focusing on the hydraulic CRDMs with

flow control system.

In this chapter, the hydraulic CRDM with hybrid control rod were analyzed using developed theoretical model based on the force equilibrium equation. In previous researches, the effects of the hybrid control rod assemblies were not considered, therefore, the modeling of hybrid control rod was needed to predict the behavior of hydraulic CRDM in PINCs. The design and modeling of hybrid control rod were explained in Chapter 2. Based on theoretical model of hybrid control rod, integrated model, including the hybrid control rod and hydraulic CRDM was proposed and validated. Moreover, a novel hydraulic CRDM for enhancing control method was designed and tested. There are two designs of hydraulic CRDM: 1) conventional hydraulic CRDM (CRDM-C) based on the IRIS reactor, and 2) a new geometry of hydraulic CRDM (CRDM-P). The test section was designed based on a 4-finger hydraulic CRDM in APR1400. To verify the characteristics of the hydraulic CRDM, the test of elevation control was conducted according to a change of the weight and geometry. And then, the rod-drop test was performed to ascertain the effects of friction to identify the control rod parameter for safe shutdown.

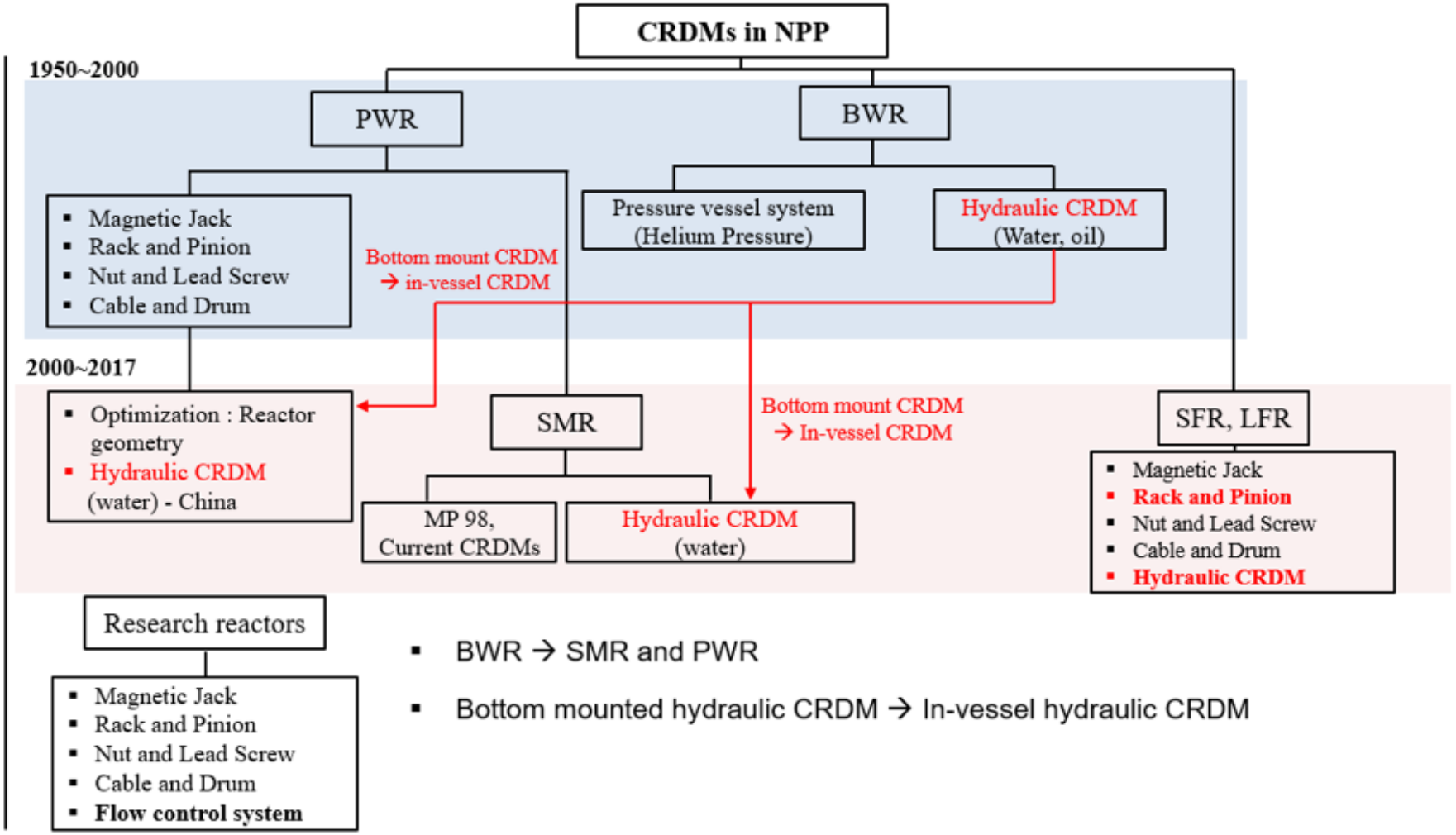

Fig. 3.1 Flow of CRDM development focusing on the hydraulic CRDMs

3.2 Driving mechanism and its theoretical models

In PINCs, the hybrid control rod and hydraulic CRDM are combined and connected during the operation. In this part, the driving mechanism and modeling of hydraulic CRDM are presented.

3.2.1 Design of the hydraulic CRDM with flow control system

The hydraulic drive units with flow control methods are proposed and tested. In previous researches, there are five different flow control systems: NHR-5, IRIS, NHR-200, SBWR, and NHR-200 (modified) [3.1, 3.6-3.8, 3.10]. The NHR systems had patterned holes with a grooved cylinder. Therefore, the NHR-5 had the various flow paths including the inlet flow, outlet flows, bypass flow, and flow passing through the holes. Initially, the flow behaviors were not analyzed owing to the complex flow paths. Therefore, the force equilibrium at hydraulic cylinder was modeled and analyzed. During the elevation control of hydraulic CRDMs, the inlet flow was controlled using the control valve, orifice, and bypass line. In hydraulic CRDM for IRIS reactor, the three valves were considered to move the hydraulic cylinder. The hold valve had a fixed cross-sectional area, therefore, the holding flow rate (named steady flow rate) was determined based on the condition of hold valve. During the elevation control, the withdrawal/insertion electro-valves were opened to increase the inlet mass flow rate. Based on the momentum equation, the modeling of the hydraulic circuit was designed, focusing on the function of the frictional loss inside hydraulic cylinder. hydraulic CRDMs of both NHR-5 and IRIS considered the driving forces such as the gravitational force, pressure differential force, and buoyancy force. The steady flow rates and the flow behavior of hydraulic cylinder were defined as the function of the inlet flow rate and flow resistance coefficient. In NHR-200 and SBWR, the researches on the flow instability and high accuracy control method were conducted. The flow control system was similar to the previous researches. To obtain the pressure loss of hydraulic cylinder, the flow resistances of flow path were calculated and validated at the fixed steady flow condition. Modified NHR-200 had the integrated valve and modified hydraulic cylinder, which enhance the structure integrity during the shutdown process. Fig. 3.2 shows the hydraulically driven rod control unit with flow control system. In PINCs, the flow control system was designed based on the integrated valve and bypass line for controlling the inlet mass flow rate of hydraulic CRDM (Fig. 3.2(f)). The closed loop has been modeled to calculate the behaviors of the mass flow, pressure, position of the driving unit. The continuity equation and momentum equation were driven by using the geometry of the flow control loop. In case of the withdrawal process, the pumping power increased, therefore, increased pressure loss of hydraulic cylinder is induced by increased pressure from the pump. The pressure drop is continuously saturated to the equilibrium state, as show in Fig. 3.3 (b).

$$\frac{dm}{dt} = \sum \dot{m}_{in} - \sum \dot{m}_{out} \qquad \text{(Continuity Equation)} \qquad (3.1)$$

$$L\frac{\partial (G_m)}{\partial t} = \Delta P_{pump} - \Delta P_f + \Delta P_b \qquad \text{(Momentum Equation)} \qquad (3.2)$$

3.2.2 Theoretical model for conventional hydraulic CRDMs

The driving mechanism of the hydraulic CRDM is highly related to the flow driven forces at the moving cylinder. The characteristics of the hydraulic forces are defined as the stepped/pattered geometry inside cylinder. In the previous studies, there are several approaches for analyzing the hydraulic CRDM. In SBWR, the design of the hydraulic cylinder is just defined as an equilibrium among the weigh and flow force according to the mass flow rate. The hydraulic system for NHR-5 was defined as a balance between pressure difference with multi-flow channel and weigh of the CRDM. In addition, to confirm the transient behaviors of the hydraulic CRDM, the kinematic equation of the step cylinder is driven by using the pressure, weight and acceleration. In IRIS reactor, the flow control methods and transient dynamic system modeling are conducted. The 1-D mechanical force balance in the hydraulic cylinder is proposed and validated. But, CAREM reactor is not consider the force balance equation and transient behaviors of the hydraulic system. In this reactor, the hydraulic CRDM is used for fast shutdown system, therefore, this system cannot use the step control during the operation condition (just use for the shutdown full strength).

In the analysis of the steady state flow condition, the force equilibrium equation is used for determining the state of the hydraulic CRDM, shown in Fig. 3.3. Therefore, the force equilibrium equation is driven by

$$F_b + P_{in}(t)A_c + F_{fr} = P_{out}A_c + m_c g \qquad (3.3)$$

In this equation, the control parameter is the pressure, therefore, the pressure difference is rearranged by

$$\Delta P = \frac{m_c g}{A_c}\left(1 - \frac{\rho_{water}}{\rho_c}\right) + f(fr) \qquad (3.4)$$

In this equation, the pressure difference is highly related to the frictional force inside cylinder. The frictional loss is assumed to be a simple major head loss.

$$f(fr) = \frac{\rho g}{A} h_{major} \tag{3.5}$$

By considering Eq. 3.4 and 3.5, the steady flow rate is defined as

$$\dot{m} = \frac{\Delta P + {m_c}/{A_c}\,({\rho_{water}}/{\rho_c} - 1)}{\frac{32\nu l}{D^2 A_c^2}} \tag{3.6}$$

Similarly, the transient kinematic equation is expressed by,

$$m\frac{d^2X}{dt^2} = F_b + F_{fr} + P_{in}(t)A_c - P_{out}A_c - m_c g \tag{3.7}$$

Table. 3.1 shows a summary of theoretical model about transient behaviors in hydraulic CRDM. Each concept of the hydraulic CRDM has different parameters to analyze the behaviors of the hydraulic cylinder. Depending on the geometrical and parametrical importance of hydraulic CRDMs, the terms of the viscosity of working fluid and spring forces were considered in the previous researches.

$$m\frac{d^2X}{dt^2} = F_b + F_{fr} + P_{in}(t)A_c - P_{out}A_c - m_c g + (F_{viscous}) + (F_{Spring}) \tag{3.8}$$

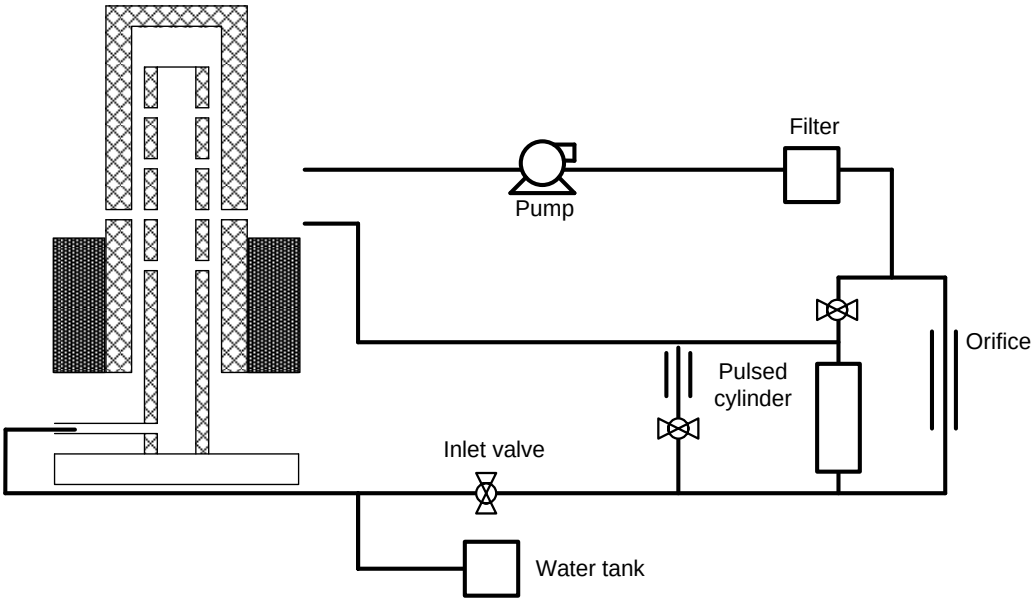

(a) NHR-5

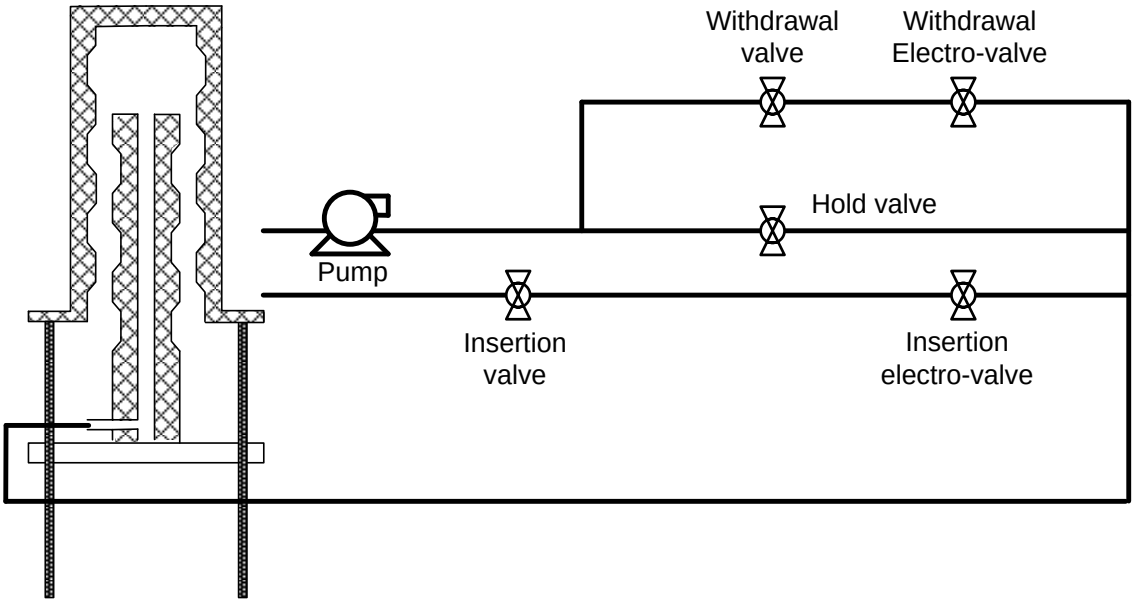

(b) IRIS

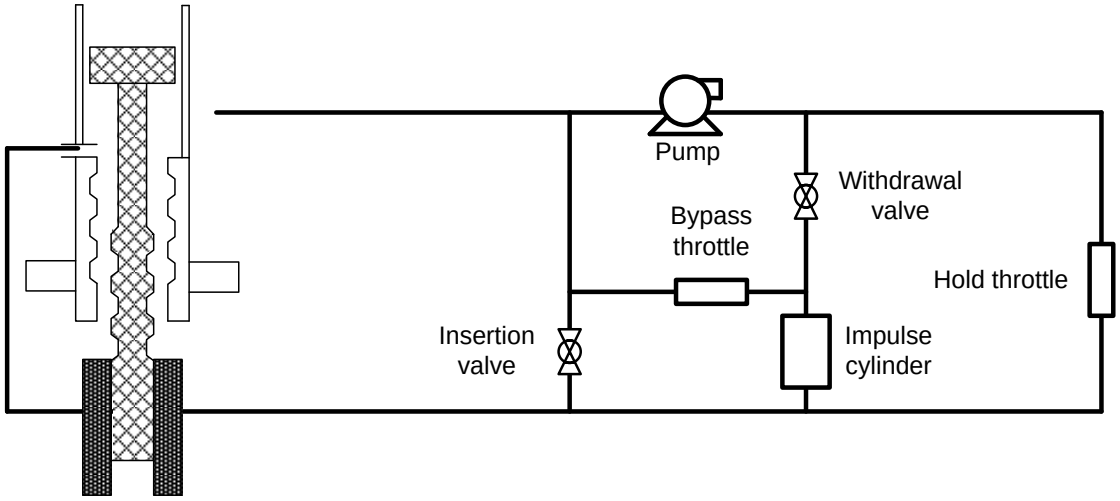

(c) NHR-200

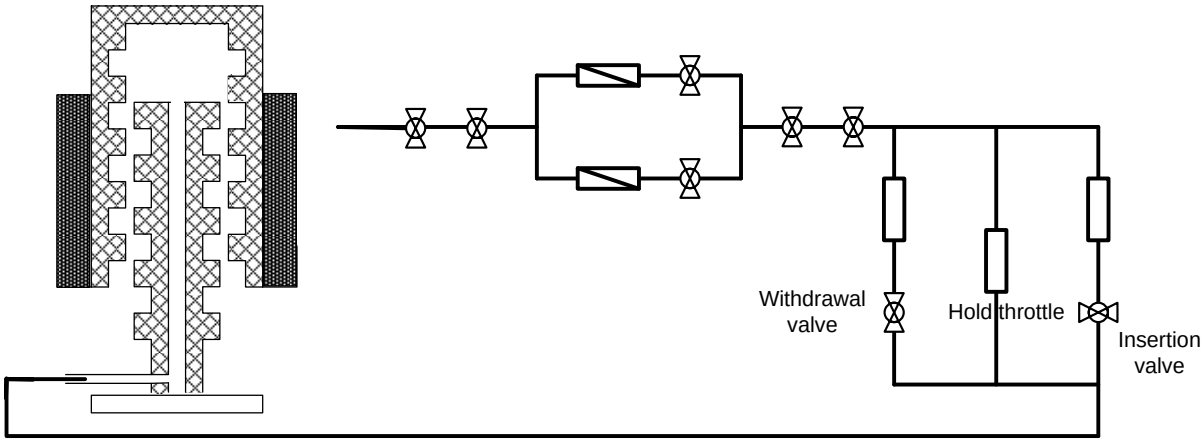

(d) SBWR

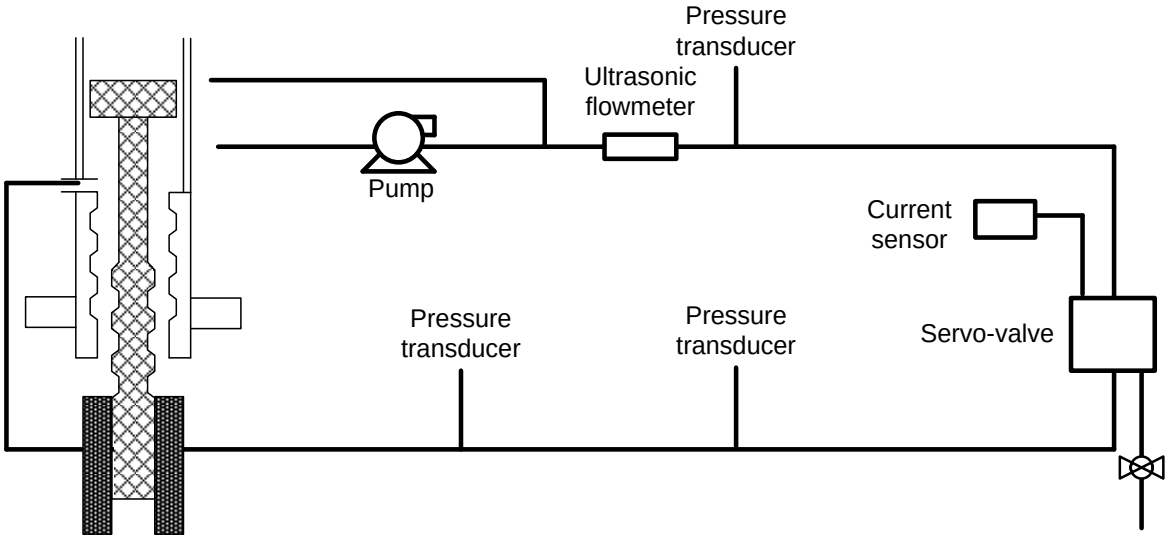

(e) Modified NHR-200 (2017-2018)

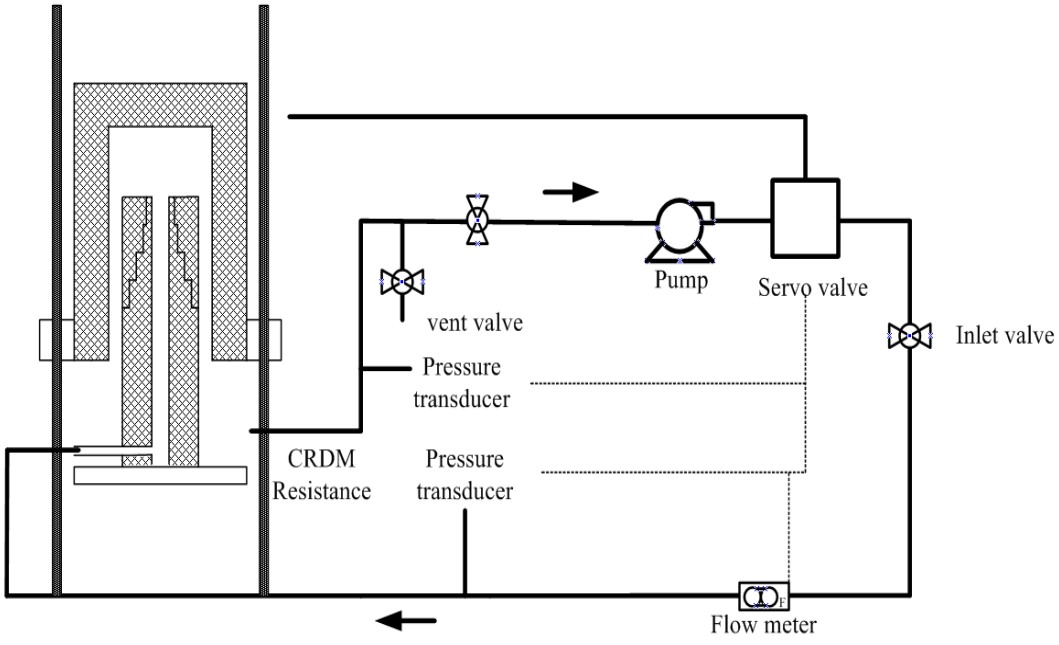

(f) PINCs

Fig. 3.2 Hydraulically driven rod control system with flow control method [3.1, 3.6-3.8, 3.10]

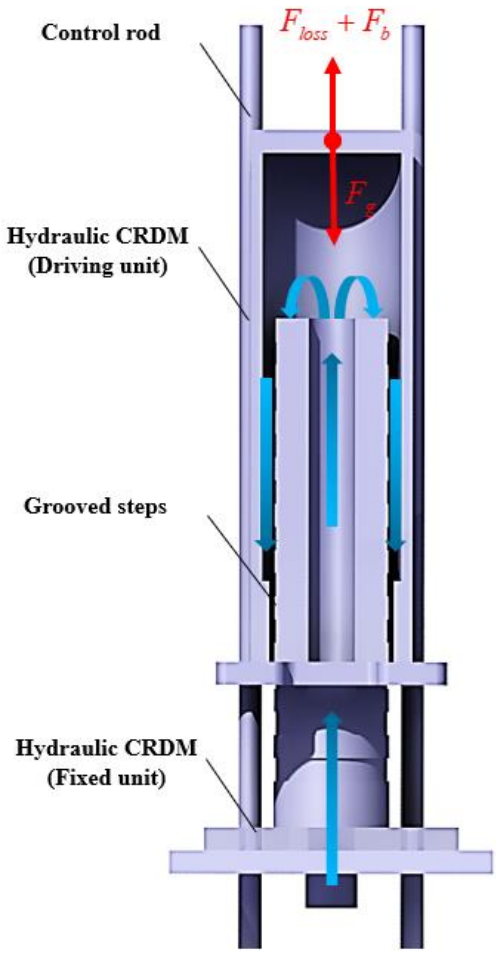

(a) Force balance of the conventional CRDM

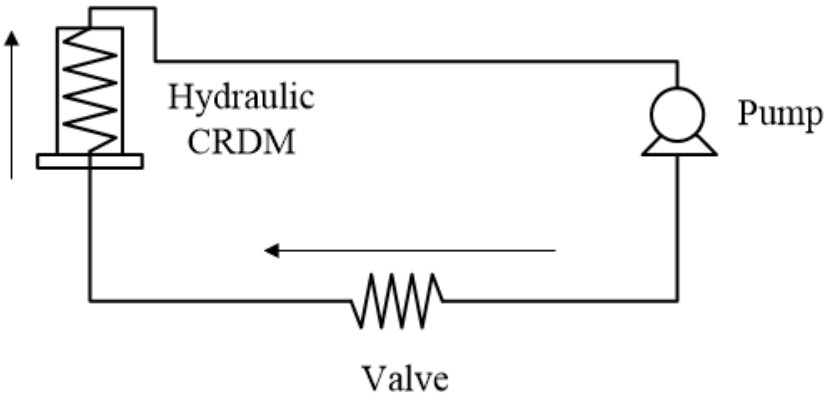

$$\Delta P_{pump} = \Delta P_{Valve} + \Delta P_{CRDM}$$

(b) Simplified flow control mechanism

Fig. 3.3 Schematic diagram of conventional CRDM with flow control mechanism

Table. 3.1 A summary of theoretical model about transient behaviors in hydraulic CRDM [3.1, 3.2 3.6, 3.7, 3.10, 3.11, 3.12]

Researcher	Theoretical model	Operating condition	Remarks
Batheja (1987)	$m\frac{d^2X}{dt^2} = P_{in}A_c - P_{out}A_c - mg$ $A_{B1} = \frac{\pi}{4}(D_{kl}^2 - d_{gt}^2)$ $A_{B2} = \frac{\pi}{4}(D_{kl}^2 - (d_{gt} - 2\cdot\Delta h\cdot tan(\alpha))^2)$ $A_{B3} = \frac{\pi}{4}(D_{kl}^2 - d_{kl}^2)$	Pressure : 25 Bar Temperature : 223 °C Mass flow rate : 1 – 2 kg/s	Test of the elevation control and free drop behaviors
Wang (1993)	$M\frac{d^2x}{dt^2} = P_{in}A_{in} - P_oA_o - m_cg(1-\frac{\rho_w}{\rho_t})$	Pressure : 1.37 Bar Temperature : 186 °C Mass flow rate : 0.388 – 0.90 kg/s	Characteristics of the flow channel and flow hole for elevation change
Bo (2002)	$M\frac{d^2x}{dt^2} = \Delta PA_c - m_cg(1-\frac{\rho_w}{\rho_t})$ $\frac{d\Delta P}{\Delta P} = \frac{1}{\rho_r/\rho - 1}\frac{d\rho}{\rho}$	Pressure : N/A Temperature : 60 °C Mass flow rate : 0.388 – 0.90 kg/s	Define the effect of the delay time for controlling the elevation
Li (2006)	$m_c\frac{d^2x}{dt^2} = \rho g(H_{in} - H_o)A_c - m_cg(1-\frac{\rho_w}{\rho_t})$	Pressure : 2.5 Bar Temperature : 240 °C Mass flow rate : ~0.0016 kg/s	Design modification for optimizing the core design (Top down CRDM)
Ricotti (2003)	$m_{rod}\frac{d^2x}{dt^2} = \Delta P_{rod}A_{thrust} - m_{rod}g - C_{viscous}\frac{dx}{dt} + \frac{\rho_{fluid}}{\rho_{rod}}m_{rod}g$	Pressure : 2.0 Bar Temperature : ~100 °C Mass flow rate : ~0.0016 kg/s	Preliminary test for hydraulic CRDM with flow control system
Liu (2017)	$\frac{dv}{dt} = \frac{(P_{in}A - P_oA - (M_p + M_s)g - M_sg - k(X - X_o) + \varepsilon(P_{in} - P_o)A_f)}{M_p + M_s}$	Pressure : 1.2 Bar Temperature : N/A Mass flow rate : ~1.6 kg/s	Weight effect of the hydraulic CRDM
Qin (2018)	$M\frac{dv}{dt} = P_uA_u - P_DA_D - F_{t1} + G - F_B - F_M + F_S - F_{t2}, 0 < x \le X_1$ $M\frac{dv}{dt} = P_UA_U - P_DA_D - F_{t1} + G - F_B - F_M + F_S - F_{t3}, X_1 < x \le X_2$ $M\frac{dv}{dt} = P_UA_U - P_DA_D - F_{t1} + G - F_B - F_M + F_S - F_{t3} - F_{t4}, X_2 < x \le X_3$	Pressure : 3.5 Bar Temperature : N/A Mass flow rate : ~4.2 kg/s	Application of spring damper for reducing the drop impact

3.3 Experimental Setup and Procedure

Two functions are essential for hydraulic CRDM: 1) Position control (high accuracy step control) and 2) free drop with a drop time of less than 4 s (design requirement) [3.13]. Experiments were performed to verify the characteristics of the step control and free drop of control rod by using a scale facility. The test facility is designed with a 1:12 length scaled 4-finger control rod assembly under room temperature [3.14]. This facility is built with reduced length and steps, and it uses water as the working fluid. The test facility includes cylinders of different shapes (conventional geometry (CRDM-C), new type geometry for PINCs (CRDM-P)), a circulating pump with a control valve, a pressure gauge, thermocouples, a flow meter, and a water tank as shown in Fig. 3.4. Two types of CRDMs are investigated to determine the effect of the position tracking model for PINCs. Table 3.2 shows the design parameters of the reference reactor and the test facility. Both CRDM-C and CRDM-P have the same step size and pitch of 9 mm and 20 mm, respectively.

3.3.1 Step Control test

The control rods control the reactor power; therefore, the insertion and withdrawal are the crucial tests for the development of PINCs. To confirm the capability of the hydraulic CRDM, both CRDM-C and CRDM-P were tested for comparative evaluation. Table 3.3 shows the test matrix of the step control including the test conditions. The test steps of CRDM-C and CRDM-P are 1–7 and 1–9, respectively. The main parameters are the control flow and weight of the CRDM, and pressure difference between the cylinder and outside pool. In the test for step control, the main parameters such as the inlet mass flow rate, CRDM position, and the pressures at the inlet flow and pool were measured. The inlet mass flow rate was controlled by using the control valve. Weight blocks were used for changing the weight of the CRDMs without geometrical modification. Each step was maintained for 5 min to confirm the fluctuations of the flow and position.

3.3.2 Rod-drop test

The rod-drop time is an important requirement of the CRDMs to ensure safe shutdown of the reactor so that the risk of accidents is mitigated. In the case of the reference reactor (APR1400), the rod-drop time is 4 s for 90% insertion into the reactor core. During the rod-drop test, the flow resistances of the control rod drive mechanism and the control rod inside the guide tube are the crucial parameters. These parameters are highly related to the CRDM weight and geometry of the flow path; therefore, in the test, different weight blocks on the top of the hydraulic CRDM and the two different geometries of the

hydraulic CRDM were considered. The drop height was 600 mm, and the tests were performed five times for each weight. During the drop test, a high-speed camera was used to measure the position of the CRDM.

Table. 3.2 The design parameters of the experimental test facility

	Reference reactor	Test facility		Ratio
		CRDM-C	CRDM-P	
CRDM assembly				
Evaporator, Core (mm)	3,810	320	320	1/11.9
Condenser, water pool (mm)	7000	400	400	1/17.5
Hydraulic CRDM (control space) (mm)	8,000 (for PINCs)	1000	1000	1/8
Cross sectional area of assembly (mm^2)	192.8×192.8	200×200	200×200	1/0.96
Step pitch (mm)	19.05	20	20	1/0.95
Steps	200	7	9	-
Hybrid control rod (ea)	4	4	4	1/1
Hybrid control rod assemblies				
Outer diameter (mm)	20.73	19.05	19.05	1/1.09
Inner diameter (mm)	19.93	18.16	18.16	1/1.10
movable part (mm)	12,000	1,400	1,400	1/12

Table. 3.3 Test condition of the step control

Parameters	Values	unit
Mass flow rate	4.2 – 24.5	kg/min
Weight of CRDM	15 – 50	kg
Steps	1-7 (CRMD-C)/1 – 9 (CRDM-P)	-
Pressure	0 – 0.5	Bar
Temperature	25	℃

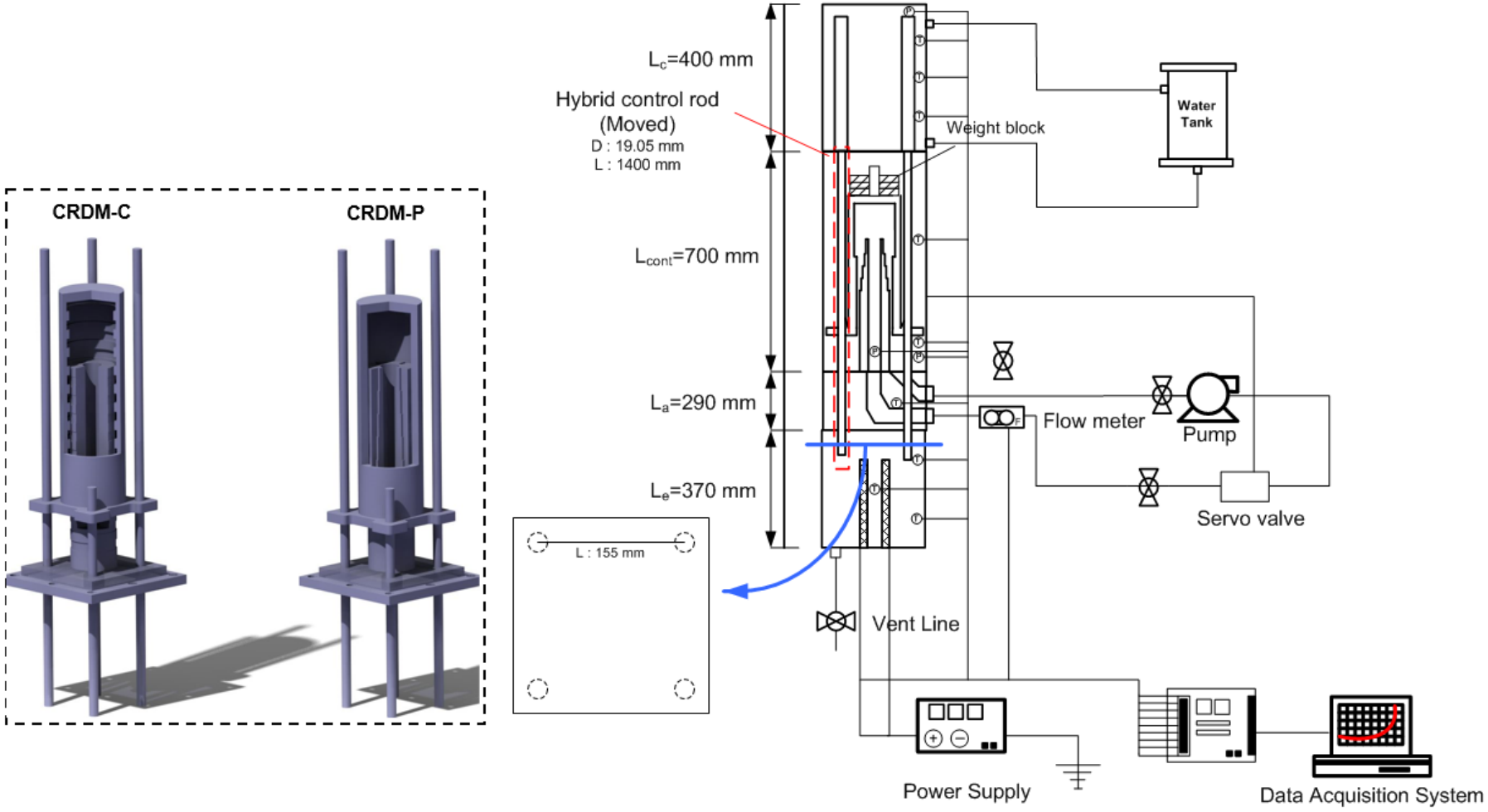

Fig. 3.4 The facility for the hydraulic CRDM test

3.4 Experimental results

To confirm the enhanced feature of the hydraulic CRDM, a comparative study between the conventional hydraulic CRDM (CRDM-C) and the new type of hydraulic CRDM (CRDM-P) was conducted experimentally.

3.4.1 Conventional hydraulic CRDM (CRDM-C)

3.4.1.1 Step control process

In the first process of the step control, at the inlet region, the mass flow rate and pressure difference increased, however, the elevation of CRDM-C was fixed due to insufficient force from the pressure difference. In case of the start-up, the lift force induced by the pressure differential was lower than the required force to move the elevation owing to the insufficient mass flow rate. The test results as the dynamic behavior of the mass flow rate and the pressure difference between inlet and outlet flows are shown in Fig. 3.5. The inlet flow must be larger than the minimum steady state flow rate in the equilibrium state. From the 24 sec to 130 sec, the pressure difference between the cylinder and outlet flow is dramatically increased because of the narrow gap inside cylinder. and the control rod was not moved. The inlet flow rate is slightly increased, remaining the range from minimum and maximum steady flow rate, the hydraulic cylinder will remain in its step with decreased pressure, as shown in Fig. 3.5 (the range from 130 sec to 200 sec). Once the inlet flow rate is larger than maximum steady state flow rate, the lift force pushes the hydraulic cylinder resulting on a decreased pressure drop owing to the increased cross-sectional area of flow path (the range from 200 sec to 300 sec).

In the CRDM-C, the steady flow rate is crucial factor to determine the performance of the pump and other flow control systems. Fig. 3.6 (a) shows the steady state flow rate of CRDM-C with calculated minimum and maximum flow rate with a fixed weight of CRDM-C. Based on using the Eq. 3.6, the steady state flow had an acceptable range from the minimum and maximum flow rate with a given weight of 30 kg. In the overall steps (1-7 steps), the steady state flow maintained the predicted flow rate between 11.43 to 14.3 kg/min. During the step-up process (withdrawal step), previous research explained the delay time owing to the diversion to the hydraulic cylinder [3.11]. The mass flow rate inside the cylinder was released to the stepped holes at the upper head. However, the hydraulic unit does not divert the flow path in following geometry. Therefore, reduced mass flow rate of the inlet region was not observed during the step-up step. The major reason of the decay time is the change of the cross-sectional area of the flow channel. With an increase of the pump head, reduced pressure was observed due to the narrow gap between bottom structure and cylinder. In this state, the lift force increases to values larger than the counterforces, including the gravitational force and frictional force. Therefore,

the hydraulic cylinder moves to the next equilibrium position. These results showed that the design of the conventional hydraulic system is sensible to pressure during the step-up process, shown in Fig. 3.6 (b). After the valve open, the fluctuated pressure was observed due to the repetitive stagnation inside cylinder. The cylinder had a patterned geometry, therefore, the step-down process had a complex pressure and flow behavior. The pressure and flow characteristics of the hydraulic CRDM during the single step-down is shown in Fig. 3.6 (c). The response time was faster than the step-up process, however, the speed of the cylinder was slower than those of the step-up process.

3.4.1.2 Drop test

Due to the limitation of the test facility, the drop tests with the range from 15 kg to 50kg were conducted. The test results of the rod drop time according to the weight of the hydraulic CRDM are shown in Fig. 3.7. The experimental test was performed at the maximum height (600 mm) of the hydraulic CRDM in the test facility. The test results had a range from the 2.1 sec to 8.4 sec, however, the drop time of the hydraulic CRDM with control rods was relatively delayed in comparison to safety requirement of the reference reactor (APR1400). The major reason of this delayed results was the properties of the water and weight of the hydraulic CRDM. To confirm the design requirement, the sensitivity analysis of the drop time with a different temperature and weight will be explained in the chapter 4.

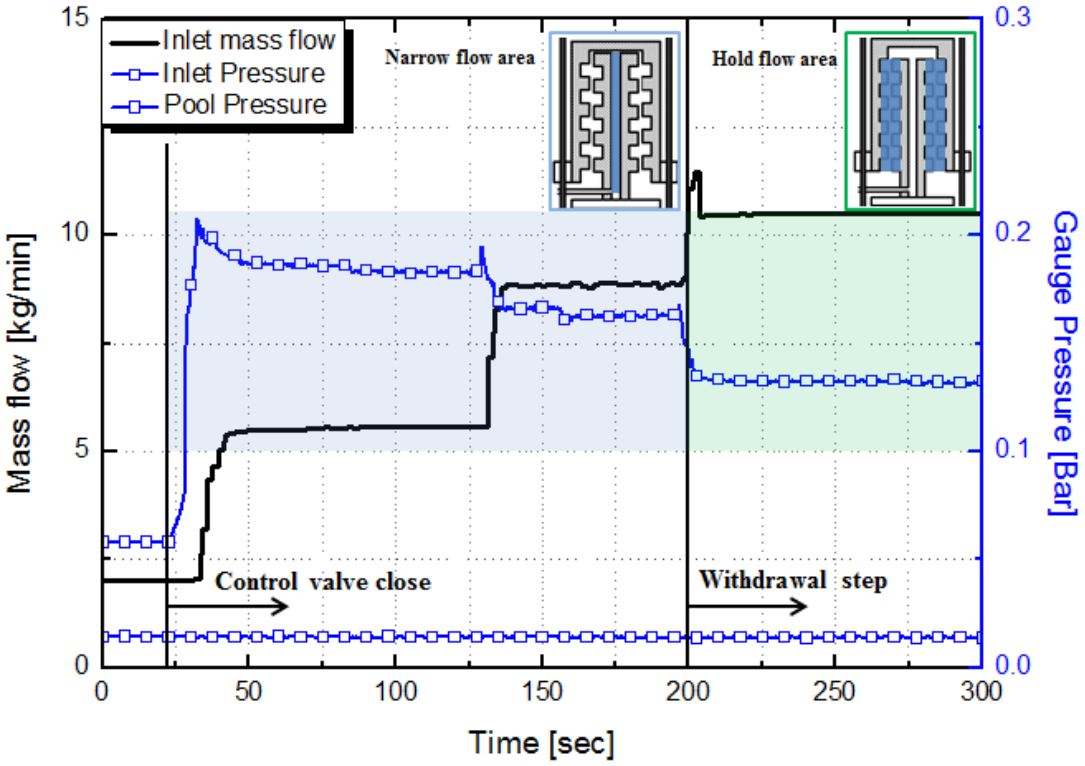

Fig. 3.5. The test results of the mass flow rate and the pressure difference between inlet and outlet flows

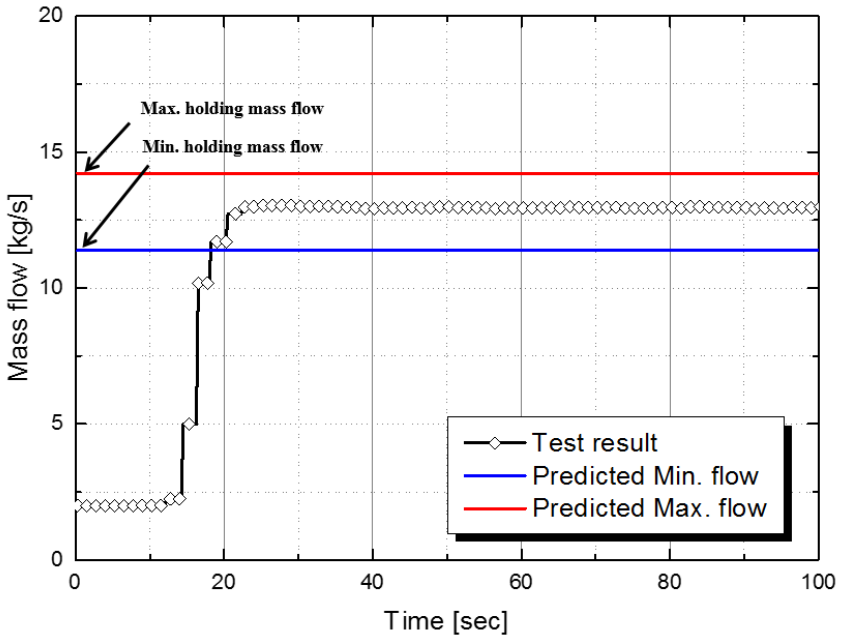

(a) Steady state flow of hydraulic CRDM with predicted results

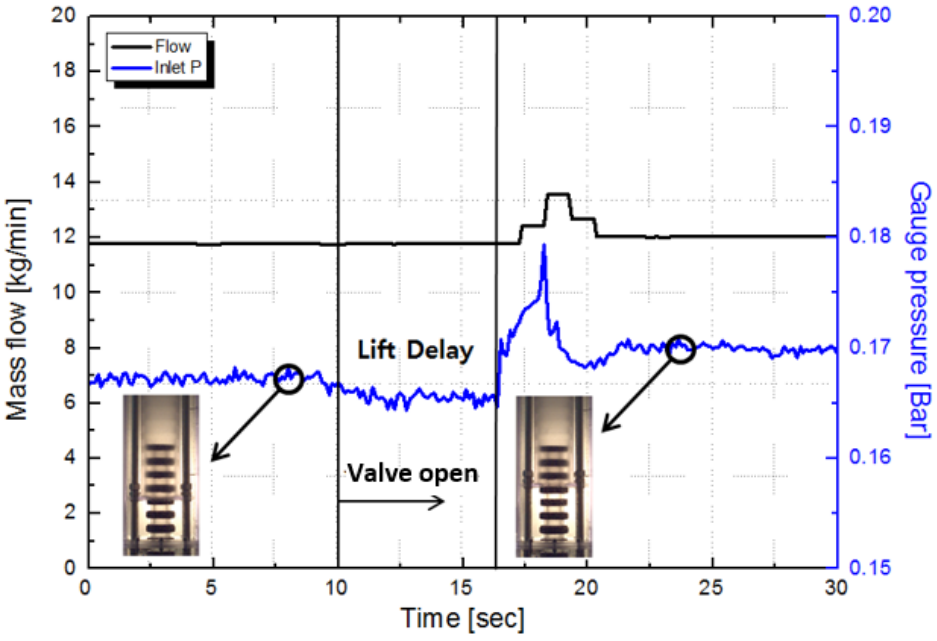

(b) Withdrawal step (Step-up)

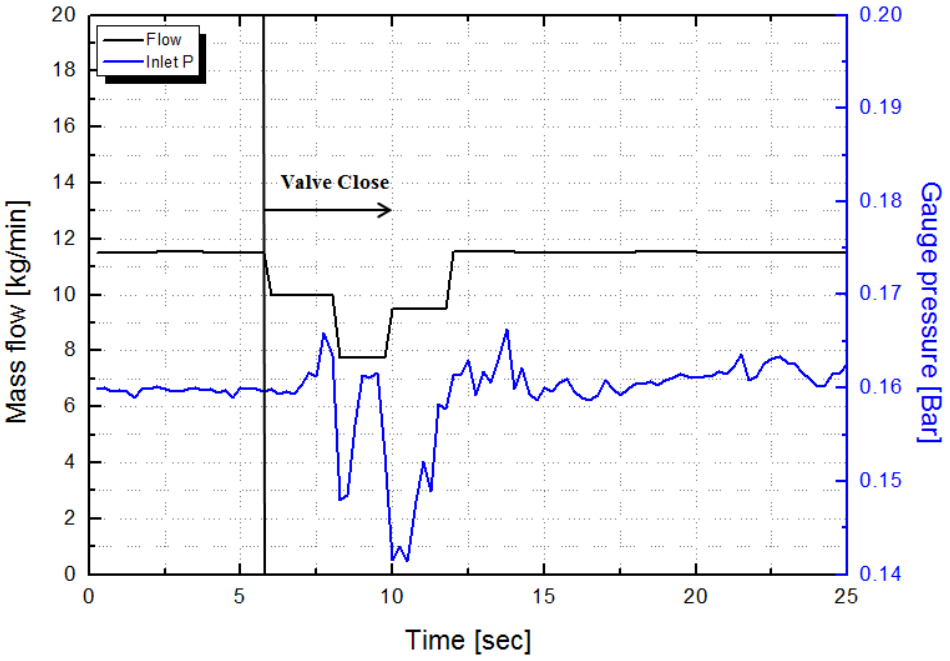

(c) Insertion step (Step-down)

Fig. 3.6 Results of step control test (30 kg)

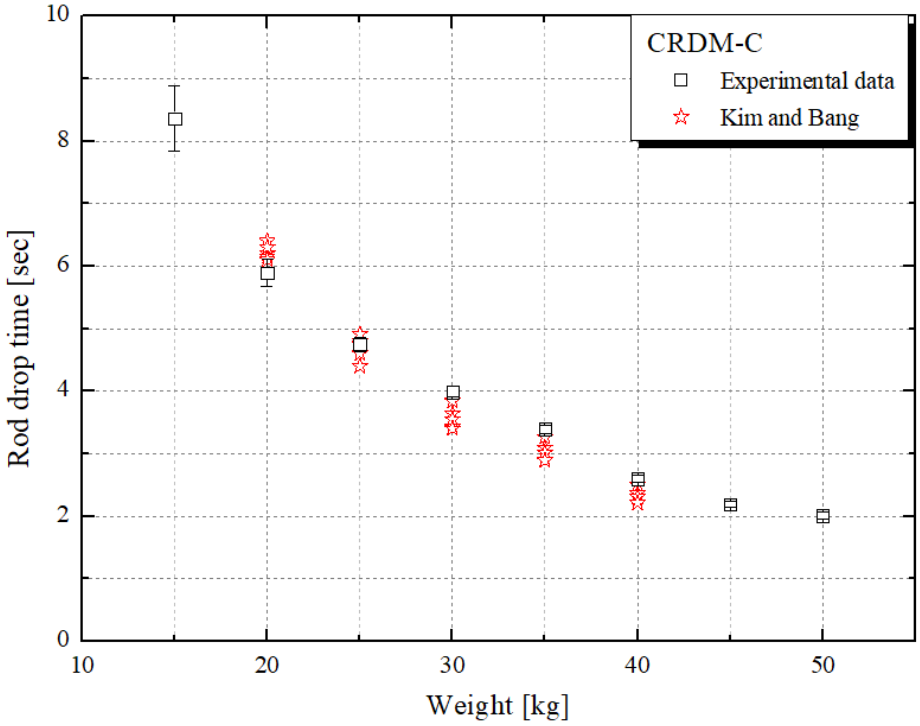

Fig. 3.7 Rod drop time according to the weight

3.4.2 Hydraulic CRDM for PINCs (CRDM-P)

To enhance the operational behavior of the hydraulic CRDM, the new type of hydraulic CRDM was developed, focusing on the simplified flow control and position indication using the inlet flow rate. The driving forces of hydraulic CRDM were same as the previous design, however, the pressure loss of the patterned cylinder was changed owing to the characteristics of the geometry. The importance of modified geometry is the steady flow rate of hydraulic CRDM. In conventional hydraulic CRDMs (including CRDM-C), the steady flow rate was a fixed range between the minimum and maximum steady flow rate depending on the cross-sectional area of each steps. However, proposed geometry (CRDM-P) has a different cross-sectional area according to the step change. Increased step position has a wide cross-sectional area inside cylinder. Therefore, at the high number of steps, the steady flow rate has a large value in comparison with those of the low step. Based on the mass flow rate, it is possible to determine the elevation of the control rod assemblies.

During the step control, CRDM-P has a single control signal for controlling the elevation of the control rod assemblies. In contrast, CRDM-C must have a complex flow control process and a considerations of control time, increased flow rate, and decreased flow rate from the steady flow, carefully. Fig. 3.8 shows the difference between hydraulic CRDM-C and CRDM-P including the design of the hydraulic CRDM-P. Therefore, in the previous studies, the control process had a complex control logic, and the step control characteristics was experimentally defined without well-defined theoretical results. Bo et al. studied the relationship among the operational pressure, mass flow rate, and control time to verify increased/decreased elevation of the control rod using the experimental results [3.11]. The prediction of step control was highly sensible to the operational conditions and geometry of the cylinder. Fig. 3.9 shows the step-up characteristics of the hydraulic CRDM of NHR-5.

3.4.2.1 Step control with pressure difference

In case of the hydraulic CRDM-P, the step (elevation of the hydraulic CRDM) can be easily predicted according to the mass flow rate. Fig. 3.10 shows the results of step control experiment with a fixed CRDM weight (30 kg). In the withdrawal step, at the inlet region, the mass flow rate and pressure increased. Due to the increased pressure, the driving force of pressure difference between cylinder and pool was increased. Therefore, CRDM-P moved to next step (upward) until force equilibrium step. The elevation of the CRDM-P with hybrid control rod changed between 5 sec (step increase signal) to 10 sec. In comparison with previous results of CRDM-C, the steady state flow rate and pressure was changed with withdrawal step process. The behavioral characteristics of CRDM-P had stable values without fluctuation of the pressure and mass flow rate.

3.4.2.2 Drop test

Fig. 3.11 shows the rod drop time according to the weight of the hydraulic CRDM-P. The test results had a range from the 1.9 sec to 6.9 sec, therefore the time until the bottom end region was shorter than the those of the CRDM-C. The grooved cylinder has a repeated stagnation of the working fluid between the steps, therefore, the head loss of the hydraulic CRDM-C was larger than the those of the CRDM-P.

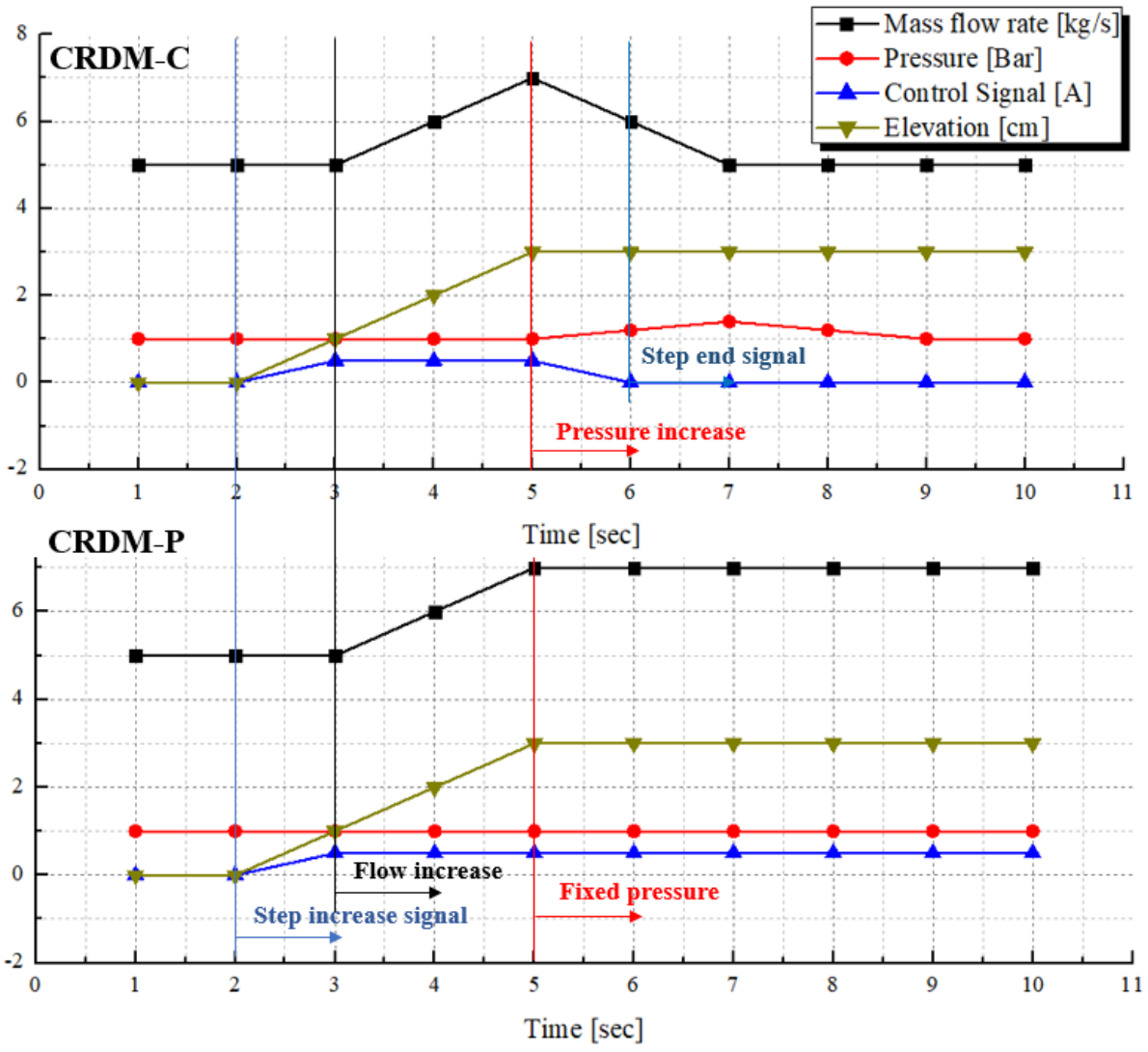

(a) Difference control method between hydraulic CRDM-C and CRDM-P

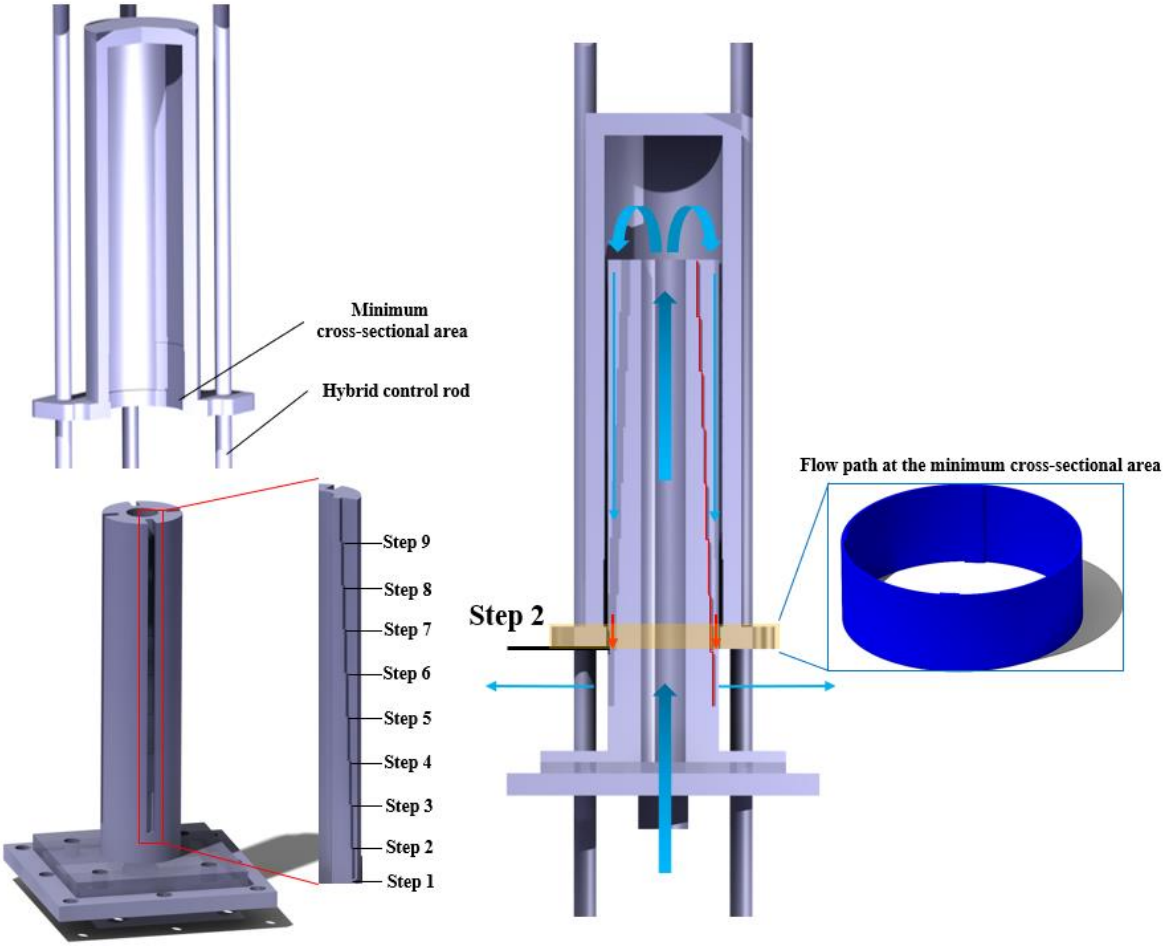

(b) The detail design of the hydraulic CRDM-P

Fig. 3.8 Difference control method between hydraulic CRDM-C and CRDM-P including the design of the hydraulic CRDM-P

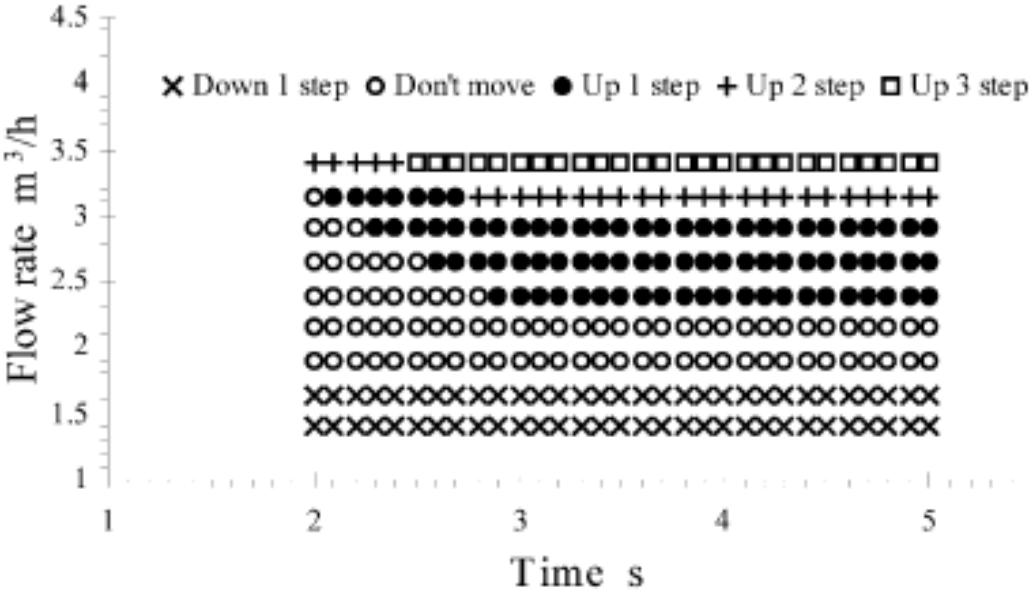

Fig. 3.9 Step up characteristics of the hydraulic CRDM for NHR-5 at 3.20 MPa [3.11]

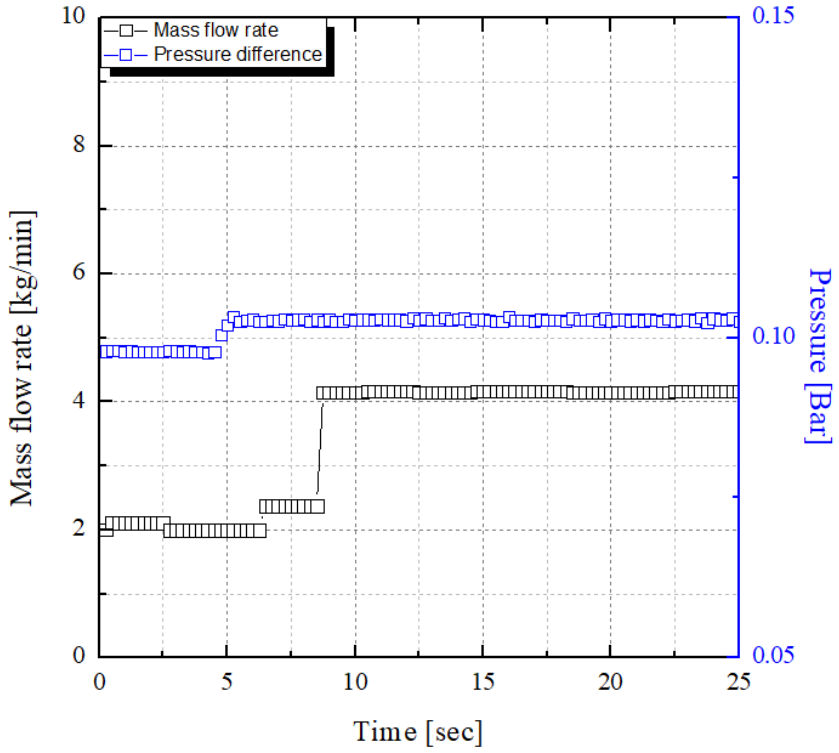

(a) Withdrawal step (Step-up; 1st step)

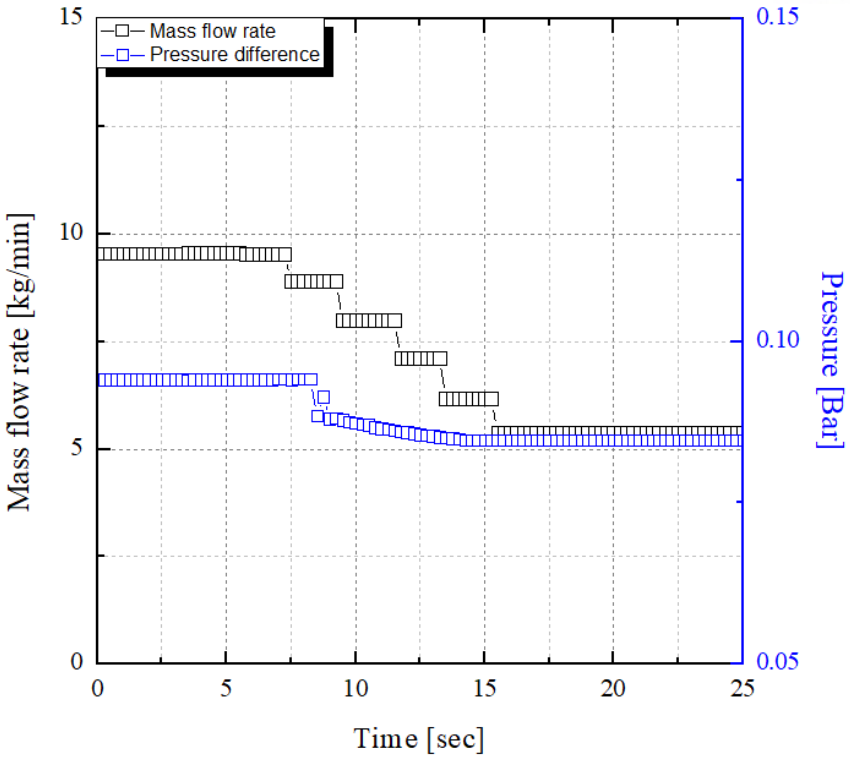

(b) Insertion step (Step-down)

Fig. 3.10 Results of step control test (15 kg, 4th step)

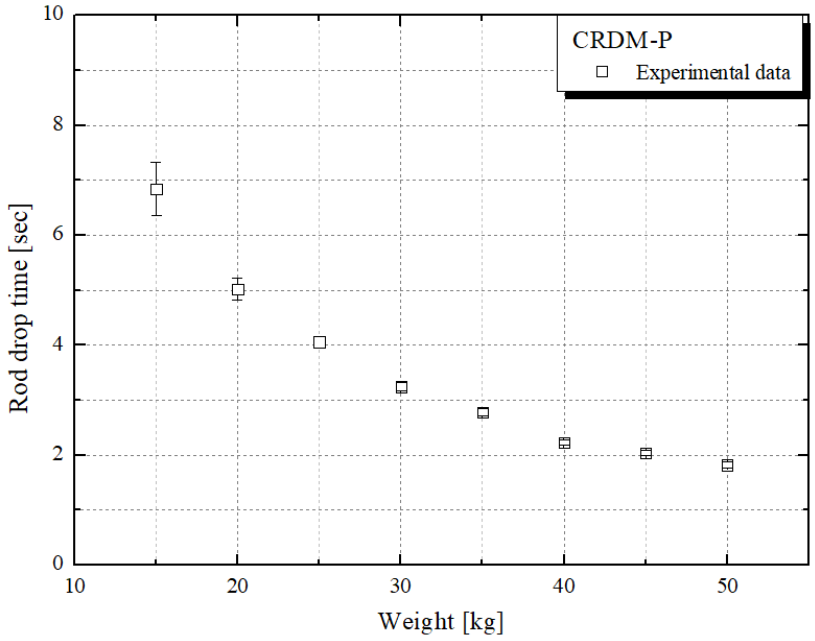

Fig. 3.11 Rod drop time according to the weight (CRDM-P)

3.5 Modified theoretical model

In the previous results, the hydraulic CRDM with hybrid control rod needs to consider the additional driving forces from the hybrid control rod components. In the chapter 2, the driving force of the single hybrid control rod was developed and validated. To enhance the theoretical model of the hydraulic CRDM, the two terms for the transient model were considered; 1) pressure differential between hybrid control rod and water pool and 2) flow frictional force between hybrid control rod and guide tube. In the studies of the hydraulic CRDM, the effect of the guide tube was neglected during the rod drop test, however, the experimental test of the CRDM-C had a geometry of the guide tube. Therefore, this geometry effect is the one of the reasons of the difference between experimental and calculated results. In the modified analysis, the force equilibrium equation is used for determining the state of the hydraulic CRDM, shown in Fig. 3.12. Therefore, the force equilibrium equation is driven by

$$M\frac{d^2y}{dt^2} = F_{loss} + F_b + F_g + \sum F_{HCR} + F_{gt} = \Delta P_{loss}A_c + F_b + F_g + num \cdot F_{HCR} + F_{gt} \tag{3.9}$$

In this equation, the driving force of the hybrid control rod is the is determined by the Eq. 2.8. Therefore, the final form of the driving force was rearranged by

$$\begin{aligned} F_{HCR} &= (m_{clad} + m_{B4C} + m_{f,\max}C_1\frac{L}{L_{\max}})g \\ &+((C_2 + C_3\frac{L}{L_i})P - P_{atm})A_c + \omega F_{bearing} + num \cdot f_{seal} \end{aligned} \tag{3.10}$$

The gravitational force for hydraulic CRDM was expressed by

$$F_g = Mg = m_{CRDM}g \tag{3.11}$$

The buoyancy force both hydraulic CRDM and hybrid control rod was considered. Therefore, the buoyancy force of the modified model is defined as

$$F_b = M\frac{\rho_w}{\rho_t}g = (m_{CR} + m_{CRDM})\frac{\rho_w}{\rho_t}g \tag{3.12}$$

The frictional force at the guide tube is simply expressed by

$$F_{gt} = \sum \frac{\rho V^2}{2A_c}(\lambda \frac{L}{d_h}) \tag{3.13}$$

Finally, the pressure difference is defined as

$$\Delta P_{loss} = \frac{\rho g}{A_c} \cdot h = \frac{\rho g}{A_c}(h_{major}) = \sum \frac{\rho V^2}{2A_c}(\lambda \frac{L}{d_h}) \tag{3.14}$$

From the Eq. 3.13, the driving force of pressure difference is rearranged by

$$F_{loss} = \sum \frac{\rho V^2}{2}(\lambda \frac{L}{d_h}) \tag{3.15}$$

During the rod drop behavior, the drop length of hydraulic CRDM is calculated by

$$\int (\int \frac{d^2 y}{dt^2} dt) dt = \frac{1}{M} \int \int ((\Delta P_{loss} A_c + \sum F_{HCR} + F_{gt}) dt) dt + F_b + F_g \tag{3.16}$$

To design of the steady state condition of hydraulic CRDMs, the steady flow and pressure loss at the fixed position are needed. Therefore, in the steady state, the force balance equation is driven by

$$F_{loss} + F_b + F_g + \sum F_{HCR} + F_{gt} = 0 \tag{3.17}$$

From the Eq. 3.9, the pressure loss and steady flow rate of hydraulic CRDM during fixed position is rearranged by

$$\Delta P_{loss} = \frac{1}{A_c}(F_b + F_g + num \cdot F_{HCR}) \tag{3.18}$$

$$\dot{m} = \sqrt{\frac{2 d_h \rho A_{cs}^2}{\lambda L}}((m_{CR} + m_{CRDM}) \frac{\rho_w}{\rho_t} g + m_{CRDM} g + num \cdot F_{HCR}) \tag{3.19}$$

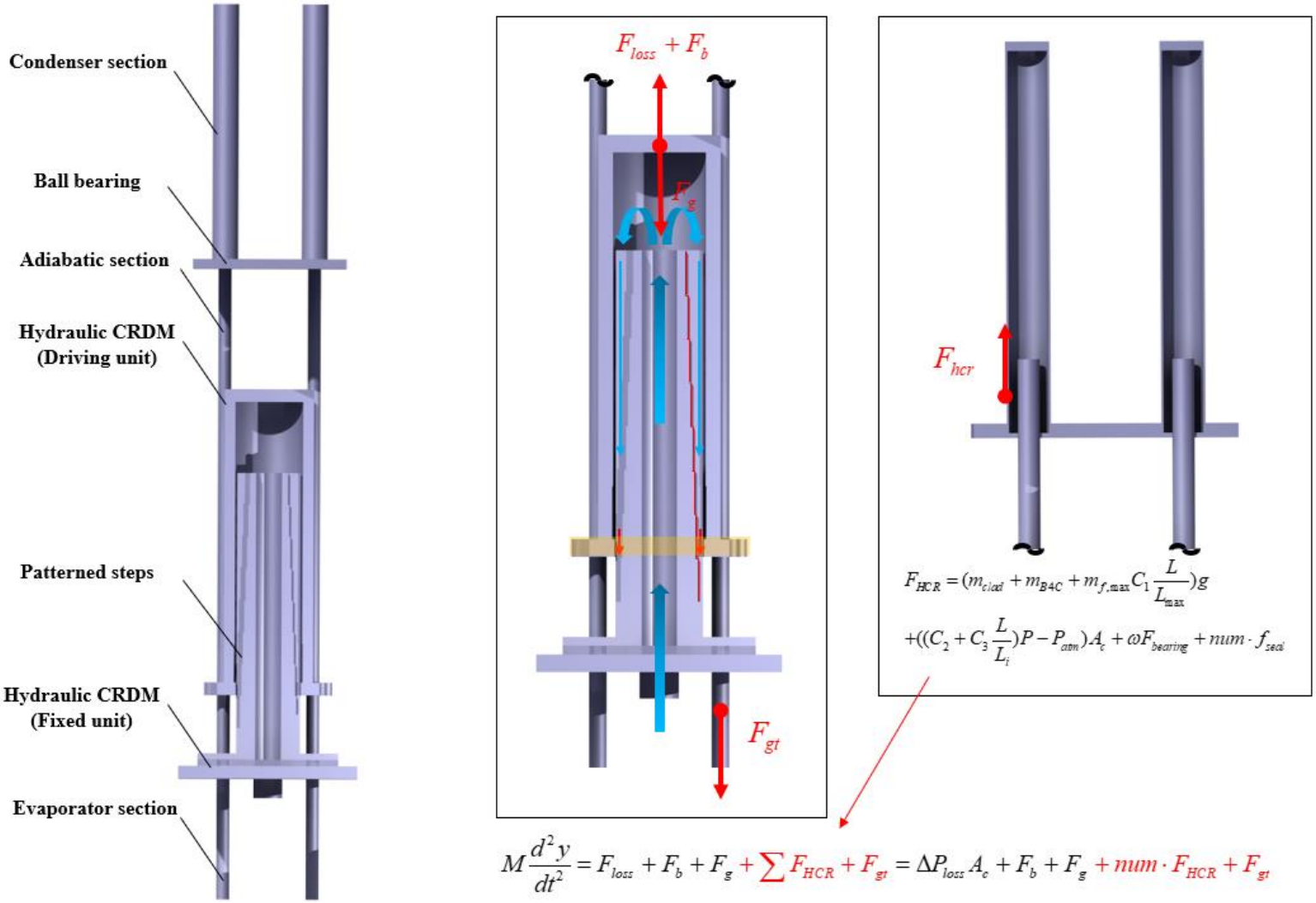

Fig. 3.12 The schematic diagram of CRDM-P

3.6 Validation of theoretical model

3.6.1 Validation of the CRDM-C

The comparison of CRDM-C and literature data was conducted to verify the effect of parameters such as pressure, mass flow rate, and elevation. In the previous researches, the various geometries and conditions are considered, however, detailed information is not presented. Therefore, the behaviors of hydraulic CRDM cannot be predicted according to the major parameters. Fig. 3.13 and 3.14 shows the pressure, mass flow rate, and elevation of CRDMs in the previous researches and experimental results. Therefore, the validation of the hydraulic CRDM was conducted by using the experimental test of CRDM-C. The detailed information of CRMD-C was shown in Table. 3.4, and Fig. 3.15 shows the validation results of theoretical model during the step-up process. The elevation of the hydraulic CRDM is determined by the mass flow rate at the steady state condition. During the steady state condition of the hydraulic CRDM, the mass flow rate was the range from 13.44 to 15.1 kg/min in case of 15kg weight. At the steady position, the frictional force and frictional coefficient of the hydraulic CRDM were minimized, therefore, the stable and minimized mass flow rate could be observed at each step, as shown in Fig. 3.15 (a). During the step-up control, the mass flow rate and pressure of the hydraulic CRDM were dramatically increased. The change of the pressure and mass flow rate yielded a good agreement within $\pm$12.9 % errors. However, the maximum peak of the pressure differential and mass flow rate were not predicted.

In case of the rod drop test, the changes of the elevation, velocity, and rod drop time were confirmed by using the high-speed camera. The theoretical results and experimental data of the rod-drop test according to the weight is shown in Fig. 3.17. In the previous study, the rod-drop time of CRDM-C was studied with the range from 15 to 50 kg. From the theoretical model, the rod-drop time is determined and the drop time of lightweight is predicted within 16.5% of deviation, including the previous data. At the low weight condition, the deviation of the drop time is larger than those of heavyweight due to the structural interactor of the test section; therefore, the deviation of the rod-drop time is gradually decreased according to the increment of the weight.

3.6.2 Validation of the CRDM-P

Various researches of hydraulic CRDM have been conducted for developing the rod control system owing to enhance the passivity and reliability. Despite the advantages, the hydraulic CRDM has a few limitations such as 1) requirement of penetration hole for inserting the additional position indicator and, 2) pressure and mass flow peak during the step control, and 3) relatively longer time to shut down the reactor upon an accident condition. A hydraulically driven control system needs to consider the sensible flow control based on the control rod position. During the control of each step, the mass flow and the pressure difference between the inlet and outside pools are carefully adjusted. In addition, a hydraulic CRDM needs a position indicator to measure the location of the control rod. In the other types of the CRDM, it is possible to measure the position of the control rod in the control units. In contrast, as the control unit of the hydraulic system is located outside the reactor vessel, it is required to penetrate the reactor vessel to insert the position indicator. Table. 3.5 shows the advantages and disadvantages of CRDMs: Magnetic jack CRDM, CRDM-C, and CRDM-P.

In this section, a novel hydraulic CRDM for application in nuclear reactors was designed and validated. The tests were conducted on a 4-finger hydraulic CRDM. The tests were based on the forces induced by the pressure difference between the horizontally patterned cylinder and water pool that controls the elevation of hydraulic cylinder (CRDM) at room temperature. The unique features of the hydraulic CRDM in PINCs are the position indication from the mass flow rate at the inlet and the heat transfer from the core to the upper heat sink. The 1D transient model based on the force balance equation was proposed, and the calculated results were experimentally validated. Dropping the control rod assembly into the active core is a critical activity for safe shutdown of reactor. To identify the function of the safe shutdown during the accident, the rod-drop test was performed to ascertain the effects of friction.

The step control behaviors of CRDM-C and CRDM-P are shown in Fig. 3.18. In CRDM-C, a fixed flow rate with different steps was observed and predicted. The minimum cross-sectional area of the CRDM-C was always fixed due to the patterned shape of the cylinders. From Eq. 3.9, the steady flow range was calculated, and its range was determined between the minimum cross-sectional area and the transient cross-sectional area of the CRDM-C. The transient cross-sectional area was continuously changed until the next step. At the half-step condition, the characteristic length of the minimum cross-sectional area was continuously decreased, therefore, the total frictional force on the surface of the cylinder was increased with the peak of the pressure difference. From the half-step to the next step, the characteristic length of the minimum cross-sectional area was linearly decreased, and the peak flow region due to the increased pressure drop was observed. The area of the valve was increased until half-step, and subsequently, the area of the valve was controlled to maintain a steady flow. The steady flow and behaviors of the transient flow showed good agreement with the theoretical results based on the Eq.

3.9, as shown in Fig. 3.19 and Fig. 20. In CRDM-P, the mass flow according to the steps was changed due to the change in area of each step. The area of the step was determined by the ratio of the step over the previous step. Therefore, the inlet flow rate of the next step needed to increase to satisfy the equilibrium of the driving forces. In comparison with CRDM-C, the pressure differences of the overall steps were stable without any peaks and fluctuations.

The hydraulic CRDMs with conventional patterned geometry need to control the mass flow rate; 1) increase of the mass flow rate until half of the step and 2) decrease of the mass flow rate at the steady flow rate. This control method needs a well-developed control system with the measurement device; however, the uncertainty of the measurement device is approximately 9–20% due to the complex conditions in the nuclear power plant [3.15]. Therefore, the hydraulic CRDMs have a problem of the multi-step increase with unexpected power change. The complex control is not used for the step control of the CRDM-P in comparison with CRDM-C. The mass flow rate increased or decreased for controlling the elevation of the hybrid control rod.

The effects of both the weight and the step of CRDM-P are shown in Fig. 3.21. In this test, the weight range is from 15 to 50 kg with 9 steps of the CRDM-P. The mass flow rates of the steps are well-predicted (within 8.6% of deviation). The driving force for controlling the hydraulic CRDM is pressure difference, and it is defined as a mass flow rate in the test. In the case of the heavyweight condition, the pressure difference increased due to the increased gravitational force. Fig. 3.22 shows the pressure difference of the CRDM-P with different step and weight conditions.

In comparison with those of the CRDM-C, the rod-drop time of the CRDM-P decreased due to the effect of the increment of the cross-sectional area on the flow resistance. Fig. 3.23 and 3.24 shows the drop behavior of the hydraulic CRDM compared with the theoretical model. To confirm the transient behavior of the hydraulic CRDM with hybrid control rod, the CRDM-P position is measured by using a high-speed camera. The trendline of the position is observed to be well-predicted. The drop location is under-predicted, and it has 17.4% of deviation; however, the other cases of the rod-drop test have a good agreement within 6.7% errors.

Table. 3.4 The detailed information of the design parameters

Parameters	CRDM-C	Unit
Weight	30	Kg
Step length	20	mm
Design temperature	25	℃
Diameter of the drive cylinder	55	mm
Gap at upper labyrinth	0.5	mm
Diameter of the connecting bar	19.05	mm
Gap at lower notch	0.5	mm
Diameter of feedwater line	19.05	mm
Head of pump	40	m
Diameter of the impulse cylinder	55	mm
Length of the impulse cylinder	Non	mm
Steady flow rate	14.2-16.4	kg/min

Table. 3.5 Advantages and disadvantages of CRDMs: Magnetic jack CRDM, CRDM-C, and CRDM-P

	Magnetic Jack	**CRDM-C**	**CRDM-P**
Strength	▪ Stable position control ▪ Low electric power at the steady state ▪ Mechanical operation (high reliability) ▪ High accuracy	▪ Good passivity ✓ Shutdown without signal and electric power ✓ Avoidance of rod ejection ▪ Compact geometry ▪ Flexible step control	▪ Good passivity ✓ Shutdown without signal and electric power ✓ Avoidance of rod ejection ▪ Compact geometry ▪ Flexible step control ▪ Position indication from the mass flow rate ▪ High accuracy
Weakness	▪ Rod ejection problem ▪ Shutdown with scram signal ▪ Large space for installation	▪ Relatively low accuracy ▪ Complex control method ▪ Fluctuated motion at steady state	▪ Fluctuated motion at steady state ▪ Relatively high mass flow rate for controlling the steps
Application	▪ Commercial PWRs and research reactors	▪ BWRs, Research reactors, and SMRs	▪ Commercial PWRs, SMRs, and Gen. IV

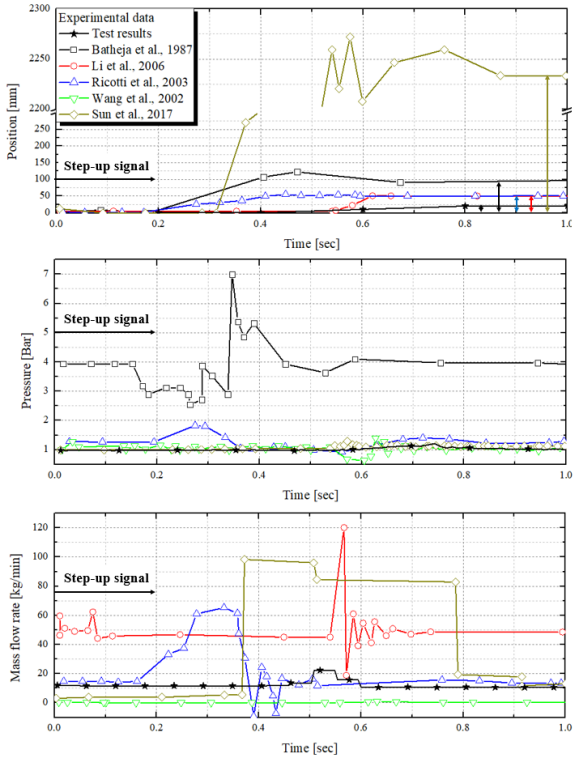

Fig. 3.13 Behaviors of the step-up process; pressure, mass flow rate, and elevation of the hydraulic CRDMs

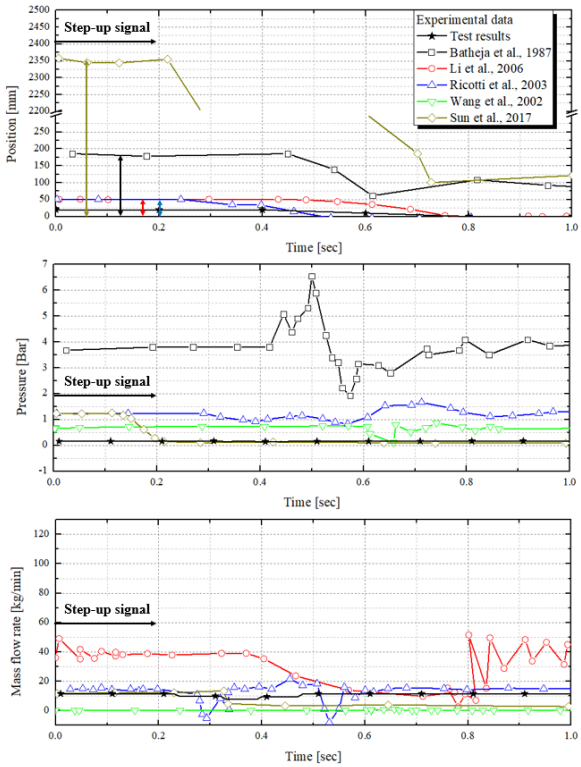

Fig. 3.14 Behaviors of the step-down process; pressure, mass flow rate, and elevation of the hydraulic CRDMs

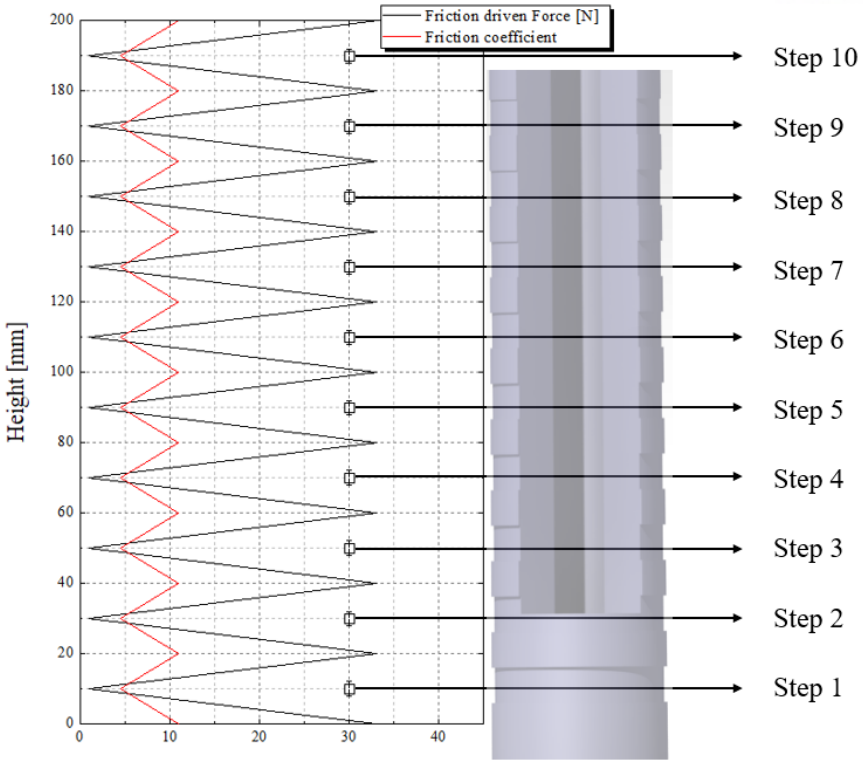

(a) Elevation of the hydraulic CRDM with theoretical results

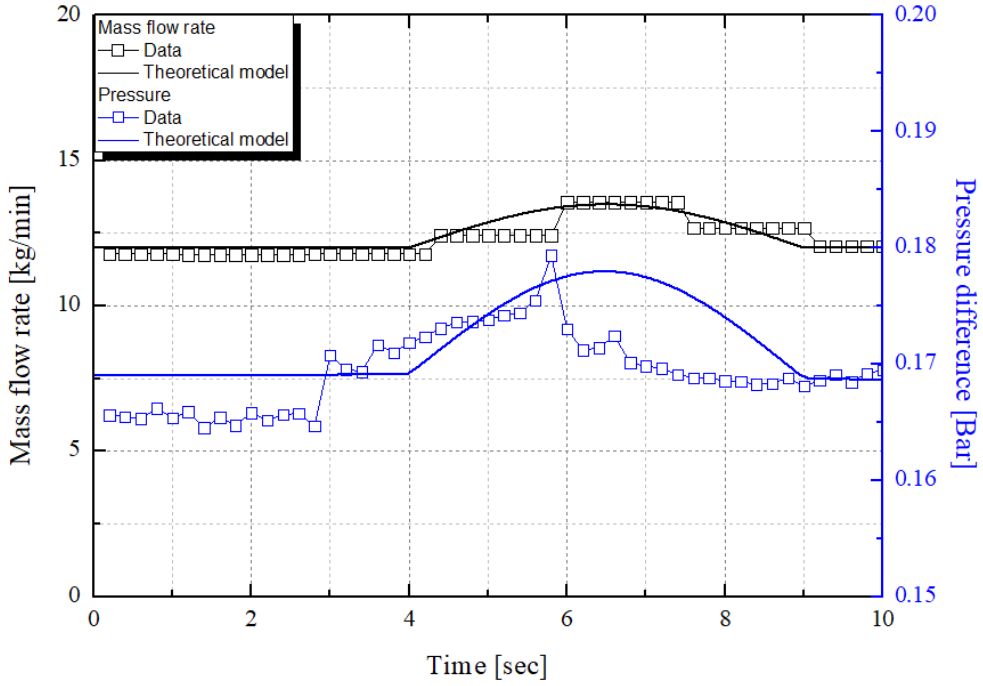

(b) Mass flow rate and pressure of the hydraulic CRDM-C with theoretical model

Fig. 3.15 Validation of the theoretical model; elevation of the hydraulic CRDM-C and step-up process and (Weight : 30 kg, Temperature : 25 °C)

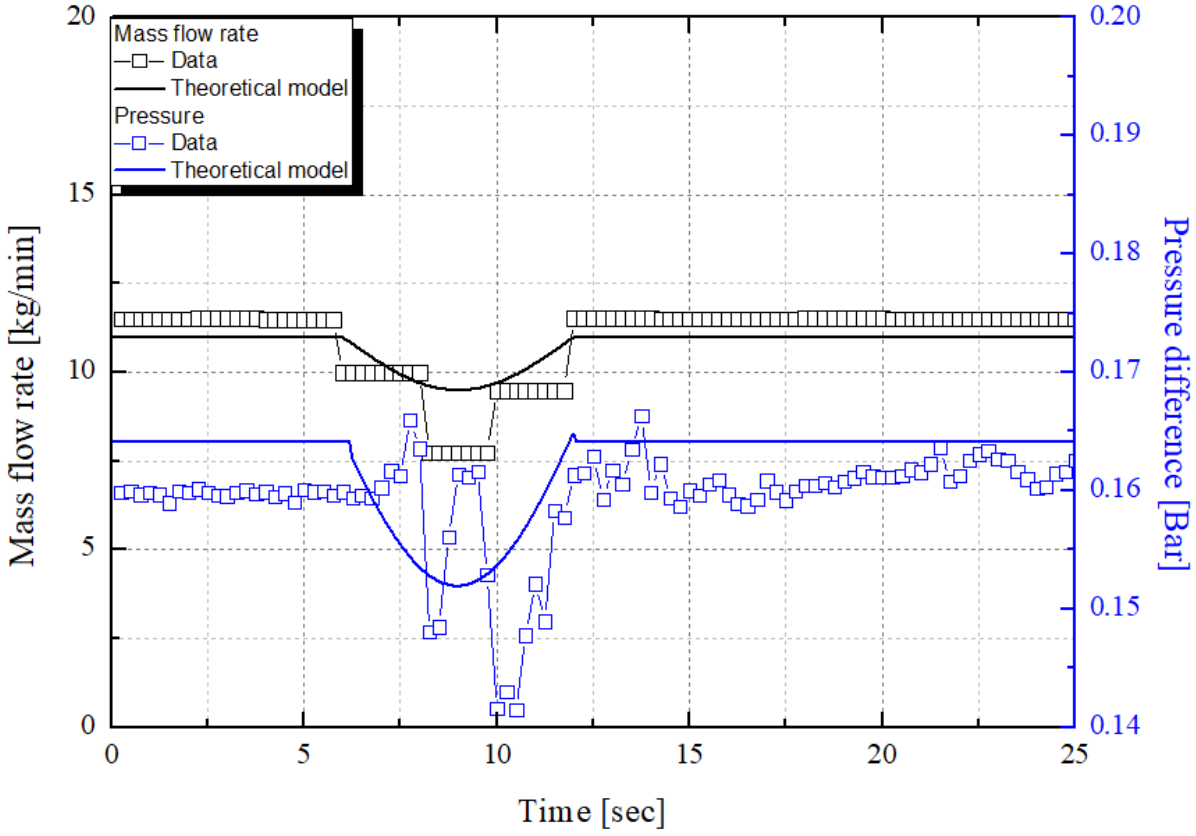

Fig. 3.16 Validation of the theoretical model; Step-down process

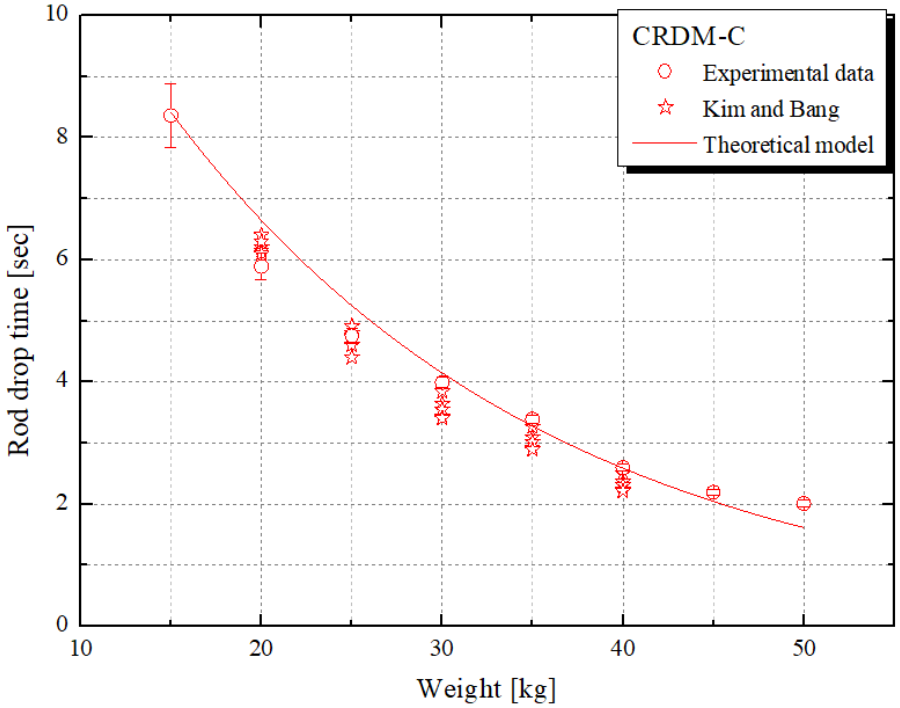

(a) Experimental results of CRDM-C with theoretical results

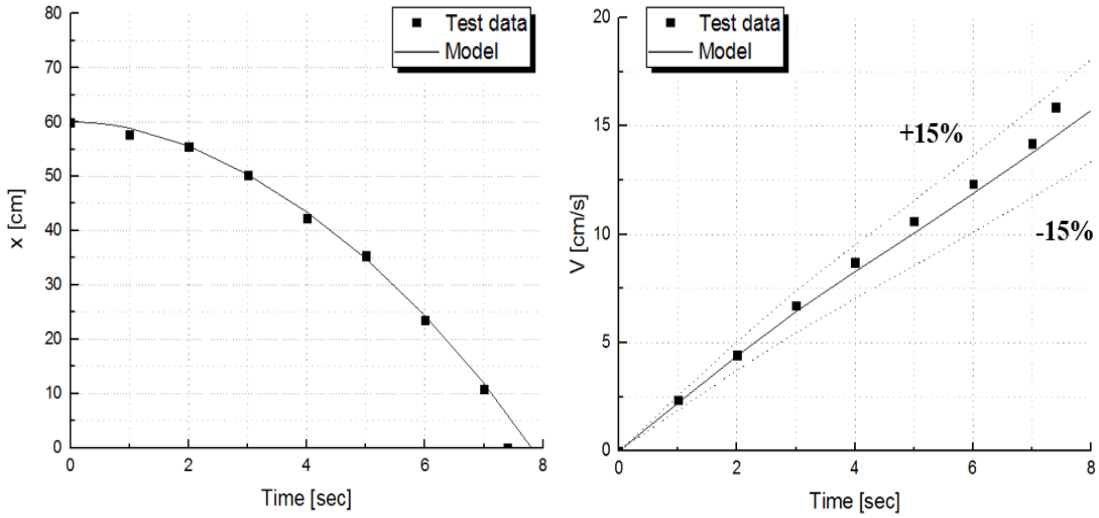

(b) Position and Velocity of the hydraulic CRDM-C during the rod-drop test

Fig. 3.17 Theoretical results and experimental data of the rod-drop test (CRDM-C)

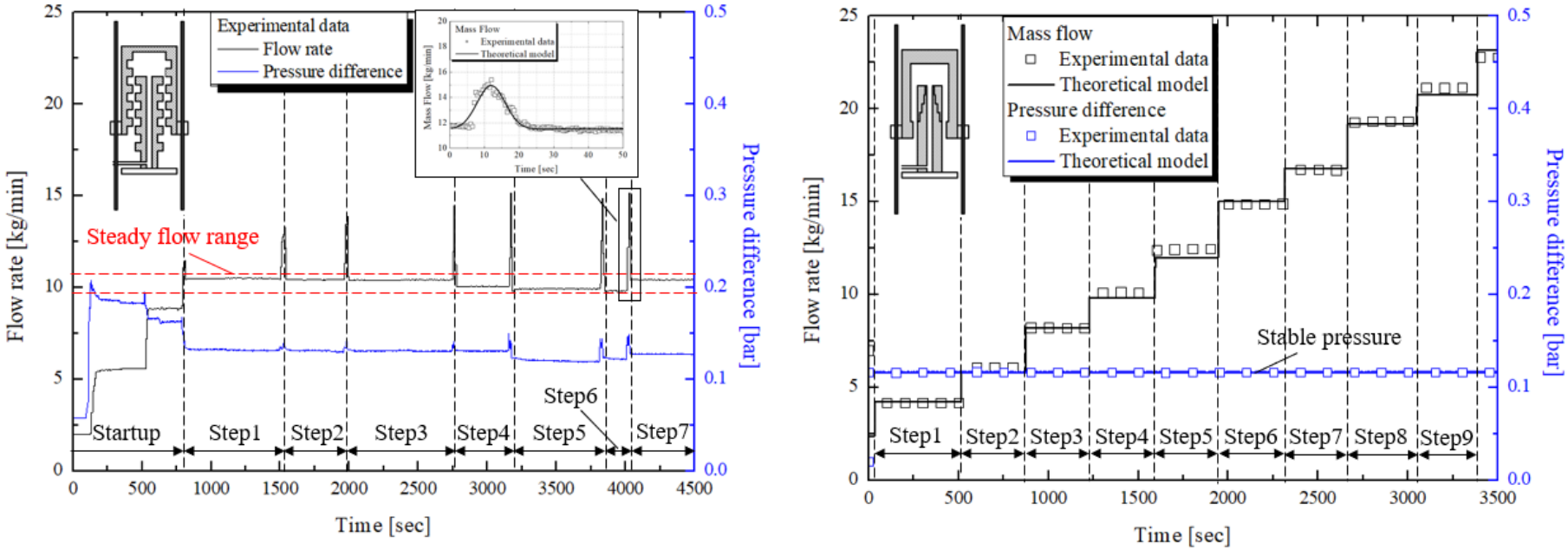

(a) Weight of CRDM : 15 kg, without hybrid control rod (CRDM-C and CRDM-P)

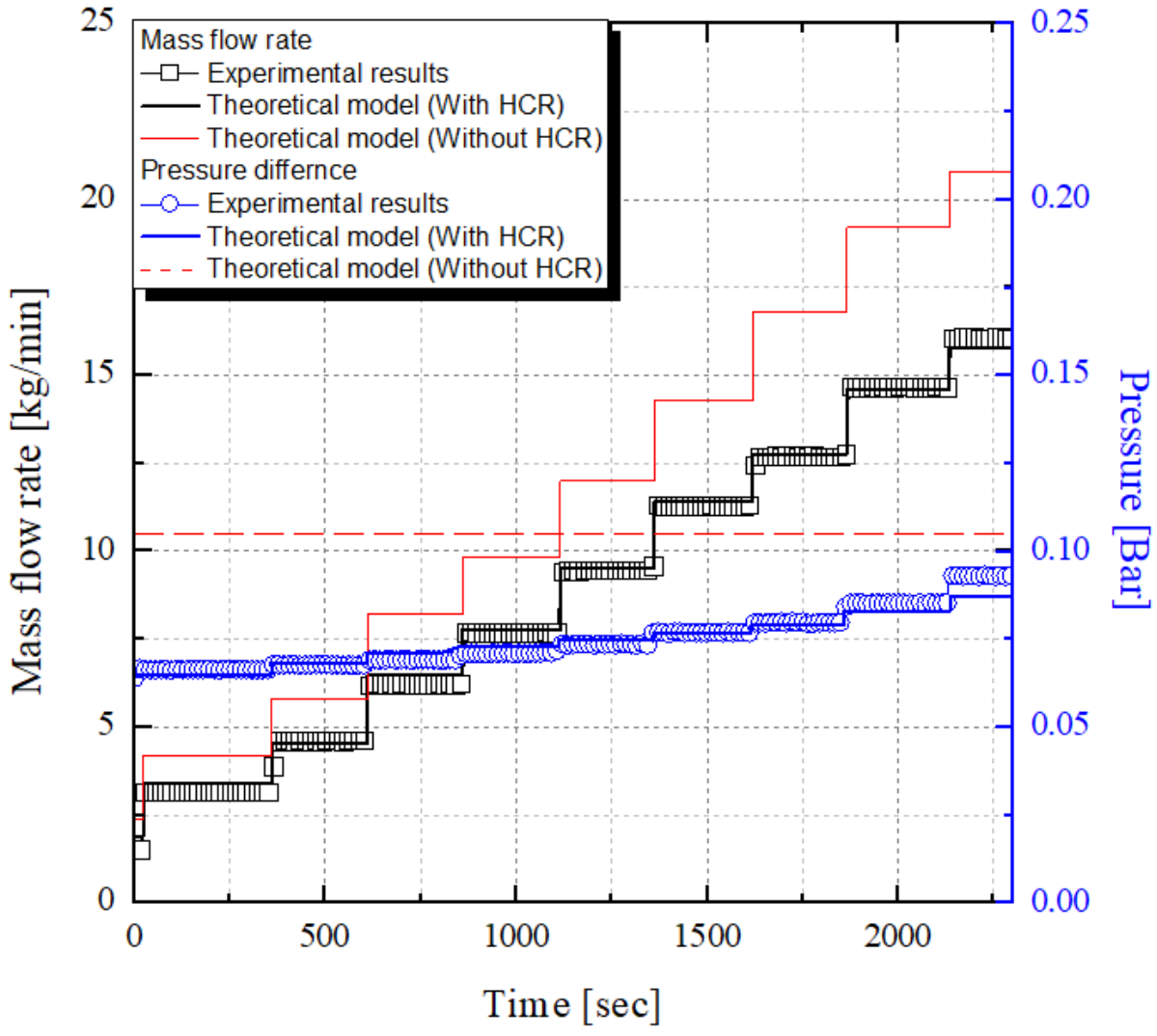

(b) Weight of CRDM : 15 kg, with hybrid control rod (CRDM-P)

Fig. 3.18 Step control behavior of CRDM-C and CRDM-P

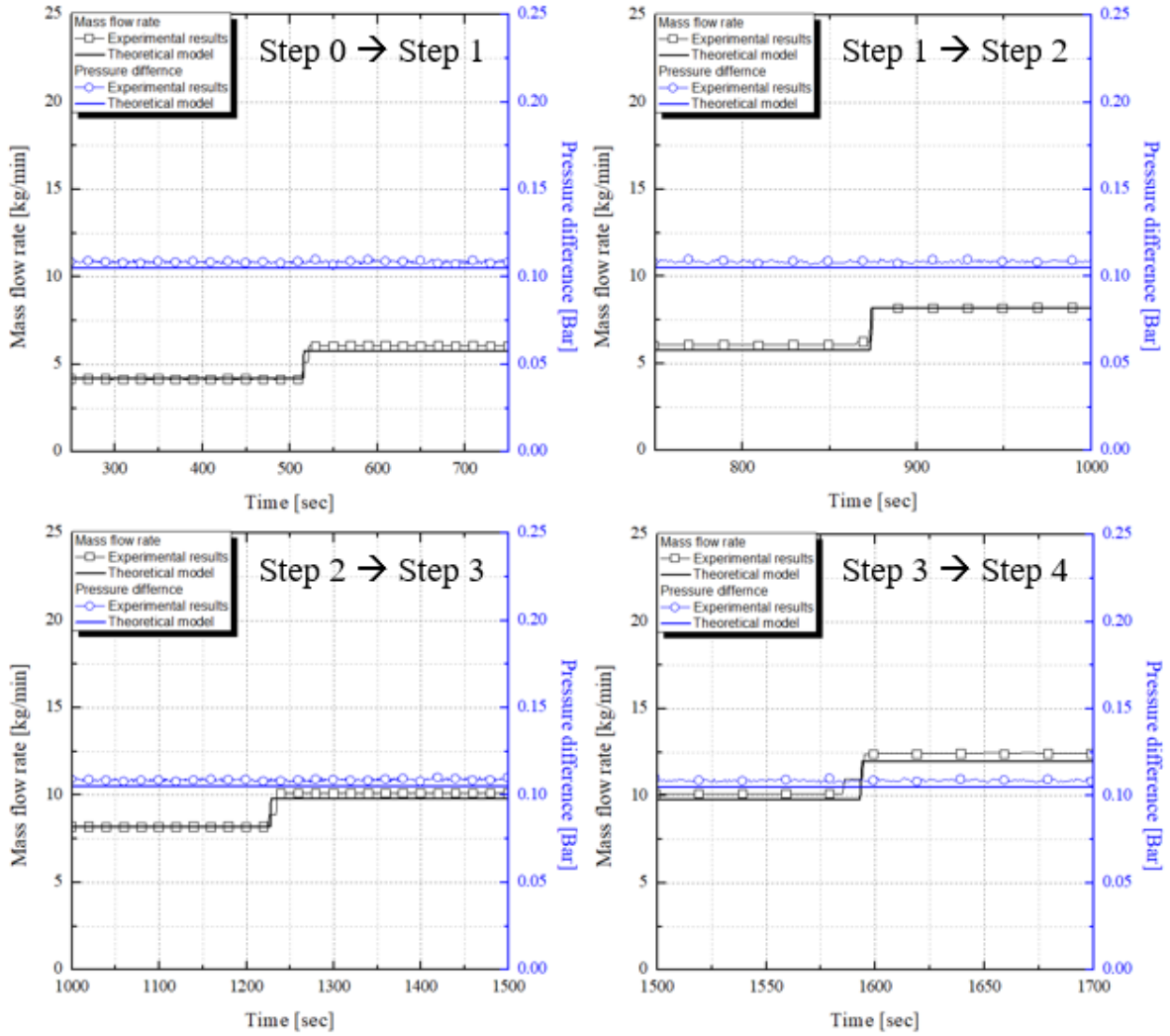

Fig. 3.19 Validation of the theoretical model; Step-up process (CRDM-P, without hybrid control rod) (Continued)

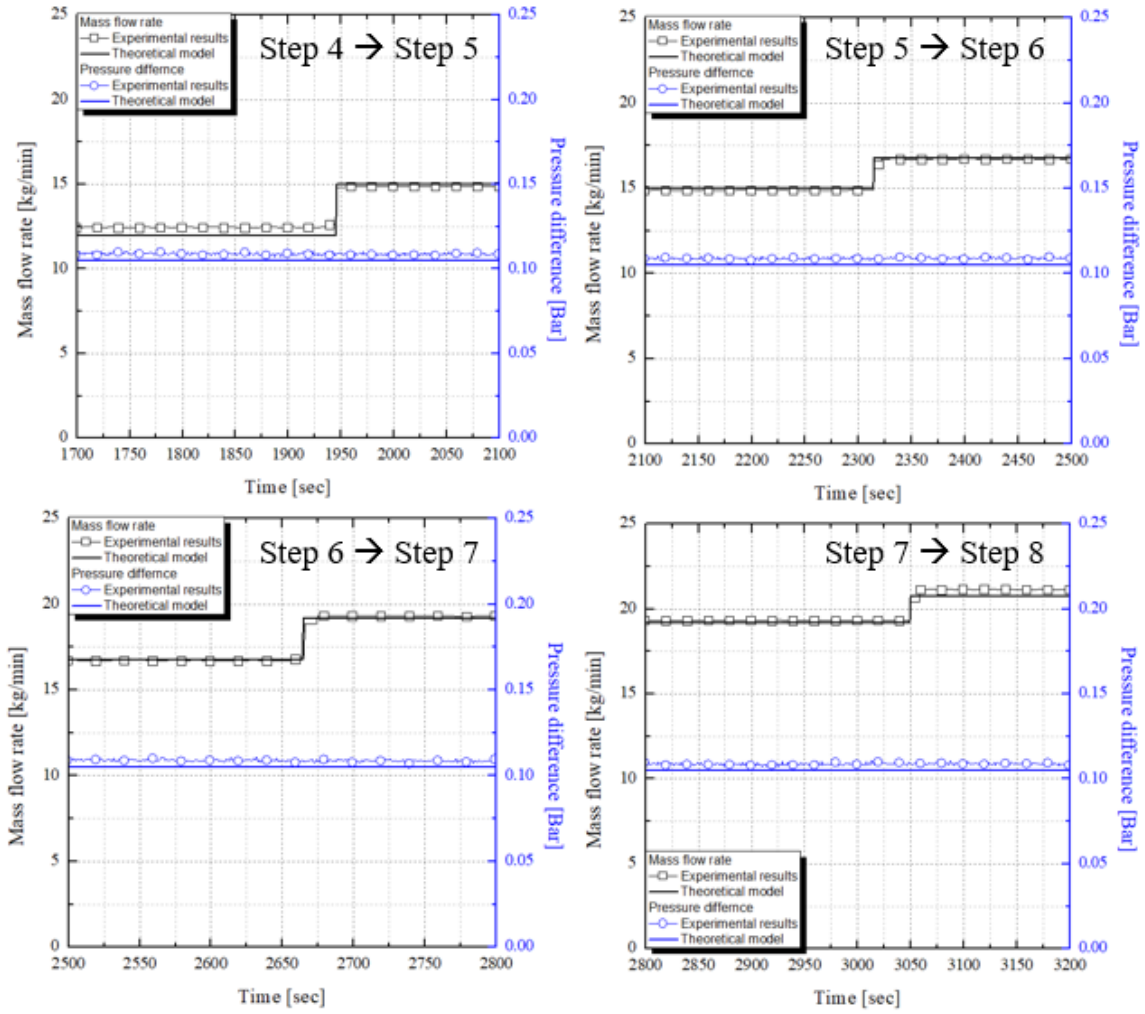

Fig. 3.19 Validation of the theoretical model; Step-up process (CRDM-P, without hybrid control rod)

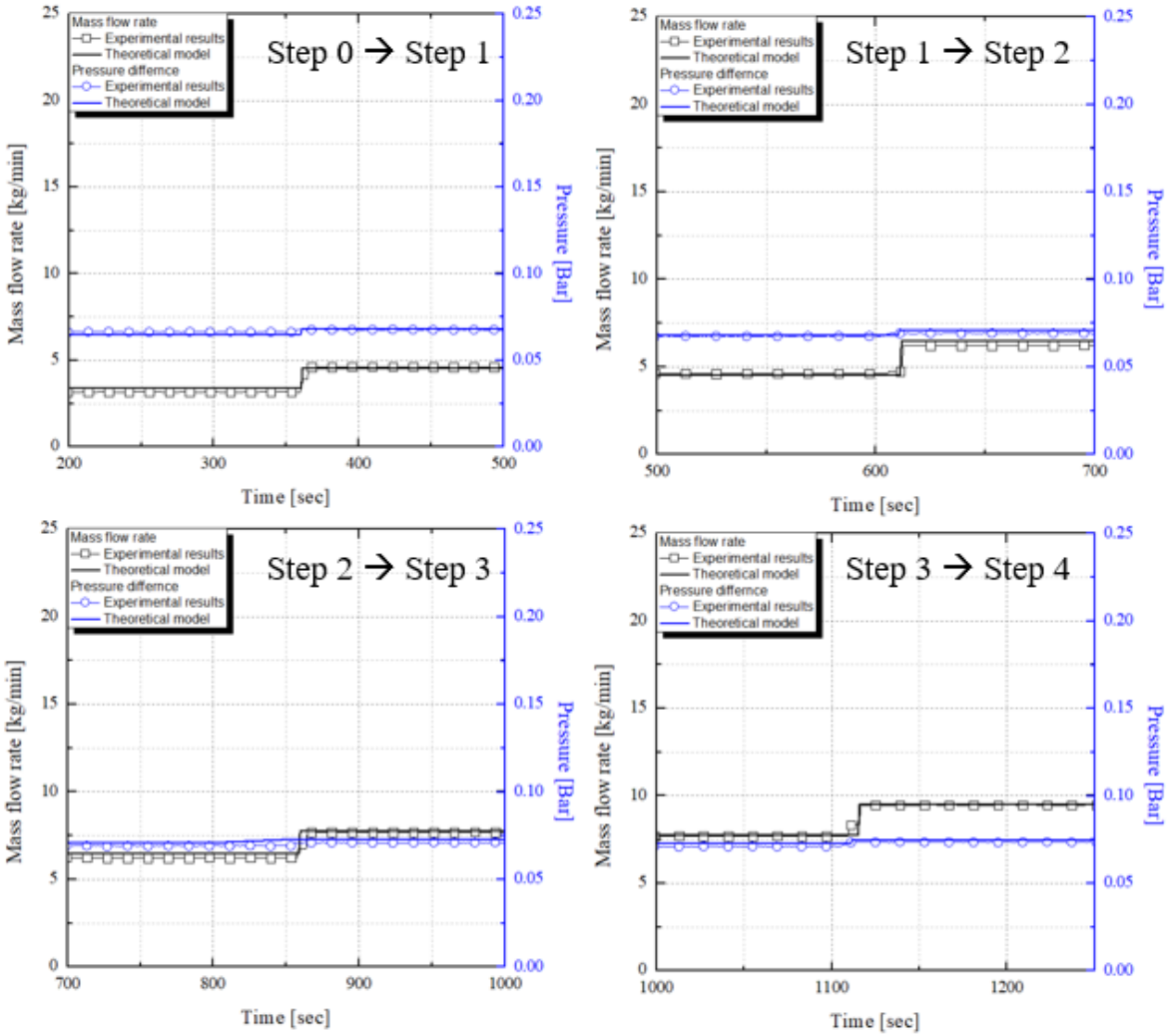

Fig. 3.20 Validation of the theoretical model; Step-up process (CRDM-P, with hybrid control rod) (continued)

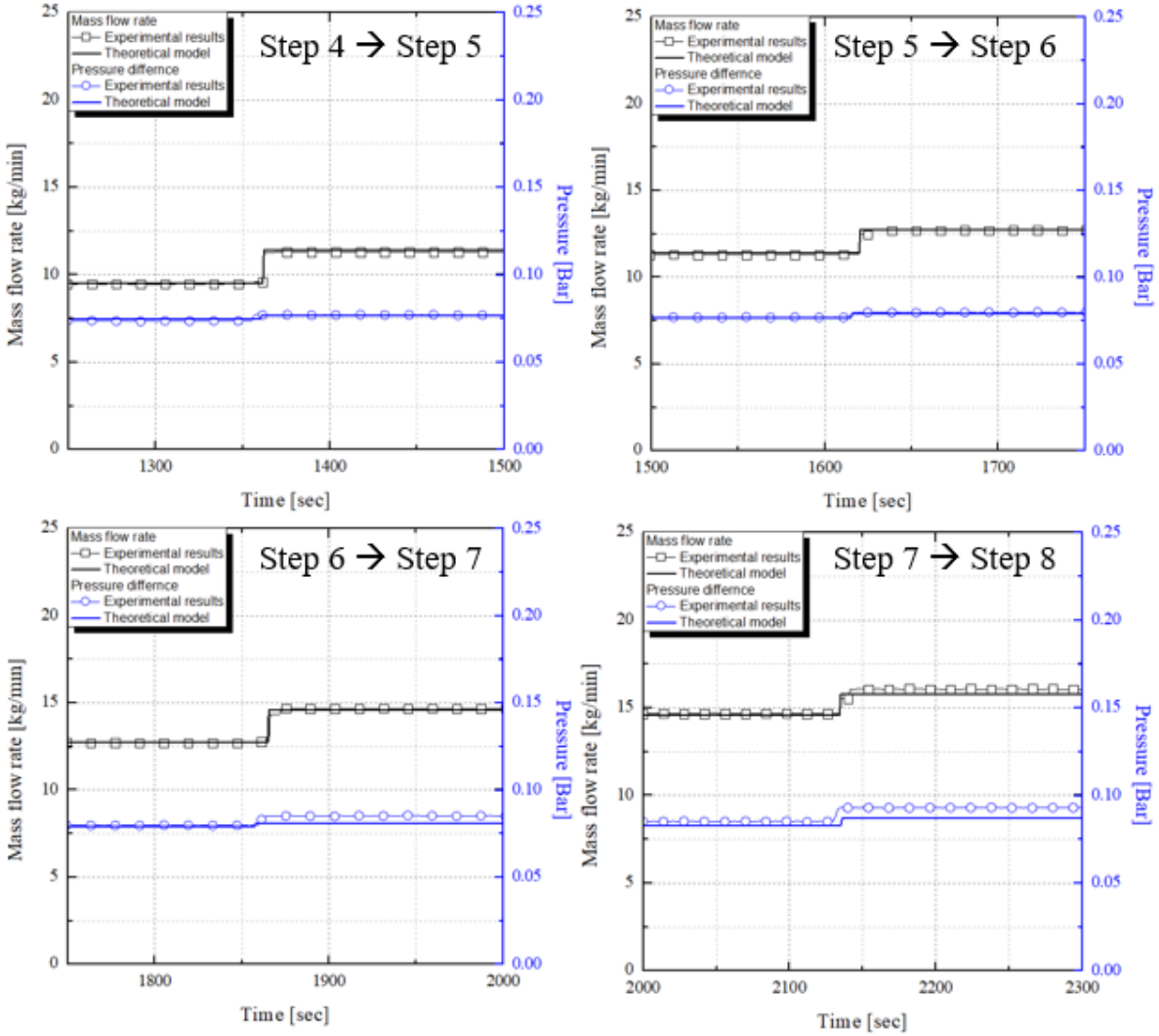

Fig. 3.20 Validation of the theoretical model; Step-up process (CRDM-P, with hybrid control rod)

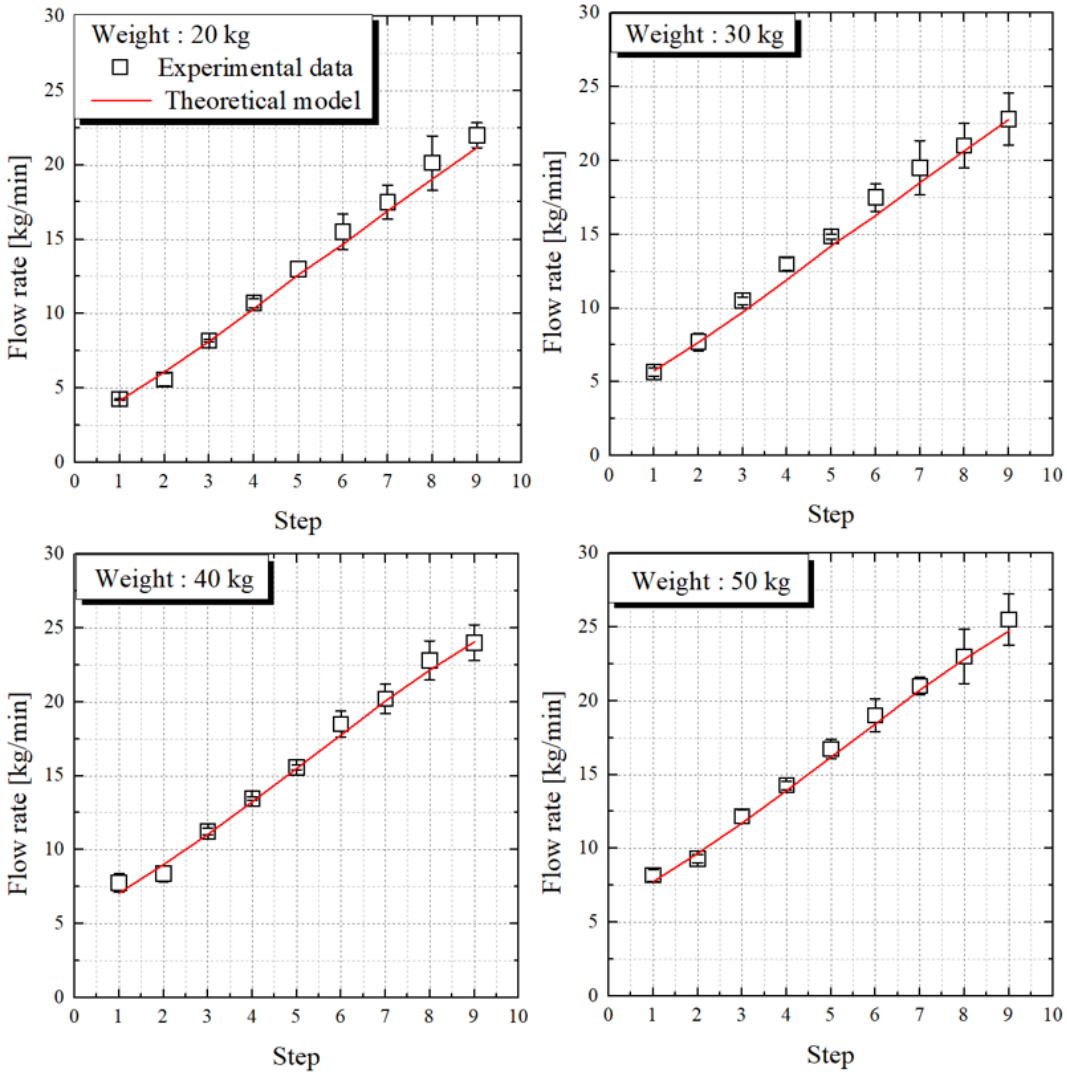

Fig. 3.21 The mass flow rate of each step according to the weight of the CRDM-P

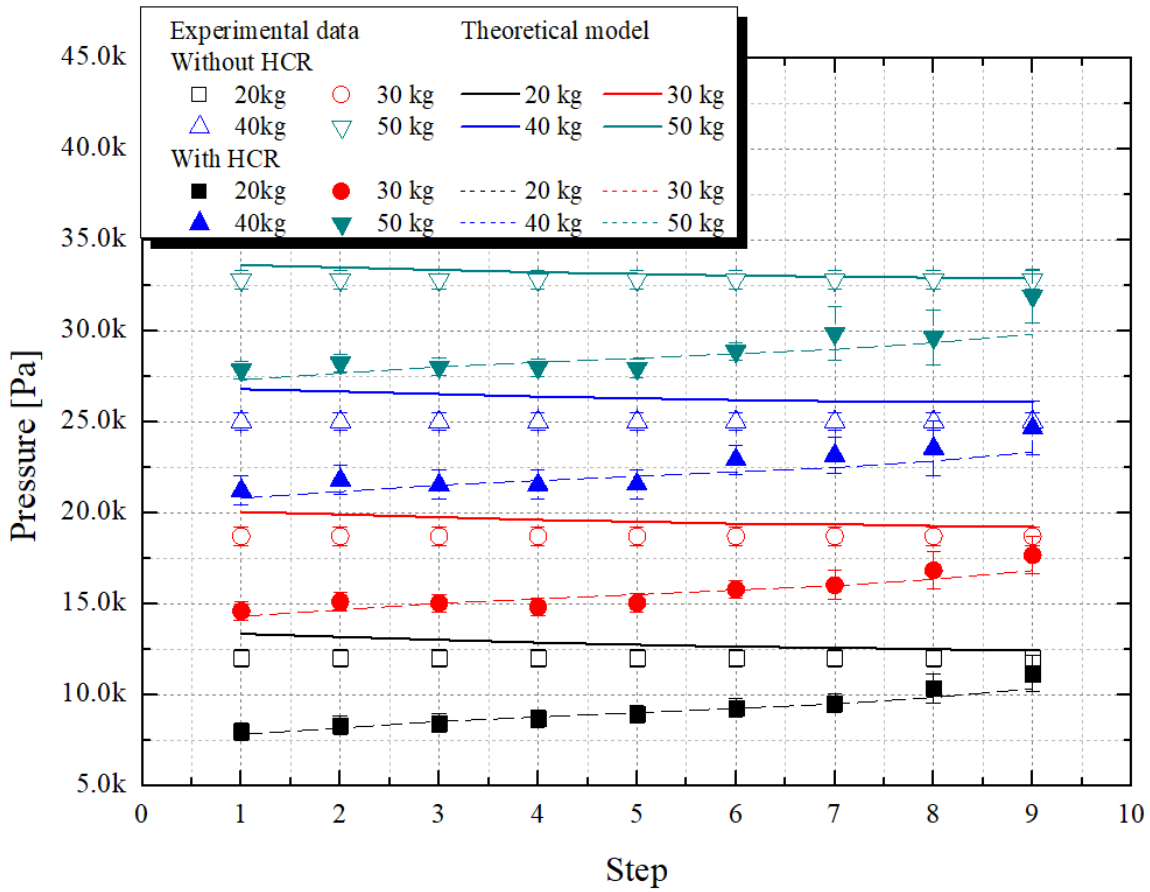

Fig. 3.22 The pressure difference of the CRDM-P according to the different step and weight conditions

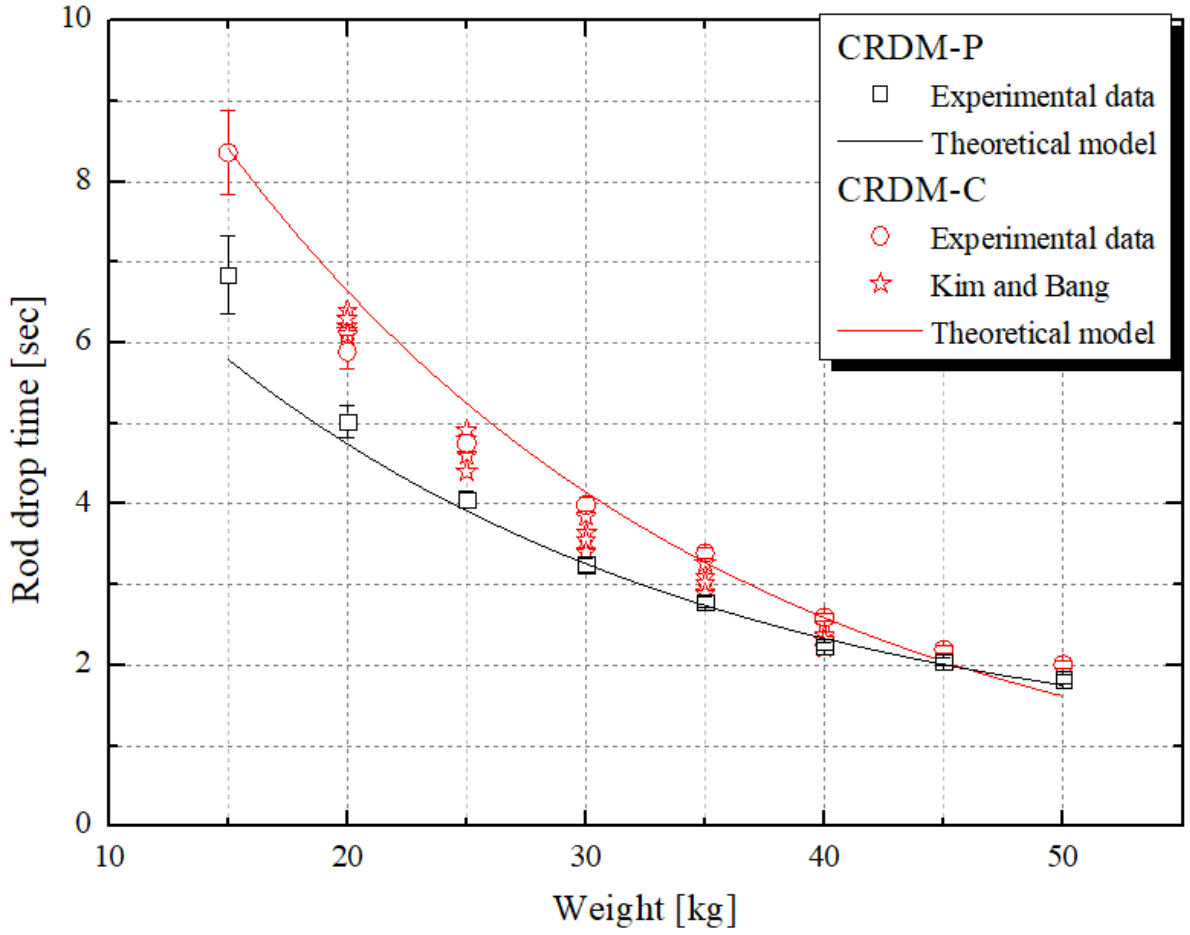

(a) Experimental results of the rod-drop test with theoretical model

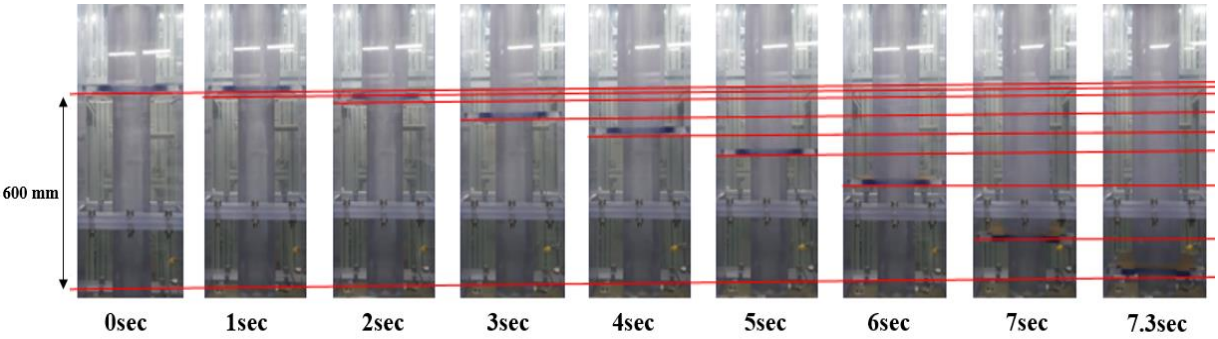

(b) Visualization of the hydraulic CRDM-P

Fig. 3.23 The drop time of the hydraulic CRDM with theoretical model

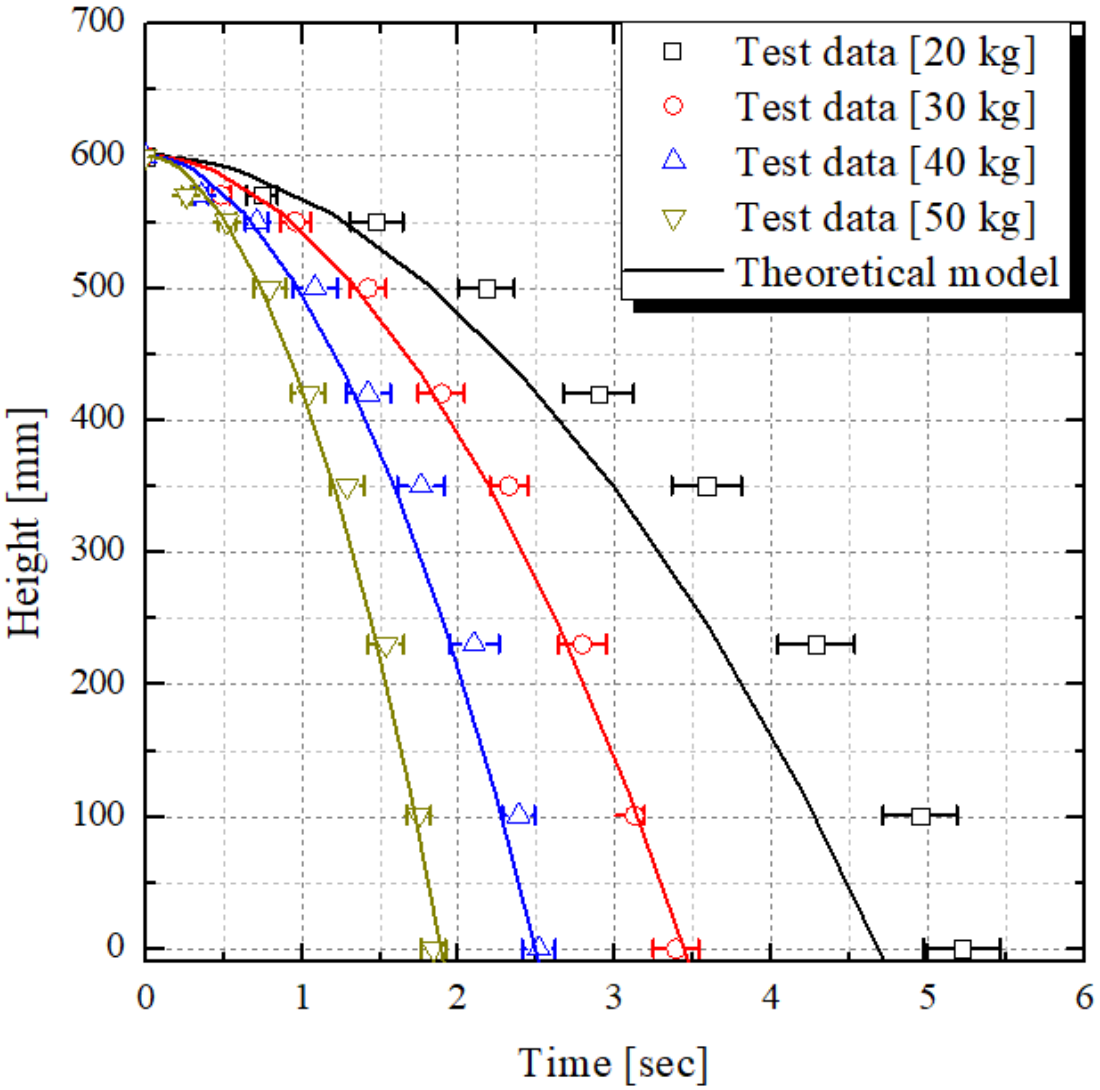

Fig. 3.24 The drop behavior of the hydraulic CRDM with theoretical model

Chapter 4. APPLICABLE DESIGN OF THE NUCLEAR POWER PLANT

4.1 Introduction

To apply the passive safety systems in nuclear power plant, the design of the full-scale system was needed. In the previous studies, one full-scale design was proposed to develop the research reactor (NHR-200) [4.1]. Before the full-scale test, the design of the hydraulic drive control rod and flow control circuits were conducted. In structure design, the conceptual design of the full-scale reactor and detail geometrical information were determined based on the experimental results of the small-scale test facilities. Especially, the major parameters such as pressure, mass flow rate, position of the hydraulic CRDM, and control velocity were confirmed by using the transient model.

In the previous chapters, the experimental tests both hybrid control rod and hydraulic CRDM were conducted to validate the theoretical models. However, the design of the integrated system was not validated due to the limitation of the experimental facility. First of all, the detail information of the commercial CRDM and modified CRDM was introduced, including the height, length, heat removal capacity, and operating condition. In a pressurized water reactor (PWR), a major portion of the CRDM is located on the upper plenum of the pressure vessel, and the shafts of control rod assembly are covered by pressure housings [4.2]. Therefore, CRDM needs penetration hole and a large space on the top of the pressure vessel. The hydraulic CRDM removes the penetration hole for CRDM nozzle combined with in-vessel strategy, and it has a shorter length in comparison with the other CRDMs such as motor driven system, magnetic jack system, and so on [4.3-4.5]. Fig. 4.1 shows the Schematics of the magnetic jack CRDM and hydraulic CRDM. Driven by the benefits of the hydraulic CRDM, several nuclear power plants have already adopted the hydraulic concept for controlling the reactor power. The suitability of the hydraulically driven CRDM for use in the spider-type PWR of IRIS reactor has been studied [4.6]. The key advantages are the elimination of the penetration-related costs, the avoidance of rod ejection accidents/transients, and a good passivity. Therefore, in this chapter, the design of the integrated system and its behaviors were confirmed by using 1-D transient models, theoretically. Second, based on the previous studies and experimental results of the PINCs, the heat removal test of PINCs was conducted to confirm the feasibility of the suggested geometry under the room temperature and pressure condition. Finally, the design of the PINCs for commercial power plant was proposed and calculated by validated theoretical model. Especially, dropping the control rod assembly into the active core is a critical activity for safe shutdown of reactor. This chapter released the rod-drop time theoretically to confirm the feasibility of the system at high-temperature.

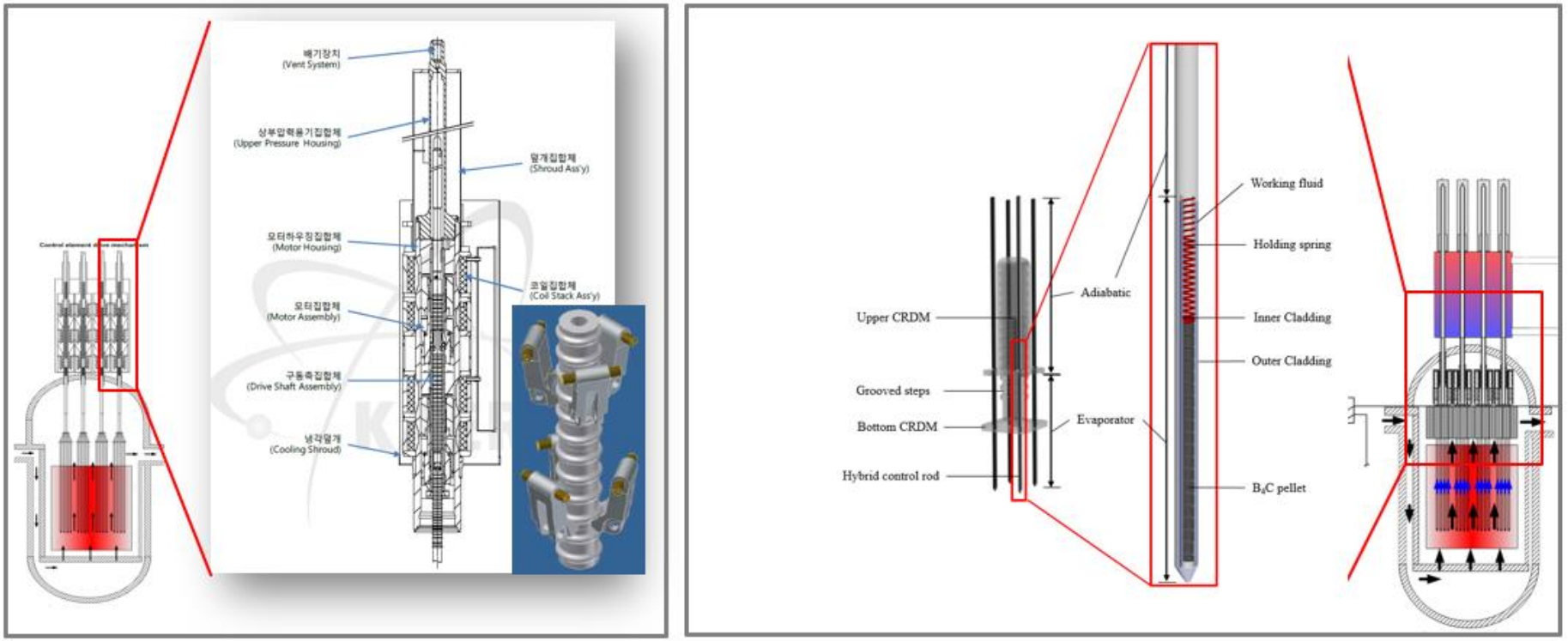

Fig.4.1 Schematics of the magnetic jack CRDM and hydraulic CRDM for PINCs [4.2]

4.2 Design of the PINCs

This section describes the PINCs and its major components. Based on the functional requirements for safe shutdown of the nuclear power plant upon an SBO, the reactor vessel, hydraulic CRDM, and water storage pool are modified. During the normal operation of the reactor, the hybrid control rod assembly (Full strength; 708 rods) used for reactor shutdown is held at the upper plenum of the reactor vessel. The reactor power is controlled by the control rods (part strength; 48 rods) [4.7]. When an accident takes place, the PINCs must be activated without any additional power to transfer the decay heat from the reactor core away from the containment building. As the first step of the reactor-shutdown operation, the inlet flow of the hydraulic CRDM decreased by shutting down the control pump. Subsequently, the hybrid control rod assemblies are inserted into the reactor core driven by the gravitational force. A hybrid control rod is a high-heat-capacity, passive heat transfer device consisting of an evaporator section, a condenser section, a neutron absorbing material (B_4C), and water (working fluid). Heat is transferred from the hybrid control rods to the natural circulation loop. The vapor generated in the hybrid control rods flows from the evaporator (inside the reactor core) to the condenser (natural circulation loop) due to the difference in vapor pressure, while the condensed liquid flows from the condenser to the evaporator due to the gravitational force. In this manner, the decay heat is transferred to a storage tank located outside the building through the natural circulation loop. In a previous study, the detailed design information was presented, and the optimal results of the heat transfer and thermal resistance were determined as 18.20 kW and 0.015 k/W, respectively [4.8, 4.9].

When the stroke length of the reactor core is 4 m, the required height of the moving part of the hydraulic CRDM is approximately 8 m. In reference reactor, control rod assemblies are considered to have both full- and part-strengths. During steady state, full-strength assemblies cannot be inserted in the reactor core, and are therefore positioned at the top of the reactor core (upper plenum). Part-strength assemblies are moved to control the reactivity of reactor power. Therefore, part-strength has separate flow control systems to allow for independent position control.

Hybrid control rods consist of a neutron absorbing material, holding spring, two layers of metal cladding, and working fluid. The decay heat of nuclear fuel is transported by the phase change heat transfer of the working fluid between inside cladding and outside cladding. Boron carbide pellets consisting of enriched B^{10}, therefore, it has a reduced diameter and space inside hybrid control rod. Table 4.1 shows the detailed information of the hybrid control rod assemblies.

In this study, a feasibility test of 4 finger CRDM-P connected with hybrid control rod was conducted. Hydraulic units were designed and modified to satisfy the heat removal and passive control requirements from previous researches [4.4-4.6, 4.10], in-vessel CRDM [4.8, 4.9, 4.11], and the magnetic jack CRDM in reference reactor [4.7]. The features for the control rod drive system include: 1) stable control,

2) accuracy under normal operating conditions, and 3) achievement of a reactor scram time that is less than the design requirement [4.9]. Most CRDMs use a mechanically driven system with a stepped geometry to control the reactivity of reactor core [4.12]. The proposed CRDM also has the stepped geometry in the hydraulic unit.

Table. 4.1 Detailed information of the hybrid control rod assemblies

Material (cladding)		Inconel 625
Material (Holding spring)		Inconel 625
Material (CRDM)		Steel alloy
Thickness of cladding, mm		0.89
Outer diameter of cladding, mm		20.73
Absorbing material		B_4C pellets
Length, mm	Evaporator	4,300, B_4C pellets location
	Adiabatic	8,000
	Condenser	4,000 (Fixed)

4.3 Applicable heat removal design and its feasibility test

4.3.1 Experimental setup and procedures

Using the scaled test facility, an experiment has been performed to test the heat removal of the PINCs concepts. The test section is designed with a 1/12 scale control rod assembly (4 hybrid control rod), and the experiments are conducted at room temperature. Fig. 4.2 shows the schematic of test facility including a pump, hydraulic cylinders with flow control system, flow meter, cartridge heaters, and water tank. Six thermocouples and two pressure gauges were installed to measure the temperature of pool and pressure difference between the inside of the hydraulic cylinder and outside pool. The test sections consist of polycarbonate (PC) material for observing the elevation of CRDM and hydraulic control rods. The information of the APR1400 and test facility are listed in Table 4.2. The hybrid control rod is inserted in the evaporator, and it is subject to constant heat from the cartridge heater when the evaporator is a 60 ℃. The surface of hybrid control rod and evaporator and the temperatures of condenser pool

are measured using the K-type thermocouples.

4.3.2 Experimental results

In general, heat pipe devices are used for transferring the heat in a fixed position , including the electric cooling systems, CPU cooling, and nuclear application [4.13-4.16]. The hybrid control rod requires the ability to move the elevation owing to enable passive shutdown during the accidents. In previous researches, the design of hydraulic CRDMs cannot satisfy the heat removal geometry owing to the use of magnetic jack and shaft-connected assemblies. Therefore, it is necessary to certify the performance of CRDM-P with hybrid control rod assemblies in removing heat by inserting control rods in the heated pool.

Fig. 4.3 shows the pool temperature and heat transfer coefficient of the hybrid control rod assemblies. After the free drop inside evaporator pool, the test results show how the pool temperature changes. During the heat removal test, fixed heat load (600W) was maintained. The removed heat from the hybrid control rod must consider stored heat of evaporator pool, therefore, the stored heat of the hybrid control rod can be determined by

$$Q_{overall} = 4 \cdot Q_e + Q_{stored} \tag{4.1}$$

$$Q_{stored} = mC_p \Delta T \tag{4.2}$$

During the test, 8 thermocouples were installed on the surface to confirm the heat transfer coefficient of hybrid control rod. The heat transfer coefficient can be determined by

$$h_{o,bundle}(W/m^2 °C) = \frac{q_e^{"}}{\overline{T_e} - \overline{T_c}} \tag{4.3}$$

The heat removal of control rods was identified from the change of the temperature. The time needed for the pool temperature to reach 90 °C was delayed by approximately 2.51 times compared to those of no hybrid control rod. The heat removal test showed the possibility of applying the in-core hydraulic drive system to PINCs.

4.4 Design of the hydraulic CRDM-P with sensitivity of the operation temperature

The hydraulic CRDM for PINCs is located in the reactor pressure vessel, therefore, it operates at high-temperature. In the reference reactor, the temperature is approximately 300 ºC. According to the governing equation, the density and viscosity are important to determine the steady flow and drop time. In previous studies, the water property table and fitting equations were used for calculating the steady flow rate and the rod drop of the control rod [4.9]. In this paper, the following equations of the working fluid properties as a function of temperature were used based on reference data [4.17].

$$\rho = -3.0115 \cdot 10^{-6} T^3 + 9.6272 \cdot 10^{-4} T^2 - 0.11052T + 1022.4, \quad 273.2K \le T \le 600K \tag{4.4}$$

$$\mu = 3.8208 \cdot 10^{-2} (T - 252.33)^{-1}, \quad 273.2K \le T \le 600K \tag{4.5}$$

In general, rod drive systems have control steps for controlling the position of the control rod assemblies systematically. In APR1400, the CRDM has 200 steps with a step pitch of 19.05 mm [4.2]. Therefore, these values were adopted for CRMD-P where the pitch represents the interval between each step. Table. 4.2 shows the design specification of the hydraulic CRDM in the nuclear power plant. Both CRDM-C and CRDM-P were designed and comparatively analyzed based on calculated results. Totally, 93 units of control rod assembly were required (48×12-finger control rod assembly, 45×4-finger control rod assembly). In the case of 12-finger control rod assembly, the maximum weight of the conventional CRDM is 156.2 kg. In contrast, the hydraulic CRDM has additional weight owing to the shape of the cylinder. Accordingly, the weights of the CRDM-P and CRDM-C were in the range of 100–200 kg and 120–220 kg, respectively.

The mass flow rates for operating the CRDM-C and CRDM-P in a nuclear power plant are shown in Fig. 4.4. The mass flow rate of the CRDM-C is a stable value of 37.5 kg/min with $\pm$2.72 kg/min deviation, whereas that of the CRDM-P is in the range of 50.0–106.2 kg/min owing to the CRDM step. These results mean that the CRDM-P needs additional pumping power; therefore, the optimization of the CRDM-P is needed to mitigate the energy demand.

The rod-drop time according to the weight of hydraulic CRDM is a critical parameter to determine the nuclear safety. The required drop time for a pressurized water reactor is maximum 4 s; therefore, in the hydraulic CRDM for PINCs, the rod-drop time of the control rod satisfied the requirement for reactor shutdown [4.2]. Fig. 4.5 shows the rod-drop time according to the weight of hydraulic CRDM in a nuclear power plant. Fig. 4.6 shows the required rod-drop time of APR1400. To confirm the effect of the geometry, weight, and operating temperature of the hydraulic CRDM, the calculation of several rod-drop conditions was shown in Fig. 4.7.

Table. 4.2 Design specification of the hydraulic CRDM for application in nuclear power plant

Parameters	CRDM-C	CRDM-P	Unit
Weight of CRDM	100-200	80-180	kg
Cylinder inner diameter	0.065	0.055	m
Cylinder outer diameter	0.075	0.065	m
Step pitch	0.01905	0.01905	m
Steps	200	200	-
Number of CRDM	48 (12-finger control rod assembly) 45 (4-finger control rod assembly)		-
Total control length	4.00	3.81	m
Mass flow rate	34.8 – 40.2 (steady flow)	50.5 – 106 (steady flow)	kg/s
Hybrid control rod	O.D. : 0.0207 I.D. : 0.0199 Total length : 12.00		m
Operation temperature	573		K
Drop height	3.81		m

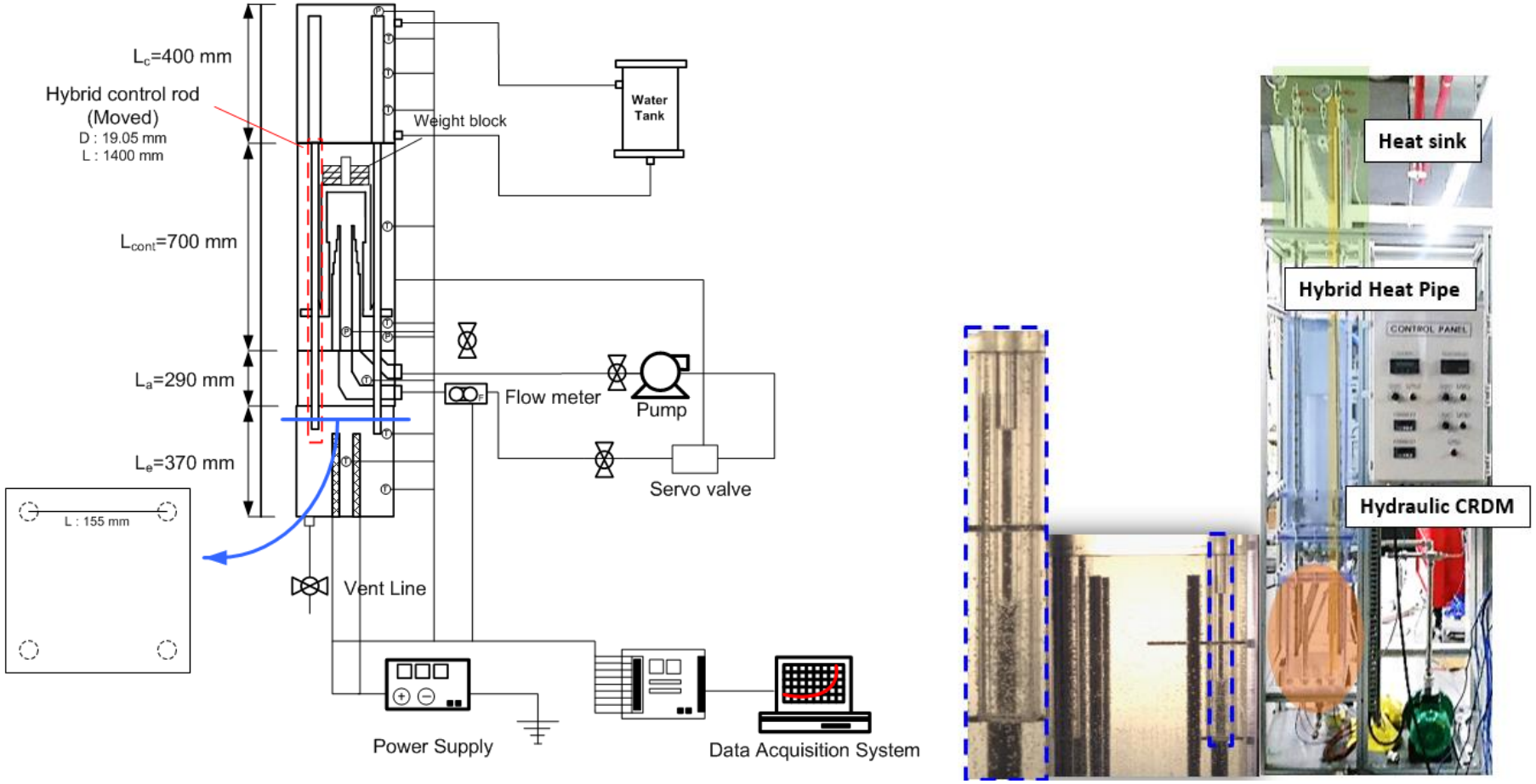

Fig. 4.2 The test facility of the hydraulic CRDM test and its schematic

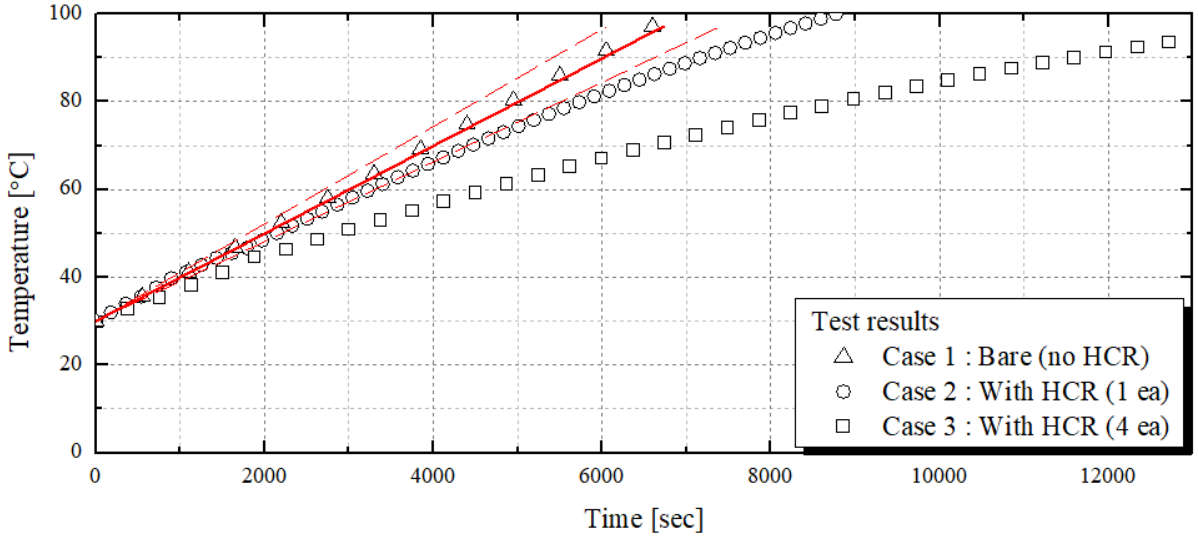

(a) The evaporator pool temperature

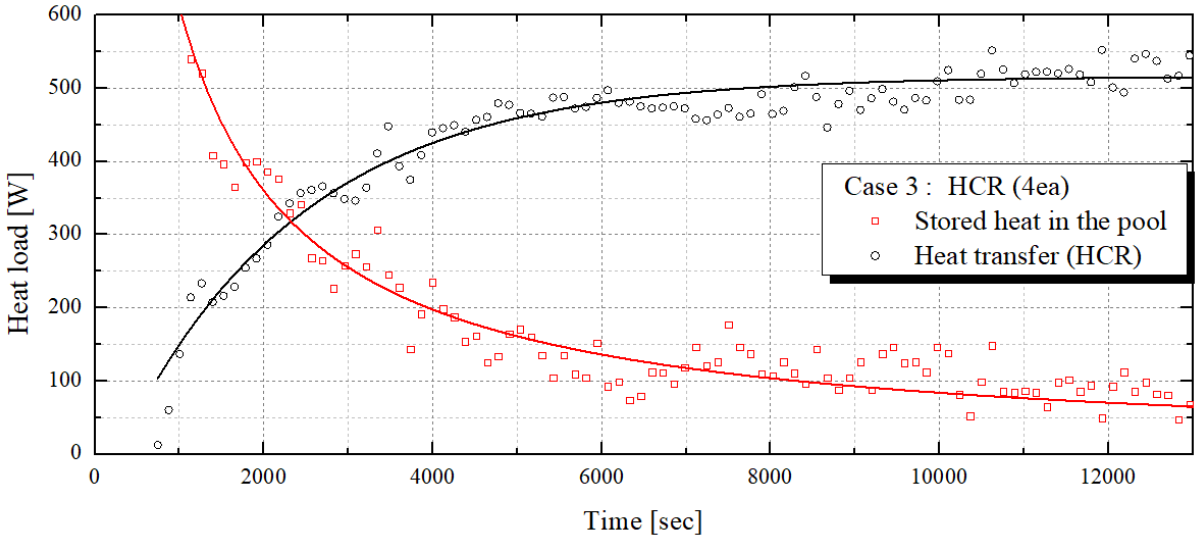

(b) Stored heat and transferred heat during experiment

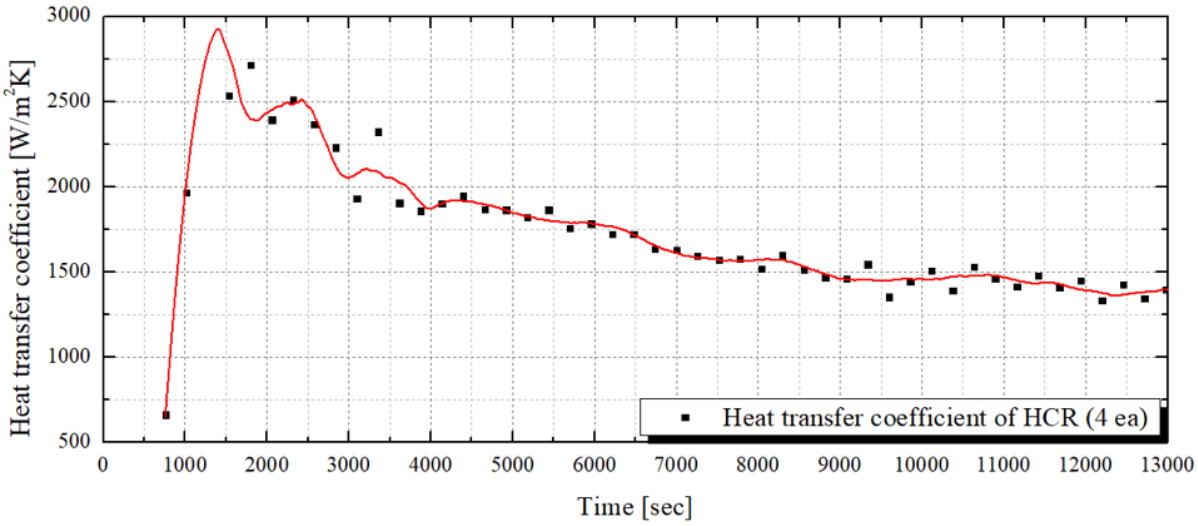

(c) Overall heat transfer coefficient

Fig. 4.3 Experimental results of the Heat removal test

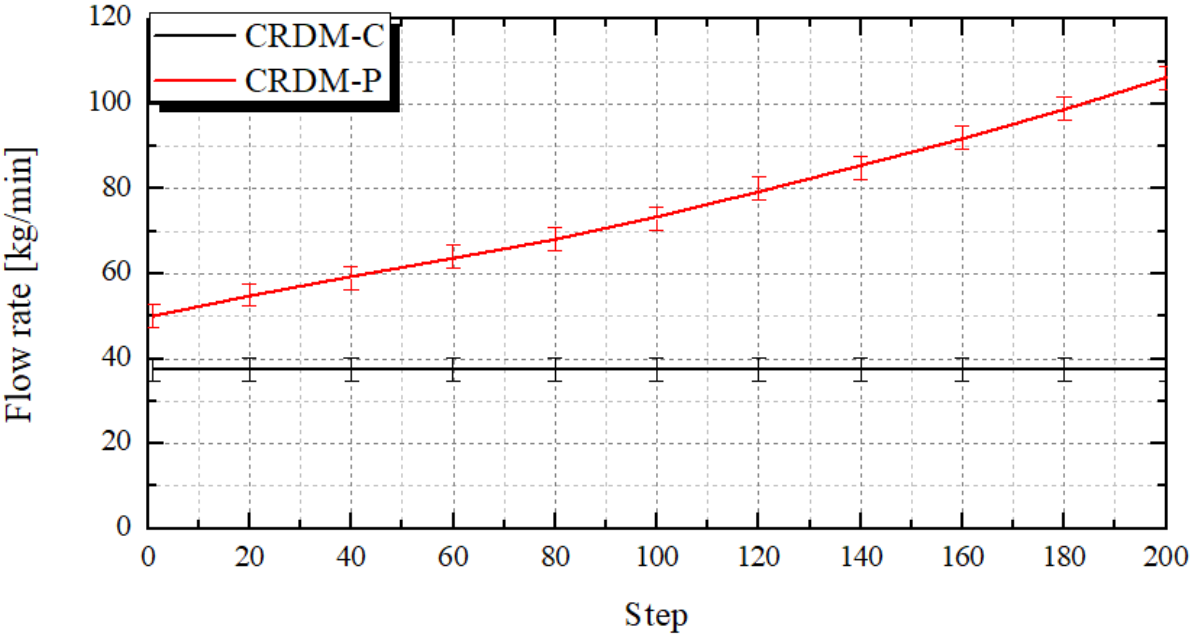

Fig. 4.4 Mass flow rate for operating the hydraulic CRDM in nuclear power plant

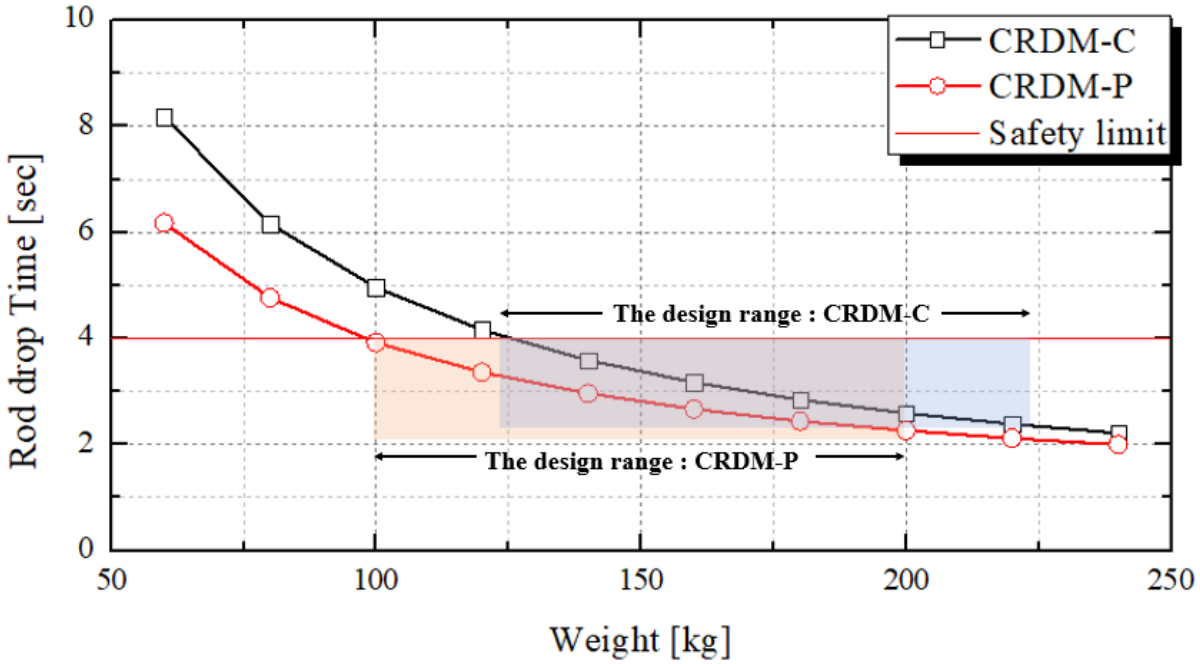

Fig. 4.5 The rod-drop time according to the weight of hydraulic CRDM in the nuclear power plant

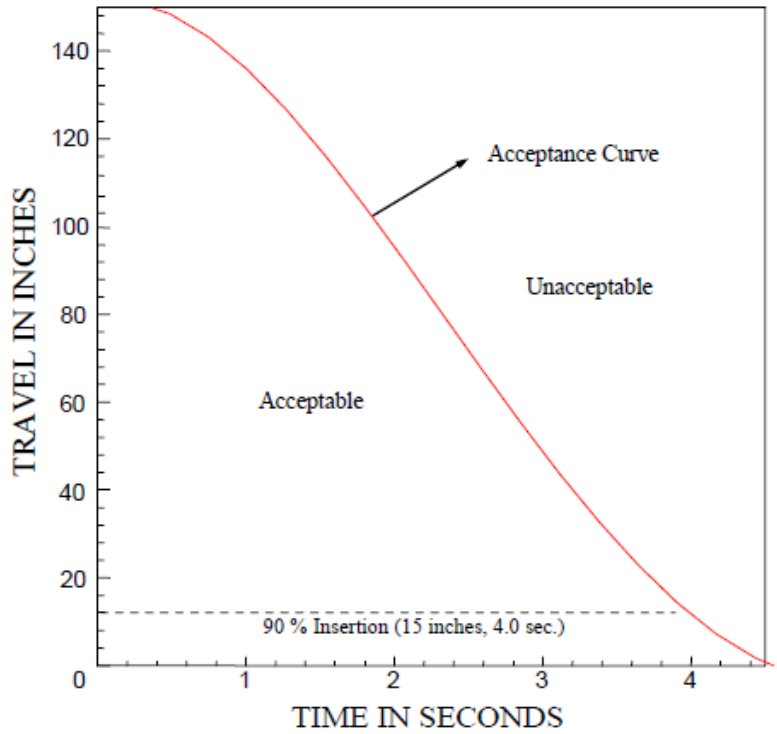

Fig. 4.6 Required rod-drop time of APR1400 [4.2]

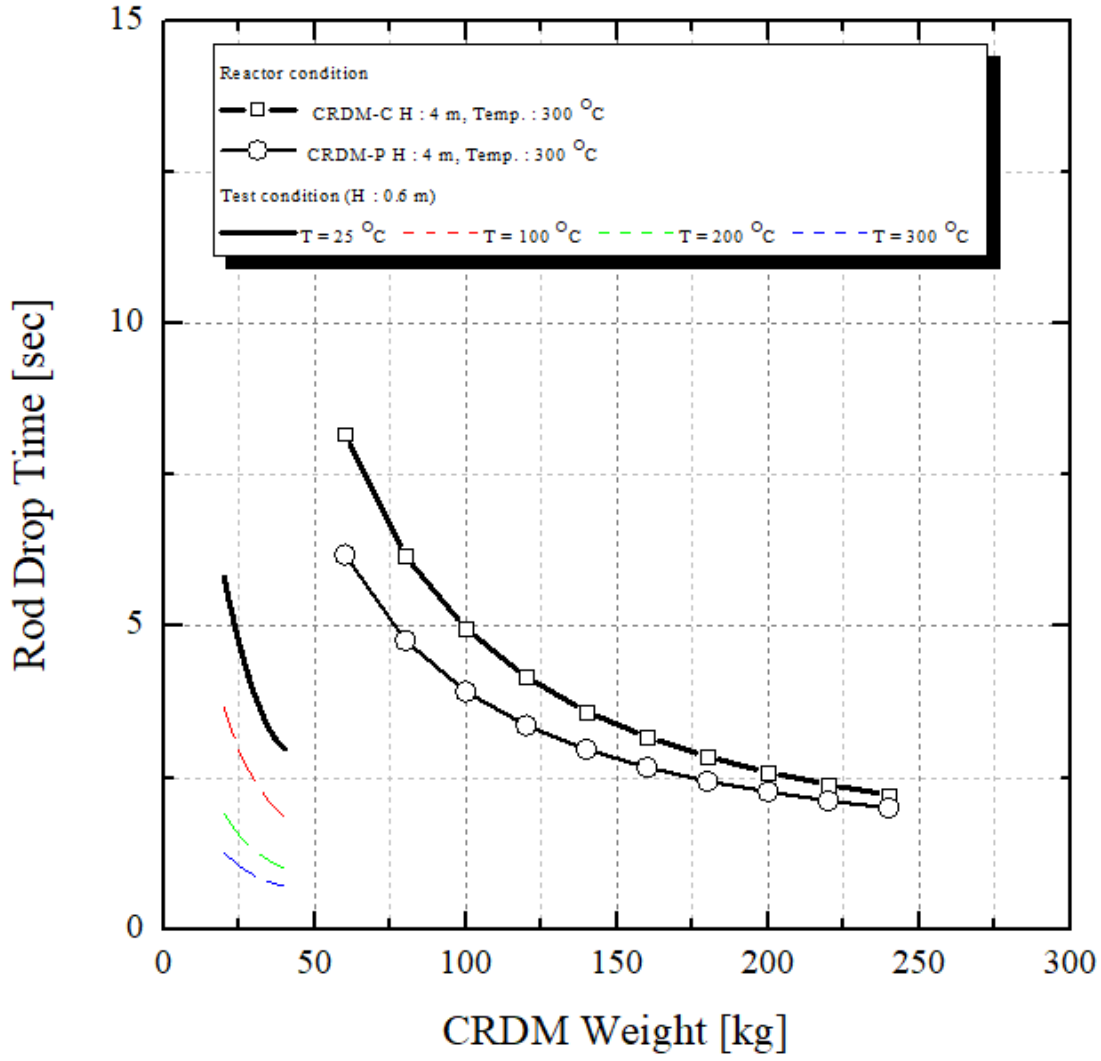

Fig. 4.7 The effect of the operating temperature, weight, and geometry of the CRDMs

4.5 Prediction of heat removal performance in nuclear power plant

In chapter 4.3, the heat removal test of bundle hybrid control rod was conducted, experimentally. Based on the proposed design, the heat removal performance of PINCs was predicted by the safety analysis using the multidimensional analysis of reactor safety code (MARS-KS) in APR1400. In previous studies, the optimal heat removal of single hybrid control rod was determined based on the merit number of thermosyphon heat pipe [4.18]. Therefore, the total heat capacity of PINCs was determined, approximately 4.248 MWth (708 control rods for shutdown CRDMs) in commercial nuclear power plant. Fig. 4.8 shows the nodalization of APR-1400 for verifying the effect of PINCs in nuclear power plant. During the station blackout, the trip of the reactor coolant pump and turbine assumed as 1.0 sec after reactor trip signal. The malfunction of the high pressure, low pressure safety injection, and turbine driven auxiliary feedwater system were assumed. Table. 4.3 describes the station blackout scenario of APR-1400. From the calculated results, the time of the fuel melting and hydrogen production were delayed. The core uncover time and the time of hydrogen production are delayed approximately 35 minute and 50 minute, respectively, as shown in Fig. 4.9. From the calculated results, it is possible to decay the critical phenomena such as the time of the peak cladding temperature and core uncover. Therefore, the response time to mitigate/defense the severe accident will be increased.

4.6 Failure/degradation of PINCs in nuclear power plant

Proposed system (PINCs) is a new concept of the passive safety system for advanced nuclear power plants, therefore, the discussions including the failure and degradation of PINCs are needed to adopt PINCs in nuclear power plants. In this chapter, the failure effects of hybrid control rod and hydraulic CRDM are explained.

4.6.1 Accident scenarios

There are various accident and transient scenarios based on the initiating events to categorize the transient conditions, as shown in Fig. 4.10. Except reactivity induced accidents, the hybrid control rod will be dropped into the reactor core during accident scenarios. The control rod ejection and control rod malfunction don’t occur due to the in-vessel strategy in case of PINCs. The critical scenario of nuclear power plant is the station blackout with the malfunction of emergency power supply (similar to Fukushima accident). In the event of this accident, the depressurization in the primary system does not occur and the active safety systems do not work. The uniqueness of PINCs is the operation without any additional power and is possible to work under the non-depressurized condition. Therefore, to verify the effect of PINCs, the station blackout condition was collected and analyzed.

4.6.2 Failure of hybrid control rod and hydraulic CRDM

The crucial failure and degradation of PINCs are 1) Failure of hybrid control rod and 2) failure of hydraulic CRDM (CRDM-P). In case of failure of hybrid control rod, the heat removal capacity is decreased and the driving force of hydraulic CRDM is changed according to the number of the failed hybrid control rods. The degraded heat capacities of hybrid control rod (Failure rate: 0%, 25%, and 50%) were calculated by using the MARS-KS code. The heat capacity was same as the previous results in chapter 4.5. Fig. 4.11 shows the effect of the failure and degradation of hybrid control rod in nuclear power plant. The core uncover times of failure: 0%, 25%, and 50% were estimated to be 140 min, 128 min, and 115 min, respectively. The times of hydrogen production are also estimated to be 167 min, 146 min, and 135 min, respectively. To mitigate the failure effect of hybrid control rod, the inspection of PINCs is required during the refueling period.

In 200 kg weight of hydraulic CRDM, the ratio of upward driving forces is approximately 8 to 18% of hydraulic CRDM according to the elevation of hydraulic cylinder. If the hybrid control rods were failed, the driving force of hybrid control rod was decreased according to the failure ratio. In case of the failure condition, the change of the driving force is shown in Fig. 4.12. The pressure difference and mass flow rate will be increased according to the increase of failure ratio, owing to decrease the driving force of hybrid control rod (upward force). Based on the experimental results, it is possible to predict the range of the mass flow rate and pressure difference during the step control. The operating range are determined by the range between with and without hybrid control rod. If the ratio of failed hybrid control rod is higher than those of well-operated hybrid control rod, the trendline is estimated to be a similar to the hydraulic CRDM without hybrid control rod. Fig. 4.13 shows the estimated range of mass flow rate and pressure difference of hydraulic CRDM with failed hybrid control rod in experimental data.

In case of failure of hydraulic CRDM, the mass flow rate was decreased (bypassed mass flow rate through crack on the cylinder), therefore, the required pumping power and inlet mass flow rate will be increased. In Fig. 4.14, the required mass flow rate is estimated according to the break area of hydraulic cylinder. In case of 25% crack ratio (crack ratio : crack area/cross-sectional area of flow path), required mass flow rate is estimated to be 156.3% of undamaged case of PINCs. It was confirmed that the effect of damage was highly significant on the mass flow rate of PINCs. Therefore, it is necessary to determine the pump performance of hydraulic CRDM by considering theses influences and to prepare manuals in case of an unexpected accident. Fortunately, however, under the conditions of failure that do not required steady flow rate, the control rod will drop to the reactor core and shutdown the nuclear power plant.

Table. 4.3 Station blackout scenario of APR-1400

Event	Remarks
Reactor trip	Trip
RCP trip	Reactor trip + 1.0
Turbine trip	Reactor trip + 1.0
SIT	Primary pressure < 4.3 MPa
HPSI and LPSI trip	Trip
MSSV	Control pressure of steam generator (Open : P > 8.1 MPa, Close : P < 7.3 MPa)
POSRV	Pressurizer pressure > 17.24 MPa (Open) < 14.07 MPa (Close)
Turbine driven auxiliary feedwater system	Trip

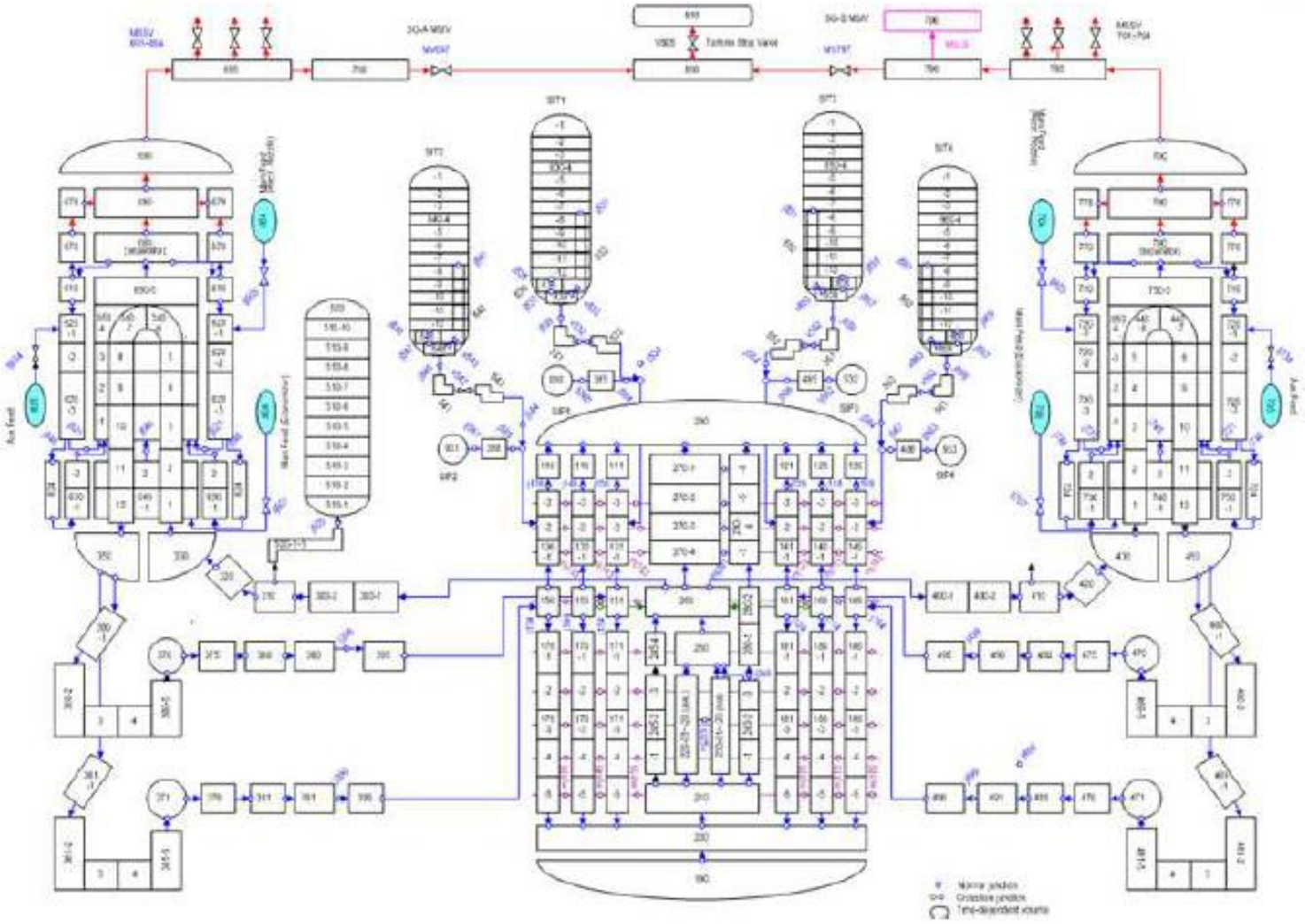

Fig. 4.8 Nodalization of APR1400

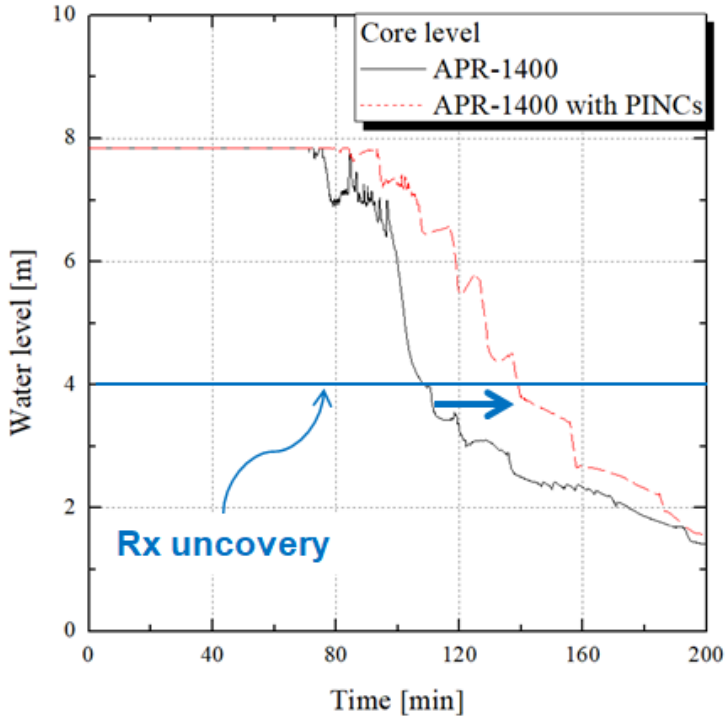

(a) Collapsed water level at the reactor core

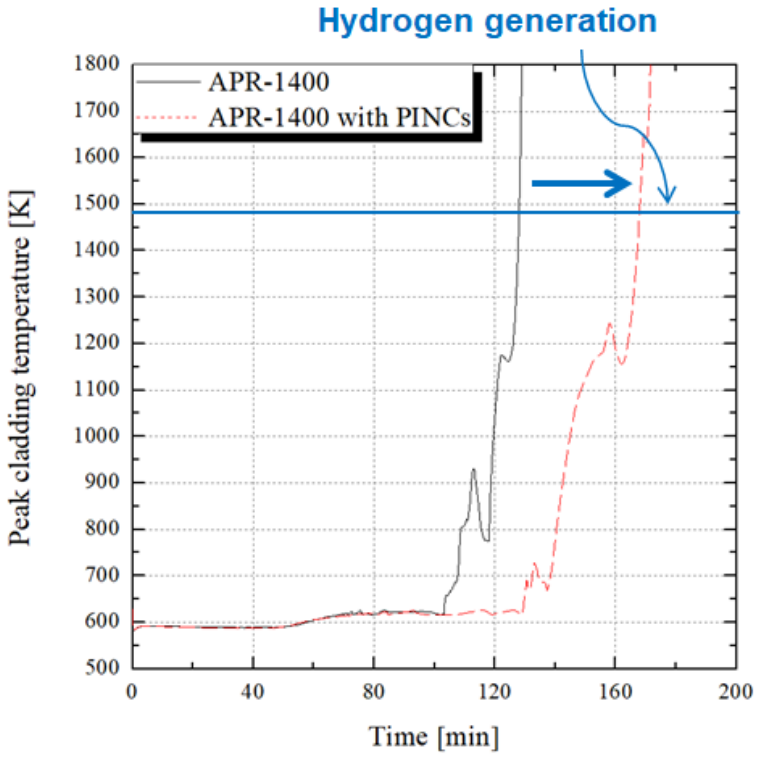

(b) Peak cladding temperature

Fig. 4.9 The effect of PINCs during the station blackout

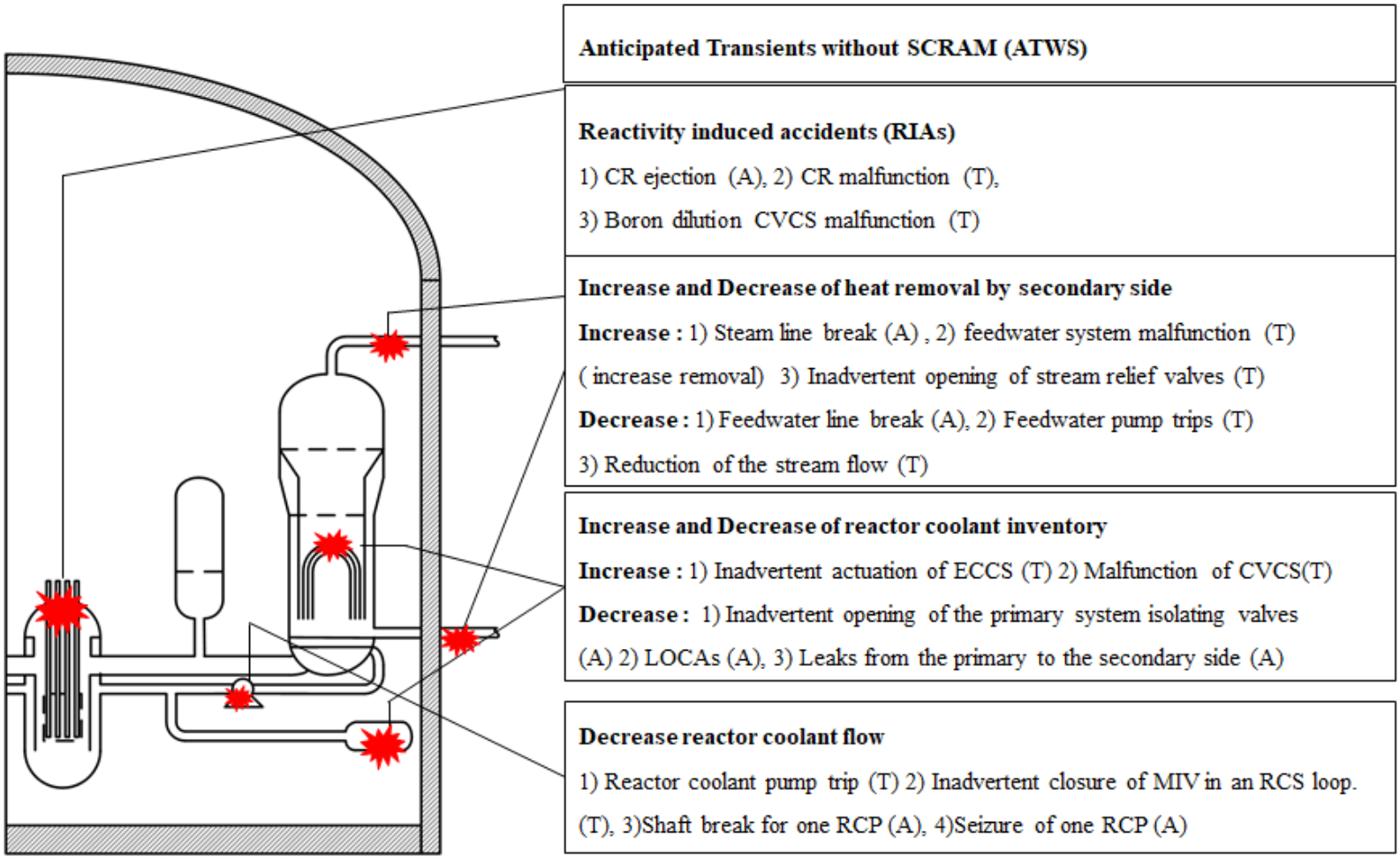

Fig. 4.10 Initiating events and their categorization

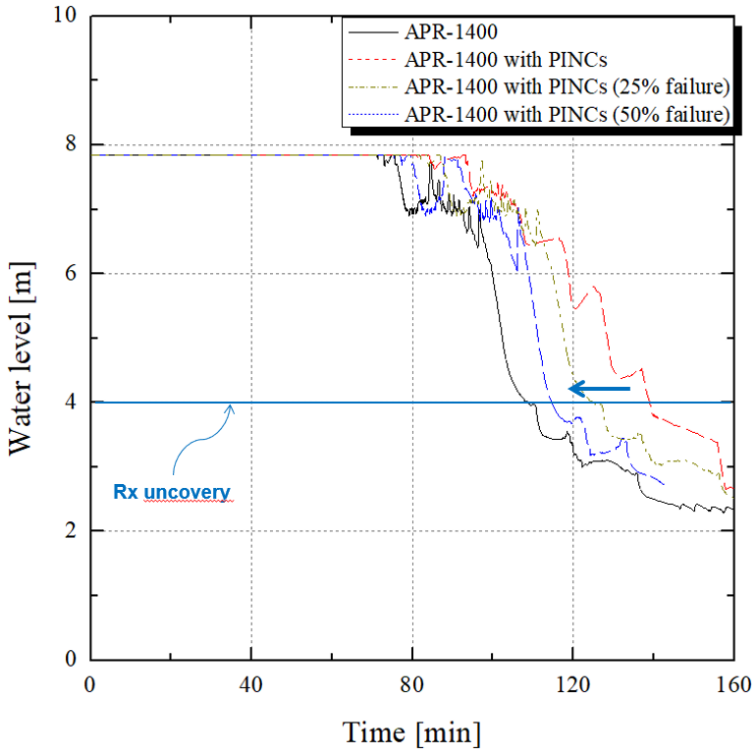

(a) Collapsed water level

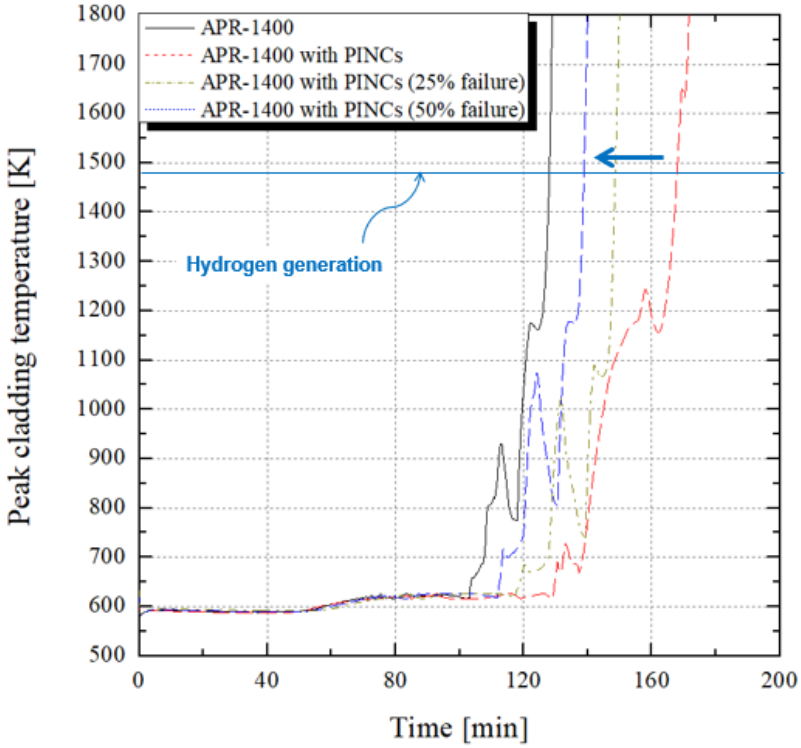

(b) Peak cladding temperature

Fig. 4.11 The effect of the failure of hybrid control rod

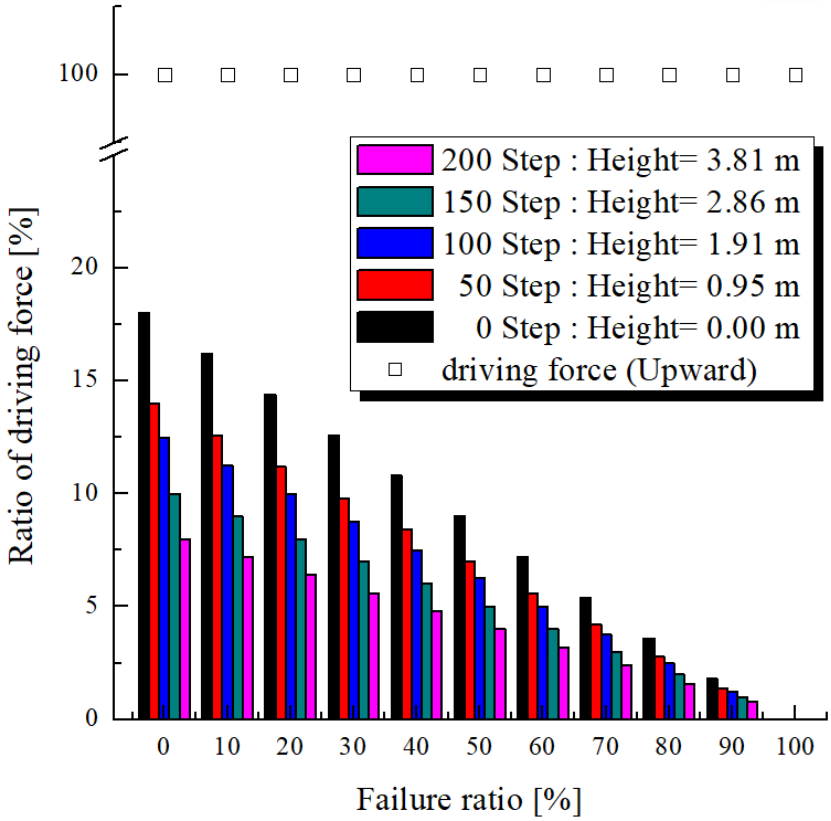

Fig. 4.12 The change of the ratio of the driving force according to the height and failure ratio

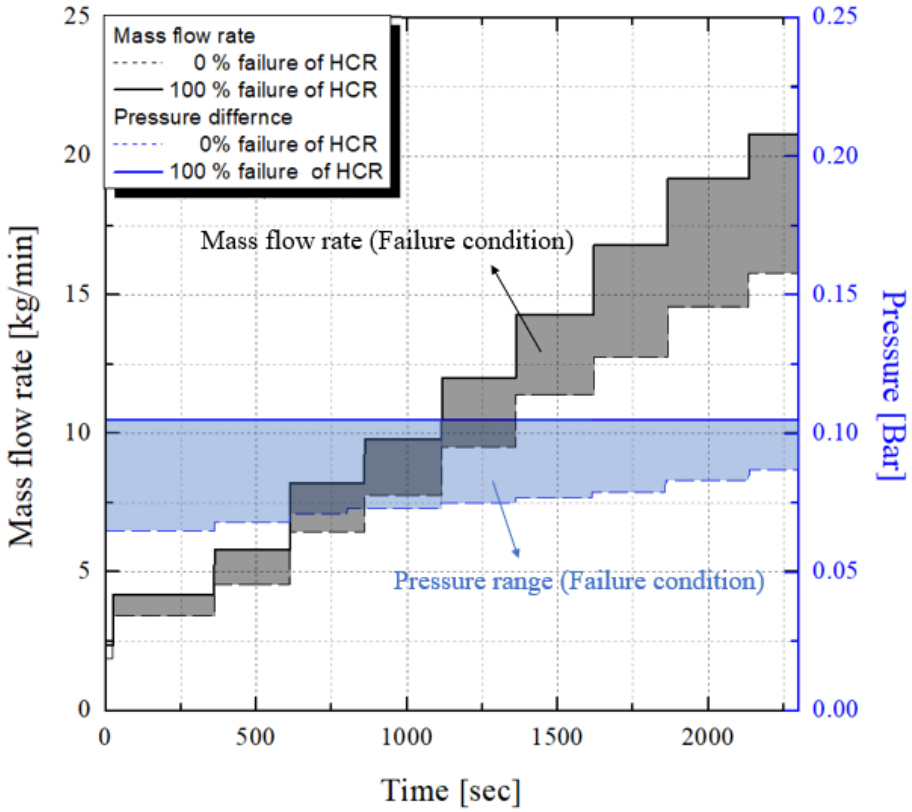

Fig. 4.13 The estimated range of mass flow rate and pressure difference of hydraulic CRDM with failed hybrid control rod

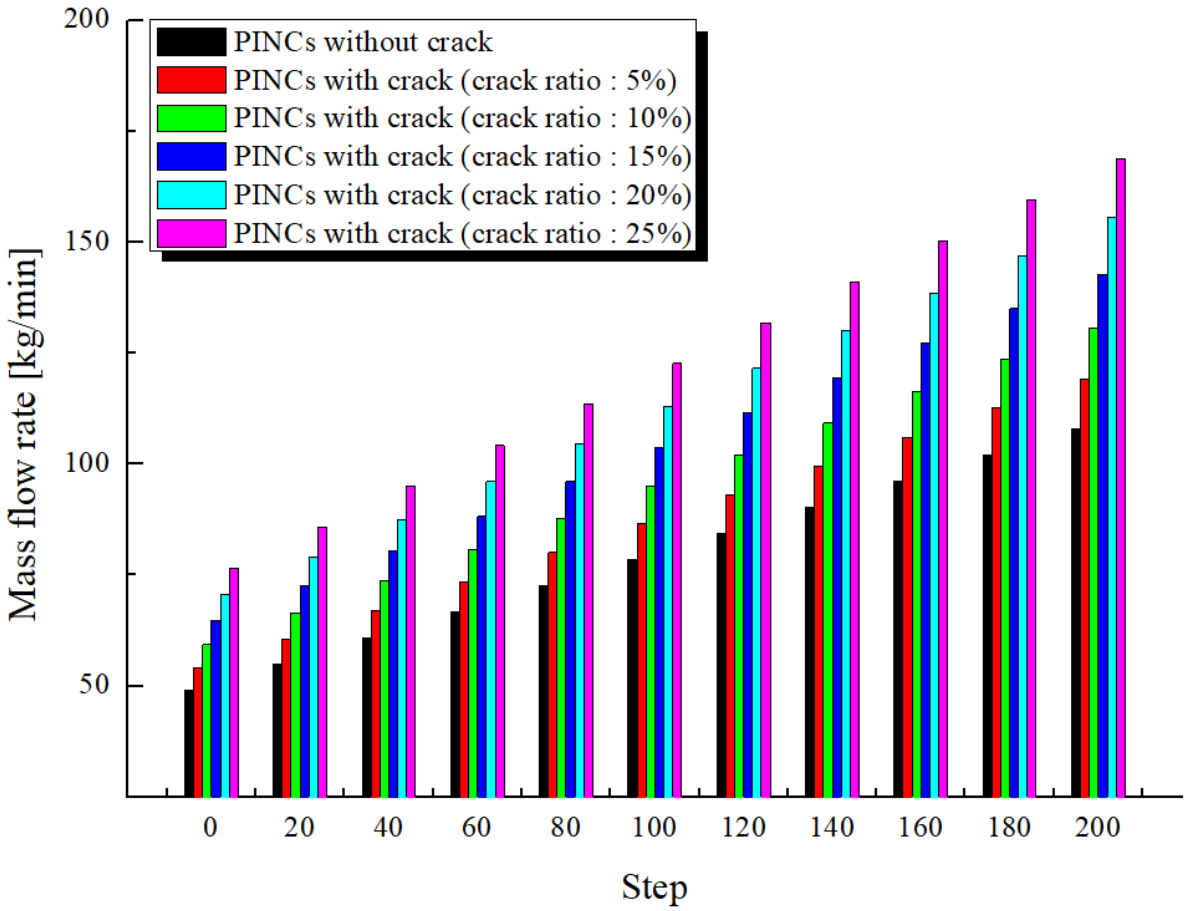

Fig. 4.14 The required mass flow rate according to the break area of hydraulic cylinder

Chapter 5. CONCLUSIONS AND RECOMMENDATIONS

5.1 Conclusion

The safety system in nuclear power plants is one of the crucial research topic owing to the massive impact of nuclear disasters such as Fukushima accident in Japan. To mitigate the impact of the design extension conditions, the importance of the passive safety system significantly increased. To achieve the enhancement of passive safety, the passive in-core cooling system (PINCs) was proposed and developed. As one of the major components of PINCs, the hydraulic control rod drive mechanism (CRDM) was designed and modeled.

5.1.1 Modeling of the hydraulic control rod drive mechanism (CRDM)

Hydraulic CRDM which control the elevation of control rod assemblies was designed and modeled including the operation strategy, control method, and geometries. The conventional designs of hydraulic CRDM had a grooved cylinder or pattered holes owing to control the position of control rod assemblies. In contrast, hydraulic CRDM for PINCs had used the stepped cylinder and hybrid control rod assemblies for achieving the functions both the decay heat removal and elevation control. The previous models for hydraulic CRDMs had large errors compared to the experimental data. Therefore, driving forces for the hydraulic CRDM was modified, including the pressure differential force between the hybrid control rod and pool, pressure differential force between hydraulic cylinder and pool, gravitational force, buoyancy force, and friction in the guide tube. Based on the force balance equation, the modeling of the hydraulic CRDM with hybrid control rod was developed, theoretically. To validate the driven models, the pressure differential force, mass flow rate, and position of the hydraulic CRDM was measured by experiments. The operational characteristics of hydraulic CRDM and the effect of major parameters were analyzed.

5.1.2 Application of the hydraulic CRDM

Based on the theoretical model, the applicable design of PINCs was proposed and tested by using the small scaled test facility. The hydraulic CRDM for PINCs exhibits unique features: Position tracking using the mass flow rate, 2) smooth flow and pressure gradient during the step control, and 3) possibility to remove heat using hybrid control rods. The heat removal test was conducted with 4-finger hybrid control rod assemblies. From the measured temperature of the hybrid control rod, evaporator pool, and condenser pool, the capacity of the heat transfer was confirmed, experimentally. Due to the high pressure and temperature condition of the nuclear power plants, the full-scale design of the hydraulic CRDM was performed. In reactor operating condition, the rod drop time satisfied the safety requirement.

In addition, the model of hydraulic CRDM can be used to the general nuclear power plants for controlling the reactor power (without hybrid control rod). In nuclear power plants, the hydraulic CRDM will be a good candidate owing to the good passivity and elimination of the rod ejection accidents.

The traditional role of the nuclear power plant was the baseload source of electricity. However, recent energy trend was changed toward mixed, small, and flexible to satisfy the electricity demand. Therefore, the load-following mode of the nuclear power plant is a key issue for sharing the role of electricity generation with renewable energies. In order to become eligible for operation in load-following control method, the high accuracy control method and enhanced safety feature are required. The proposed hydraulic CRDM could be a good candidate to load-following operation due to the high accuracy and passivity in comparison with the previous concept of hydraulic CRDMs.

5.2 Recommendations

The passive safety is an important issue in the nuclear field, especially commercial nuclear power plants and Gen.IV reactors. Passive in-core cooling system with hydraulic CRDM is a good candidate to enhance the passive safety owing to no signals and power for removing the decay heat. Especially, hydraulic CRDM have good advantages such as passive shutdown, elimination of the rod ejection accident (in-vessel system), and compact CRDM. Therefore, the application of hydraulic CRDM will make a strong contribution to the enhanced passive safety in nuclear power plants. The present study provides the validated modeling to design of the hydraulic system with a solution of the critical issues of PINCs. Therefore, this study can be used for applicating the decay heat removal and reactor power control systems in the passive in-core cooling system and various type of nuclear power plants.

References

1.1. Jeon IS, Kang HG. Development of an operation strategy for a hybrid safety injection tank with an active system. *Nucl Eng Technol.* 2015;47(4):443-453. doi:10.1016/j.net.2015.01.008

1.2. Chang SH, Kim SH, Choi JY. Design of integrated passive safety system (IPSS) for ultimate passive safety of nuclear power plants. *Nucl Eng Des.* 2013;260:104-120. doi:10.1016/j.nucengdes.2013.03.018

1.3. Bae BU, Yun BJ, Kim S, Kang KH. Design of condensation heat exchanger for the PAFS (Passive Auxiliary Feedwater System) of APR+ (Advanced Power Reactor Plus). *Ann Nucl Energy.* 2012;46:134-143. doi:10.1016/j.anucene.2012.03.029

1.4. Kang KH, Bae BU, Kim S, Cho YJ, Park YS, Kim BD. Experimental Study on the Operational and the Cooling Performance of the APR + Passive Auxiliary Feedwater System. 2012;44(6):2081-2087.

1.5. Wu P, Gou J, Shan J, Zhang B, Li X. Preliminary safety evaluation for CSR1000 with passive safety system. *Ann Nucl Energy.* 2014;65:390-401. doi:10.1016/j.anucene.2013.11.031

1.6. Yan W. Preliminary study for the passive containment cooling system analysis of the advanced PWR. *Energy Procedia.* 2013;39:240-247. doi:10.1016/j.egypro.2013.07.210

1.7. Kim IG, Bang IC. Hydraulic control rod drive mechanism concept for passive in-core cooling system (PINCs) in fully passive advanced nuclear power plant. *Exp Therm Fluid Sci.* 2017;85. doi:10.1016/j.expthermflusci.2017.03.013

1.8. Jeong YS, Kim KM, Kim IG, Bang IC. Hybrid heat pipe based passive in-core cooling system for advanced nuclear power plant. *Appl Therm Eng.* 2015;90:609-618. doi:10.1016/j.applthermaleng.2015.07.045

1.9. Kim IG, Kim KM, Jeong YS, Bang IC. Flow visualization and heat transfer performance of annular thermosyphon heat pipe. *Appl Therm Eng.* 2017;125. doi:10.1016/j.applthermaleng.2017.07.116

1.10. Kim KM, Bang IC. Thermal-hydraulic phenomena inside hybrid heat pipe-control rod for passive heat removal. *Int J Heat Mass Transf.* 2018;119:472-483. doi:10.1016/j.ijheatmasstransfer.2017.11.138

1.11. Development of the CEDM motor assembly for the APR+ reactor, KAERI/TR-4081/2010

1.12. Ricotti ME, Cammi A, Carelli M, et al. Hydraulically driven control rod concept for integral

reactors: Fluid dynamic simulation and preliminary test. *Glob 2003 Atoms Prosper Updat Eisenhowers Glob Vis Nucl Energy*. 2003;1:596-604.

1.13. Wang J, Bo H, Zheng W. Experimental study of the pressure discharge process for the hydraulic control rod drive system stepped cylinder. *J Nucl Sci Technol*. 2002;39(12):1294-1298. doi:10.1080/18811248.2002.9715324

1.14. Hanliang B, Wenxiang Z, Duo D. Studies on the performance of the hydraulic control rod drive for the NHR-200. *Nucl Eng Des*. 2000;195(1):117-121. doi:10.1016/S0029-5493(99)00200-9

1.15. Delmastro DF, Magan HB, Markiewicz M, et al. CAREM project status. *Sci Technol Nucl Install*. 2011:1-7. doi:10.1155/2011/140373

1.16. Batheja P, Meier WJ, Rau PJ. Design and testing of the reactor-internal hydraulic control rod drive for the nuclear heating plant. *Nucl Technol*. 1987;79:186-195

1.17. Jeong YS, Kim KM, Kim IG, Bang IC. Hybrid heat pipe based passive in-core cooling system for advanced nuclear power plant. *Appl Therm Eng*. 2015;90. doi:10.1016/j.applthermaleng.2015.07.045

1.18. Kim KM, Jeong YS, Kim IG, et al. Development of Passive In-Core Cooling System for Nuclear Safety Using Hybrid Heat Pipe. *Nucl Technol*. 2017;5450. doi:10.13182/NT16-32

1.19. CFD Analysis of a Concept of Nuclear Hybrid Heat Pipe with Control Rod. *The KSFM Journal of Fluid Machinery*. 2014;17(6);109-114

1.20. Seo S Bin, Kim IG, Kim KM, Jeong YS, Bang IC. Annals of Nuclear Energy Risk mitigation strategy by Passive IN-core Cooling system for advanced nuclear reactors. *Ann Nucl Energy*. 2018;111:554-567. doi:10.1016/j.anucene.2017.09.030

1.21. Kim IG, Bang IC. Hydraulic control rod drive mechanism concept for passive in-core cooling system (PINCs) in fully passive advanced nuclear power plant. *Exp Therm Fluid Sci*. 2017;85. doi:10.1016/j.expthermflusci.2017.03.013

1.22. Dazhong W, Dafang Z, Duo D, et al. Experimental study and operation experiences of the 5 MW Nuclear Heating Reactor. *Nucl Eng Des*. 1993;143(1):9-18. doi:10.1016/0029-5493(93)90272-

1.23. Hanliang B, Yanhua Z, Wenxiang Z, Duo D. Study on step-up characteristic of hydraulic control rod driving system. *Nucl Eng Des*. 2002;216(1-3):69-75. doi:10.1016/S0029-5493(02)00030-4

1.24. Li X, He S. Dynamic behavior of upper hydraulic drive control rod. *Nucl Eng Des*. 2006;236(24):2556-2566. doi:10.1016/j.nucengdes.2006.03.009

1.25. Magan HB, Delmastro DF, Markiewicz M, et al. IAEA-CN-164-5S01, CAREM Prototype Construction and Licensing Status. 2009:1-8. http://www-pub.iaea.org/MTCD/Publications/PDF/P1500_CD_Web/htm/pdf/topic5/5S01_D. Delmastro.pdf.

1.26. Hibi K, Ono H, Kanagawa T. Integrated modular water reactor (IMR) design. *Nucl Eng Des.* 2004;230:253-266. doi:10.1016/j.nucengdes.2003.11.025

1.27. Qin B, Li L, Bo H. Study on the decelerating mechanism of the new control rod hydraulic decelerator for the CRHDS based on numerical simulation and experiment. *Ann Nucl Energy.* 2018;120:814-827. doi:10.1016/j.anucene.2018.06.044

1.28. Sun X, Qin B, Bo H. Transient flow analysis of the single cylinder for the control rod hydraulic driving system. *Ann Nucl Energy.* 2017;101:151-158. doi:10.1016/j.anucene.2016.09.039

1.29. Vasilyev BA, Prospects of nuclear power industry with sodium-cooled fast reactors. XI International Public Dialogue Forum "Nuclear energy, environment, safety – 2016" http://www.osatom.ru/mediafiles/u/files/XI%20forum-dialog%202016/1_5_Boris_Vasiliev_ SC_reactors_eng.pdf

2.1. Grover GM, Cotter TP, Erikson GF, Structures of very high thermal conductance. *J. Appl. Phys.* 1964; 35;1990-1991

2.2. Intel Corp, Specifications of the New Intel Core i7-980 Processor, 2011 (last accessed 15.05.25), ark.intel.com/nl/products/58664/Intel-Core-i7-980-Processor-12M-Cache-3_33-GHz-4_8-GTs-Intel-QPI.

2.3. Kole M, Dey TK, Thermal performance of screen mesh wick heat pipes using water-based copper nanofluids. *Appl. Therm. Eng.* 2013;50;763-770 doi :10.1016/j.applthermaleng.2012.06.049

2.4. De Schampheleire S, De Kerpel K, Deruyter T, De Jaeger P, De Paepe M. Experimental study of small diameter fibres as wick material for capillary-driven heat pipes. *Appl Therm Eng*. 2015;78:258-267. doi:10.1016/j.applthermaleng.2014.12.027

2.5. Maziuk V, Kulakov A, Rabetsky M, Vasiliev L, Vukovic M. Miniature heat-pipe thermal performance prediction tool - software development. *Appl Therm Eng*. 2001;21(5):559-571. doi:10.1016/S1359-4311(00)00066-1

2.6. Faghri A, Thomas S, Performance characteristics of an annular heat pipe, Performance characteristics of a concentric annular heat pipe : Part I – Experimental prediction and analysis

of the capillary limit. *Journal of heat transfer* 1989; 111;844–850
doi:10.1115/1.3250795

2.7. Faghri A, Thomas S, Performance characteristics of an annular heat pipe, Performance characteristics of a concentric annular heat pipe : Part II – Vapor Flow Analysis. *Journal of heat transfer* 1989; 111;844–850
doi:10.1115/1.3250796

2.8. Faghri A, Heat Pipes : Review, Opportunities and Challenges, Frontiers in Heat Pipes 5 (2014)

2.9. Kim DH, Park SY, Boo JH, A Study on the Thermal Performance of Concentric Annular Heat Pipes, *Korean Society of Mechanical Engineers* 2014;19(4);1412-1417
https://link.springer.com/content/pdf/10.1007%2FBF02919187.pdf

2.10. Hung YM, Seng Q. Effects of geometric design on thermal performance of star-groove micro-heat pipes. *Int J Heat Mass Transf*. 2011;54(5-6):1198-1209. doi:10.1016/j.ijheatmasstransfer.2010.09.070

2.11. Asirvatham LG, Nimmagadda R, Wongwises S. Heat transfer performance of screen mesh wick heat pipes using silver-water nanofluid. *Int J Heat Mass Transf*. 2013;60(1):201-209. doi:10.1016/j.ijheatmasstransfer.2012.11.037

2.12. Yang X, Yan YY, Mullen D. Recent developments of lightweight, high performance heat pipes. *Appl Therm Eng*. 2012;33-34(1):1-14.
doi:10.1016/j.applthermaleng.2011.09.006

2.13. Zhang J, Diao YH, Zhao YH, Tang X, Yu WJ, Wang S. Experimental study on the heat recovery characteristics of a new-type flat micro-heat pipe array heat exchanger using nanofluid. *Energy Convers Manag*. 2013;75:609-616.
doi:10.1016/j.enconman.2013.08.003

2.14. Reay DA, Kew PA, heat pipes, Elsevier, New York, 2006

2.15. Busse CA, Pressure drop in the vapour phase of long heat pipes. *Thermionic Conversion Specialists Conference*, Palo Alto, Calif, October 1967;391-398

2.16. Shukla KN, Solomon AB, Pillai BC, Singh BJR, Kumar SS. Thermal performance of heat pipe with suspended nano-particles. *Heat Mass Transf und Stoffuebertragung*. 2012;48(11):1913-1920.
doi:10.1007/s00231-012-1028-4

2.17. Wang C, Zhang D, Qiu S, Tian W, Wu Y, Su G. Study on the characteristics of the sodium heat pipe in passive residual heat removal system of molten salt reactor. *Nucl Eng Des*. 2013;265:691-700.
doi:10.1016/j.nucengdes.2013.09.023

2.18. Jouhara H, Anastasov V, Khamis I. Potential of heat pipe technology in nuclear seawater

desalination. *DES*. 2009;249(3):1055-1061.
Doi:10.1016/j.desal.2009.05.019

2.19. Kim IG, Kim KM, Jeong YS, Bang IC. Flow visualization and heat transfer performance of annular thermosyphon heat pipe. *Appl Therm Eng*. 2017;125. doi:10.1016/j.applthermaleng.2017.07.116

2.20. Kim IG, Bang IC. Hydraulic control rod drive mechanism concept for passive in-core cooling system (PINCs) in fully passive advanced nuclear power plant. *Exp Therm Fluid Sci*. 2017;85. doi:10.1016/j.expthermflusci.2017.03.013

2.21. Development of the CEDM motor assembly for the APR+ reactor, KAERI/TR-4081/2010

2.22. Schmalhofer J, Faghri A, A study of circumferentially-heated and block-heated heat pipes – I. Experimental analysis and generalized analytical prediction of capillary limits. *Int. J. Heat Mass Transfer* 1993; 36;201–212. doi.org/10.1016/0017-9310(93)80080-E

2.23. Lin TF, Lin TF, Tsay YL, Wu JC, Experimental investigation of geyser boiling in an annular two-phase closed thermosyphon. *Int, J. Heat Mass Transfer* 1995; 38;295–307. doi.org/10.1016/0017-9310(95)90019-5

2.24. Casarosa C, Latrofa E, Shelginski A, The geyser effect in a two-phase thermosyphon. *Int. J. Heat Mass Transfer* 1983; 26;933–941. doi.org/10.1016/S0017-9310(83)80117-3

2.25. Ong KS, Goh G, Tshai KH, Chin WM. Thermal resistance of a thermosyphon filled with R410A operating at low evaporator temperature. *Appl Therm Eng*. 2016;106:1345-1351. doi:10.1016/j.applthermaleng.2016.06.080

2.26. Kim KM, Bang IC. Comparison of flooding limit and thermal performance of annular and concentric thermosyphons at different fill ratios. *Appl Therm Eng*. 2016;99:179-188. doi:10.1016/j.applthermaleng.2015.12.137

2.27. Kim Y, Shin DH, Kim JS, You SM, Lee J. Boiling and condensation heat transfer of inclined two-phase closed thermosyphon with various filling ratios. *Appl Therm Eng*. 2018;145(July):328-342. doi:10.1016/j.applthermaleng.2018.09.037

3.1. Batheja P, Meier WJ, Rau PJ, Design and testing of the reactor-internal hydraulic control rod drive for the nuclear heating plant. *Nucl. Tech.* 1987;79:186-195.

3.2. Dazhong W, Dafang Z, Duo D, et al. Experimental study and operation experiences of the 5 MW Nuclear Heating Reactor. *Nucl Eng Des*. 1993;143(1):9-18. doi:10.1016/0029-5493(93)90272-B

3.3. Magan HB, Delmastro DF, Markiewicz M, Lopasso E, Diez F, Gimenez M, Rauschert A,

Halpert S, Chocron M, Dezzutti JC, Pirani H, Balbi C, Fittipaldi A, Schlamp M, Murmis GM, Lis H, CAREM Project Status. *Sci. Technol. Nucl. Ins.* 2011;140373 doi:10.1155/2011/140373

3.4. Magan HB, Delmastro DF, Markiewicz M, Lopasso E, Diez F, Gimenez M, Rauschert A, Halpert S, Chocron M, Dezzutti JC, Pirani H, Balbi C. CAREM Prototype Construction and Licensing Status. *IAEA-CN-164-5S01*

3.5. Mazzi R, CAREM: An innovative-integrated PWR, 18th International Conference on Structural Mechanics in Reactor Technology (SMiRT 18) Beijing, China, August 7-12, 2005 SMiRT18-S01-2

3.6. Ricotti ME, Cammi A, Carelli M, et al. Hydraulically driven control rod concept for integral reactors: Fluid dynamic simulation and preliminary test. *Glob 2003 Atoms Prosper Updat Eisenhowers Glob Vis Nucl Energy*. 2003;1:596-604. http://www.scopus.com/inward/record.url?eid=2-s2.0-2642577579&partnerID=40&md5=8bafb1ea75c03d05fdaa6e8fb0f47595%0Ahttps://www.ipen.br/biblioteca/cd/genes4/2003/papers/1028-final.pdf%0Ahttps://cn.bing.com/search?q=CAREM+REACTOR++control&first=96&FORM=PORE

3.7. Qin B, Li L, Bo H. Study on the decelerating mechanism of the new control rod hydraulic decelerator for the CRHDS based on numerical simulation and experiment. *Ann Nucl Energy*. 2018;120:814-827. doi:10.1016/j.anucene.2018.06.044

3.8. Sun X, Qin B, Bo H. Transient flow analysis of the single cylinder for the control rod hydraulic driving system. *Ann Nucl Energy*. 2017;101:151-158. doi:10.1016/j.anucene.2016.09.039

3.9. Dazhong W, Zuying G, Wenxiang Z. Technical design features and safety analysis of the 200 MWt Nuclear Heating Reactor. *Nucl Eng Des*. 1993;143(1):1-7. doi:10.1016/0029-5493(93)90271-A

3.10. Li X, He S. Dynamic behavior of upper hydraulic drive control rod. *Nucl Eng Des*. 2006;236(24):2556-2566. doi:10.1016/j.nucengdes.2006.03.009

3.11. Hanliang B, Yanhua Z, Wenxiang Z, Duo D. Study on step-up characteristic of hydraulic control rod driving system. *Nucl Eng Des*. 2002;216(1-3):69-75. doi:10.1016/S0029-5493(02)00030-4

3.12. Qin B, Li L, Bo H. Annals of Nuclear Energy Study on the decelerating mechanism of the new control rod hydraulic decelerator for the CRHDS based on numerical simulation and

experiment. *Ann Nucl Energy*. 2018;120:814-827. doi:10.1016/j.anucene.2018.06.044

3.13. Development of the CEDM motor assembly for the APR+ reactor, KAERI/TR-4081/2010.

3.14. Development of the CEDM Motor Assembly for the APR+ Reactor, AR-805/2008.

3.15. Nishimura T, Nakayama H, Saitoh M, Yaguch S, CRDM motion analysis using machine learning technique. *Proceedings of ICAPP* 2017 April 24-28, 2017 - Fukui and Kyoto (Japan)

4.1. Qin B, Li L, Bo H. Annals of Nuclear Energy Study on the decelerating mechanism of the new control rod hydraulic decelerator for the CRHDS based on numerical simulation and experiment. Ann Nucl Energy. 2018;120:814-827. doi:10.1016/j.anucene.2018.06.044

4.2. Development of the CEDM Motor Assembly for the APR+ Reactor, AR-805/2008.

4.3. Ishida T, Imayoshi S, Yoritsune T, Nunokawa H, Ochiai M, Ishizaka Y. Development of In-vessel Type Control Rod Drive Mechanism for Marine Reactor. *J Nucl Sci Technol*. 2001;38(7):557-570. doi:10.1080/18811248.2001.9715067

4.4. Park JS, Lee MG, Chang SY, Lee DH. Conceptual Design of a Magnetic Jack Type In-Vessel Control Element Drive. *Trans. Korean Soc. Mech. Eng. C* 2015;3(3):225-232.

4.5. Divandari M, Hashemi-Tilehnoee M, Khaleghi M, Hosseinkhah M. A novel control-rod drive mechanism via electromagnetic levitation in MNSR. *Nukleonika*. 2014;59(2):73-79. doi:10.2478/nuka-2014-0008

4.6. Ricotti ME, Cammi A, Carelli M, et al. Hydraulically driven control rod concept for integral reactors: Fluid dynamic simulation and preliminary test. *Glob 2003 Atoms Prosper Updat Eisenhowers Glob Vis Nucl Energy*. 2003;1:596-604. http://www.scopus.com/inward/record.url?eid=2-s2.0-2642577579&partnerID=40&md5=8bafb1ea75c03d05fdaa6e8fb0f47595%0Ahttps://www.ipen.br/biblioteca/cd/genes4/2003/papers/1028-final.pdf%0Ahttps://cn.bing.com/search?q=CAREM+REACTOR++control&first=96&FORM=PORE

4.7. Development of the CEDM motor assembly for the APR+ reactor, KAERI/TR-4081/2010.

4.8. Jeong YS, Kim KM, Kim IG, Bang IC. Hybrid heat pipe based passive in-core cooling system for advanced nuclear power plant. *Appl Therm Eng*. 2015;90. doi:10.1016/j.applthermaleng.2015.07.045

4.9. Kim IG, Bang IC. Hydraulic control rod drive mechanism concept for passive in-core cooling system (PINCs) in fully passive advanced nuclear power plant. *Exp Therm Fluid Sci*. 2017;85. doi:10.1016/j.expthermflusci.2017.03.013

4.10. Mazzi R, CAREM: An innovative-integrated PWR, 18th International Conference on Structural Mechanics in Reactor Technology (SMiRT 18) Beijing, China, August 7-12, 2005 SMiRT18-S01-2

4.11. Yoritsune T, Ishida T, Imayoshi S. In-vessel type control rod drive mechanism using magnetic force latching for a very small reactor. *J Nucl Sci Technol*. 2002;39(8):913-922. doi:10.1080/18811248.2002.9715276

4.12. Dazhong W, Dafang Z, Duo D, et al. Experimental study and operation experiences of the 5 MW Nuclear Heating Reactor. *Nucl Eng Des*. 1993;143(1):9-18. doi:10.1016/0029-5493(93)90272-B

4.13. Lu J, Shen L, Huang Q, Sun D, Li B, Tan Y. International Journal of Thermal Sciences Investigation of a rectangular heat pipe radiator with parallel heat fl ow structure for cooling high-power IGBT modules. 2019;135(January 2018):83-93. doi:10.1016/j.ijthermalsci.2018.09.004

4.14. Liang K, Li Z, Chen M, Jiang H. Comparisons between heat pipe, thermoelectric system, and vapour compression refrigeration system for electronics cooling. *Appl Therm Eng*. 2019;146(August 2018):260-267. doi:10.1016/j.applthermaleng.2018.09.120

4.15. Lai K, Wang W, Yi C, Kuang Y, Ye C. The study of passive cooling system assisted with separate heat pipe for decay heat removal in spent fuel pool. *Ann Nucl Energy*. 2018;111:523-535. doi:10.1016/j.anucene.2017.08.062

4.16. Liu M, Zhang D, Wang C, Qiu S, Su GH, Tian W. Experimental study on heat transfer performance between fluoride salt and heat pipes in the new conceptual passive residual heat removal system of molten salt reactor. *Nucl Eng Des*. 2018;339(March):215-224. doi:10.1016/j.nucengdes.2018.09.015

4.17. Zografos AI, Martin WA, Sunderland JE. Equations of properties as a function of temperature for seven fluids. *Comput Methods Appl Mech Eng*. 1987;61(2):177-187. doi:10.1016/0045-7825(87)90003-X

4.18. Flexible heat pipe-baed passive decay haet removal system and element technology development, 2013M2A8A1041440

Acknowledgement (감사의 글)

울산에서 태어나 29 년동안 고향에서 수학하며 박사학위를 마칠지는 꿈에도 몰랐습니다. 뒤돌아보면, 대학원 생활은 제 인생을 가장 큰 변화와 성장을 가져왔던 기간이었습니다. 학위과정동안 얻은 많은 경험과 교훈을 잊지 않고 살아가도록 하겠습니다. 지금의 제가 있기까지 너무도 많은 도움을 받았지만 전하지 못한 마음을, 감사의 글을 빌려 전하고자 합니다.

먼저 저의 선택을 믿고 지금까지 든든한 버팀목이 되어준 부모님께 감사드립니다. 어머니, 항상 미안하고 고맙습니다. 그리고 아버지, 제 졸업이 조금 늦었지만 하늘에서 보기에 부끄럽지 않은 아들이 되겠습니다. 그리고 외할머니, 사랑으로 길러주셔서 감사합니다.

대학원 생활동안 걱정해주시고 가야할 방향을 알려주신 교수님께 감사의 말을 올리고 싶습니다. 교수님이 있었기에 제가 여기까지 올 수 있었습니다. 교수님의 조언과 질책이, 지금 졸업을 앞두고 돌아보니 모두 저를 위한 마음이었습니다. 끝까지 이끌어 주셔서 감사합니다.

그리고 지금까지 함께한 연구실 선 후배님들에게 감사의 인사를 올립니다. 처음 대학원에 들어와, 어린 저를 가르쳐준 승원이형, 연구실 분위기를 책임진 성대형, 안전해석 코드를 가르쳐준 사라누나, 제가 가장 힘들 때 고민을 함께해준 한이형, 연구실의 해결사 경모, 밥과 커피 그리고 아이디어를 함께 나눈 석빈, 항상 예상치 못한 이야기로 즐거움을 준 성보, 연구실의 궂은 일을 맡아서 해준 영신, 우리 랩의 패션리더 효, 부족한 선배 때문에 고생한 유경이, 힘없은 선배들 때문에 몸 쓰는 일을 항상 도맡은 민호, 항상 어두운 얼굴이 이제 밝아졌으면 좋겠는 한얼이까지, 저의 5 년 반의 학위과정에서 빼놓을 수 없는 인연이었습니다. 평생동안 잊지 못할 소중한 추억을 함께하여 정말 고맙습니다.

또한 학부때부터 대학원까지 많은 것을 가르쳐주신 김지현 교수님, 대학교 OT 부터 제 학위 마지막 발표까지 함께해 주신 박영빈 교수님, 바쁘신 와중에도 흔쾌히 심사를 맡아주신 이재영 교수님, 최기용 박사님께도 감사의 말씀을 올립니다.

저의 학위 동안의 실험장치들을 제작해주시고 실험의 문제들을 해결해주신 이종수 사장님께도 깊은 감사를 드립니다.

끝으로, 학부, 대학원 생활동안 저의 아군이 되어 지지해준 친구들과 선배, 후배들에게 감사를 전합니다. 감사합니다.